

## Reservoir characteristics and diagenesis of the Buntsandstein sandstones in the Campine Basin (NE Belgium)

PIETER BERTIER 

*KU Leuven, Geology, Celestijnenlaan 200E, B-3001 Heverlee; current address: Qmineral BV, Gaston Geenslaan 1, 3001 Heverlee, Belgium; [pbertier@qmineral.com](mailto:pbertier@qmineral.com).*

RUDY SWENNEN 

*KU Leuven, Geology, Celestijnenlaan 200E, B-3001 Heverlee, Belgium; **corresponding author:** [Rudy.Swennen@Kuleuven.be](mailto:Rudy.Swennen@Kuleuven.be).*

RAYMOND KEMPS 

*Research Group for Materials Technology, VITO, Boeretang 200, B-2400 Mol, Belgium; [Raymond.kemps@vito.be](mailto:Raymond.kemps@vito.be).*

BEN LAENEN 

*VITO NV, Boeretang 200, B-2400 Mol, Belgium; [Ben.Laenen@vito.be](mailto:Ben.Laenen@vito.be).*

ROLAND DREESEN 

*Geological Survey of Belgium, Royal Belgian Institute of Natural Sciences, Directorate Earth and History of Life, Jennerstraat 13, B-1000 Brussels, Belgium; [Roland.dreesen@telenet.be](mailto:Roland.dreesen@telenet.be).*

### ABSTRACT

The red beds of the Buntsandstein (Early Triassic) in the Campine Basin (NE Belgium) display porosities between 5.3–20.2% (average 13.7%) and permeabilities varying between 0.02–296.4 mD (average 38.7 mD). Knowledge of their reservoir controlling properties, which today are missing, is important in view of potential geological storage of CO<sub>2</sub> or natural gas and geothermal reservoir potential within these sandstones. Therefore the effects of diagenesis were assessed based on petrography, stable isotope analyses, fluid inclusion microthermometry, X-ray diffraction, electron microprobe and porosity-permeability core analyses.

These sandstones were deposited by a dryland river system, in a warm, mostly arid climate with episodic rainfall and high evaporation rates. During wetter periods especially feldspars were dissolved. Strong evaporation during dry periods led to reprecipitation of the dissolved species as K-feldspar and quartz overgrowths, smectite and calcite/dolomite. Sediment reworking resulted in framework grains becoming clay coated. The clay coats are better developed in finer than in coarser grained sediments. The original smectite composing the rims converted to illite during burial. The tangential orientation of the clay platelets in the rims led to illite-mica-induced dissolution of quartz during burial/compaction, which is manifested as bedding parallel dissolution seams that are filled with clays and micas, especially in the fine-grained sandstone/siltstone/claystone. These constitute important barriers to the vertical flow within the reservoir. The released silica did not really affect the red sandstones but was exported (often on mm to cm scale) to nearby bleached horizons, where nucleation inhibiting clay rims are less well developed. The red colour of the sandstones arises from the presence of small amounts of Fe-oxides in the inherited clay rims. Migration of fluids enriched in organic acids, expelled from underlying Carboniferous coal-bearing strata, resulted in local bleaching of coarser grained horizons. In the finer grained sediments, the red colour was mostly preserved, which suggests that the reductive capacity of the fluid was limited.

### KEYWORDS

sedimentology,  
diagenesis,  
reservoir properties,  
clay rims,  
dissolution,  
compaction

### Article history

Received 05.10.2020, accepted in revised form 21.09.2022, available online 22.12.2022.

## 1. Introduction

Lower Triassic red beds are widespread in the Southern North Sea area. Their regional extent roughly stretches from eastern Ireland to western Lithuania and from Bavaria in the south to the north of Denmark. These red beds were deposited in extensive, arid sandy alluvial plains bordering an intracratonic lake, which occupied the deepest central parts of the basin (Geluk, 2005; Feist-Burkhardt et al., 2008; Bachmann et al., 2010). They host important hydrocarbon accumulations where underlying Zechstein (Permian) evaporites did not effectively seal them from the Carboniferous source rocks, as is the case at the basin margins, where the salts are thinner or absent, and in a couple of areas that underwent inversion tectonics (Johnson & Fisher, 1998). In the Netherlands, the Buntsandstein is the second major gas-producing horizon (van Hulten, 2006). In the UK sector, several important reservoirs are producing from the equivalent Hewett sandstone.

The Buntsandstein is also an important target for natural- and greenhouse gas storage since it underlies heavily industrialised and densely populated regions. Also, their geothermal potential has recently been investigated (Dufour & Heederik, 2019; Mijnlief, 2020 and references therein; Scorgie

et al., 2021).

Despite its potential, reservoir quality of the Buntsandstein, especially regarding diagenesis, received only limited attention in the literature. Van Hulten (2006) and Soyk (2015) qualify the diagenetic overprint as an important exploration risk, respectively in the Netherlands and the Upper Rhine Graben in SW Germany. Several authors report early diagenetic cements that locally completely obliterate porosity (Fontaine et al., 1993; Purvis & Okkerman, 1996; Spain & Conrad, 1997). Muchez et al. (1992) recognised the importance of secondary porosity in the Buntsandstein of the Campine Basin. Wendler et al. (2012) attributed bleaching and related feldspar alteration and carbonate cementation in central Germany to circulation of CO<sub>2</sub>-rich fluids.

The sandstones of the Buntsandstein Formation were sampled from five boreholes in the Campine Basin (i.e., KB64, KB98, KB169; KB172 & KB201; Figs 1, 2). This contribution aims at presenting a detailed description of the diagenetic history of the Buntsandstein in the Campine Basin (NE Belgium) and its effect on reservoir quality. It provides insight into the processes that potentially can be modelled geochemically, however, the latter is out of the scope of this contribution. Special attention will be paid to:

- early diagenetic alterations and how they link to depositional

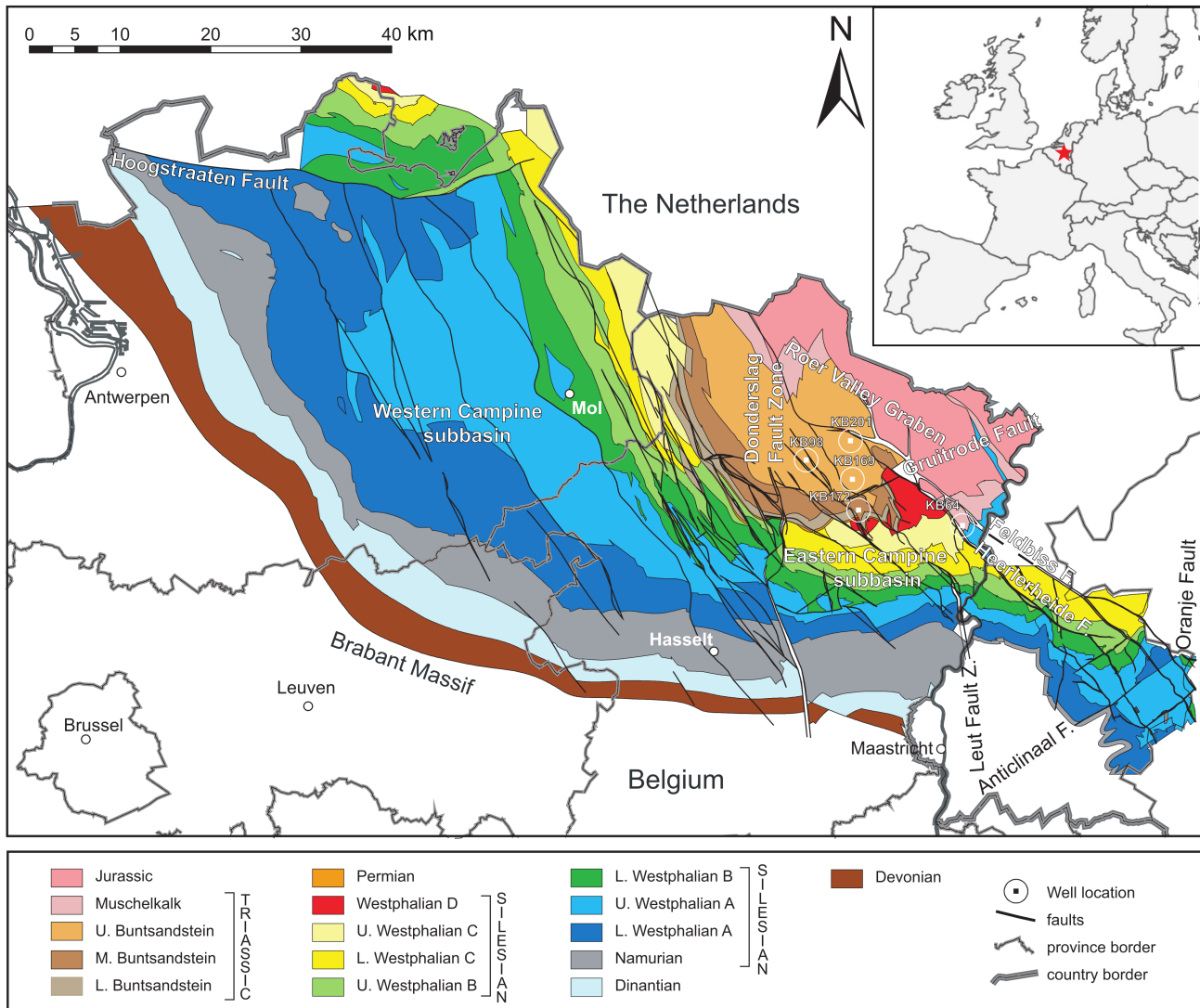


**Figure 1.** Pre-Cretaceous subcrop map of the Belgian Campine Basin (compiled after Langenaeker, 2000 and Patijn & Kimpe, 1961). The northern and north-eastern borders consist of the Hoogstraaten fault and the NW–SE striking boundary faults of the Roer Valley Graben. Eastward the basin extends into Dutch Limburg, where the NE–SW striking Variscan Anticlinaal Fault/Oranje Fault system constitutes the boundary with the German Carboniferous Wurm Basin. To the south and west, the basin is bounded by the subcropping early Palaeozoic rocks of the Caledonian London–Brabant Massif.

settings. Here the impact of sedimentological subenvironments on reservoir heterogeneity is addressed.

- burial diagenetic processes related to fluid migrations. How these can explain the development of secondary porosity and bleaching of the original sandstones will be addressed. These burial processes will be placed into the temperature-depth history of the basin.

Thus the aim of this paper is to address the composition of the Buntsandstein sandstones and to infer which diagenetic processes affected these reservoir rocks. The latter will also help to assess the reactivity of these sandstones with regard to their subsurface reservoir use (Carbon Capture Storage, geothermal energy).

## 2. Geological setting

The Campine Basin is situated in NE Belgium (Fig. 1), between the Roer Valley Graben in the NE and the Brabant Massif in the SW. The Buntsandstein in this basin encompasses all predominantly red-coloured and sandy siliciclastic sediments assigned to the Lower Triassic (Dusar et al., 2001). These sediments constitute, together with the Permian Helchteren Formation, a wedge between the Carboniferous Coal Measure Group and the Cretaceous Chalk Group, in the NE part of the Campine Basin (Fig. 1).

The transition between Permian and Triassic is concordant, where the former strata are present. Where the Permian deposits are absent, the Buntsandstein discordantly overlies Westphalian strata. The top of the Buntsandstein Formation in the Campine Basin corresponds to the Cimmerian Unconformity, which is overlain by Cretaceous chalks and marls (Fig. 2). Towards the north, in the Roer Valley Graben, Jurassic shales cover the Buntsandstein.

Three members have been distinguished in the Buntsandstein. The Gruitrode Member (basal unit) consists of an alternation of red thick-bedded siltstones to silty claystones and sandstones of varying granulometry. The Bullen Member (middle unit) with the best reservoir potential consists of red and bleached sandstones with some conglomerate layers. The Bree

Member (top unit) is composed of more fine-grained sandstones, which are variably rich in calcareous cements, with claystone layers at the base and the top. The maximum preserved thickness of the Buntsandstein in the Campine Basin is about 490 m (Dusar et al., 2001). In the Roer Valley Graben its thickness is estimated to be only 430 m (Laenen, 2002).

## 3. Depositional environment

The Buntsandstein strata consist of a tilted sequence, resulting in a subcrop with the oldest deposits situated near the contact with the Carboniferous and the youngest strata located more in the direction of Roer Valley Graben. Dusar et al. (1987b) determined the depositional environment of the Buntsandstein deposits based on a detailed sedimentological facies analysis of cores of borehole KB172. They describe the Buntsandstein as a floodplain association in which three subenvironments can be distinguished. The base consists of parallel laminated fine sediments, deposited by flood sheets and as clay playa, which are typical for distal floodplain settings in dry environments. The medial sequence shows features of both channel flows and flood sheet deposits. The youngest deposits represent a proximal environment that is characterised by coarse sandstones and conglomerates deposited by channel flows. Dusar et al. (1987b) regarded these continental deposits as a braid-plain prograding basinwards by means of channel flows that spread out as flood sheets covering vast areas.

Correlation of KB172 with other boreholes that traversed the Triassic in the Campine Basin and the Roer Valley Graben, as made by Langenaeker (1998) and van Tongeren (2001), showed that the three-fold division made by Dusar et al. (1987b) does not correspond to the lithostratigraphic subdivision. The youngest, most proximal sequence of Dusar et al. (1987b) constitutes the lower part of the Bullen Member, while both the medial and distal sequences make up the Gruitrode Member. The Bree Member and the upper part of the Bullen Member were removed by erosion at the location of KB172.

The Bree Member was intersected by boreholes KB201 and KB169 in the Campine Basin. The lower part consists of an

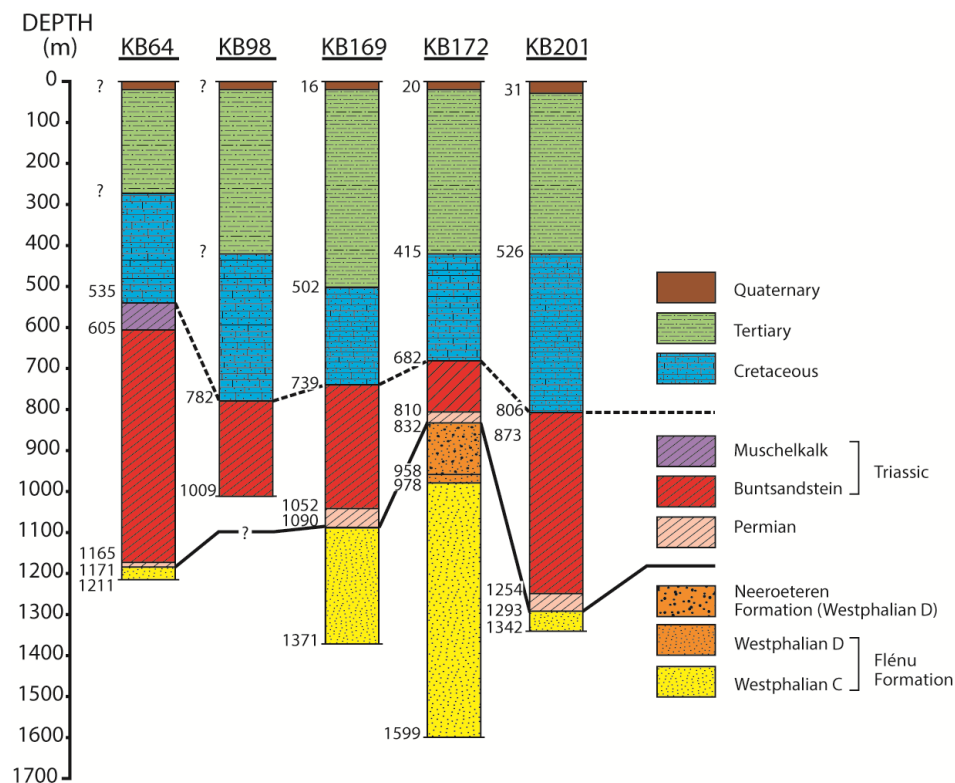


Figure 2. Stratigraphy of the sampled boreholes.

intercalation on a centimetre to metre scale of sandstones and red shales. The top part consists of fine to medium, and sometimes coarse-grained sandstones (Laenen, 2002). The presence of thin gypsum/anhydrite and carbonate layers, nodules and fractures filled with the latter phases in the upper 100 m of the Bree Member indicate the onset of a transgressive trend with fluvial deposits interfingering with lagoonal evaporites and shallow marine limestones (Wouters & Vandenberghe, 1994; Langenaeker, 1998).

#### 4. Burial history

The burial history of the five wells was reconstructed based on the geological history of the basin and coalification data of the underlying Westphalian sequence and organic-rich Namurian shales (*sensu* Suggate, 1998), with the integration of published data from Fermont et al. (1994), Van Keer et al. (1998), Helsen & Langenaeker (1999), Bertier et al. (2008) and Wei et al. (2022). Figure 3 shows the burial curve of KB172, as an example. This burial history is used as a reference frame for the reconstruction of the diagenetic history of the reservoir, allowing to differentiate eo-, meso- and telogenetic regimes (*sensu* Choquette & Pray, 1970):

- Eogenetic regime during and after deposition, in the early Triassic. This regime lasted till the early Jurassic, when deposition of thick sequences of marls and shales of the Alena Group sealed the Buntsandstein from meteoric influence and caused the temperature in the reservoir to rise above 70 °C.
- Mesogenetic regime during which the Buntsandstein reached its maximal burial (middle Jurassic). For KB172, maximum temperatures reached about 115 °C for the base and about 95 °C for the top of the Buntsandstein reservoir.
- Telogenetic regime during Cretaceous uplift whereby the Buntsandstein at all studied locations was again influenced

by near-surface diagenesis.

- Renewed burial with transition of eo- to mesogenetic regime II. By the end of the Cretaceous, sedimentation resumed and continued almost uninterrupted throughout the Cenozoic. Sequences of varying thicknesses were deposited at the studied locations, yet in none of the wells, temperatures never reached values higher than during the Middle Jurassic.

The five wells that were sampled for this study are located on different fault blocks (Fig. 1), and consequently underwent slightly different burial histories (Table 1).

#### 5. Methodology

Forty-five thin sections (from cores all accessible at the core repository of the Belgian Geological Survey) were examined by conventional and for the first time by cathodoluminescence (CL) petrography. Calcite and iron-rich carbonate phases were identified by staining with alizarine red S and potassium ferricyanide (Dickson, 1966). Also new was that thin section porosity was highlighted by a fluorescent dye in the epoxy of vacuum-impregnated sandstones. The mineralogy of 32 thin sections was quantified using an automated point counter (1000 counts/thin section). CL petrography was carried out with a Technosyn Cold Cathodo Luminescence Model 8200 MkII (Technosyn Limited, Cambridge, UK). Operational conditions were 16–20 kV, 500–650 µA gun current, 5 mm beam width and 0.05 Torr vacuum. Further petrography on broken rock surfaces was done by scanning electron microscopy (SEM). A JEOL JSM 6340f SEM (JEOL (Europe) B.V., Zaventem, Belgium) equipped with a PGT Spirit (Princeton Gamma-Tech Instruments Inc., Princeton, USA) energy dispersive detector and a Centaurus (K.E. Developments, Cambridge, UK) backscatter detector was used. All EDX-spectra were obtained after a counting period of 100 s. New data on porosity and

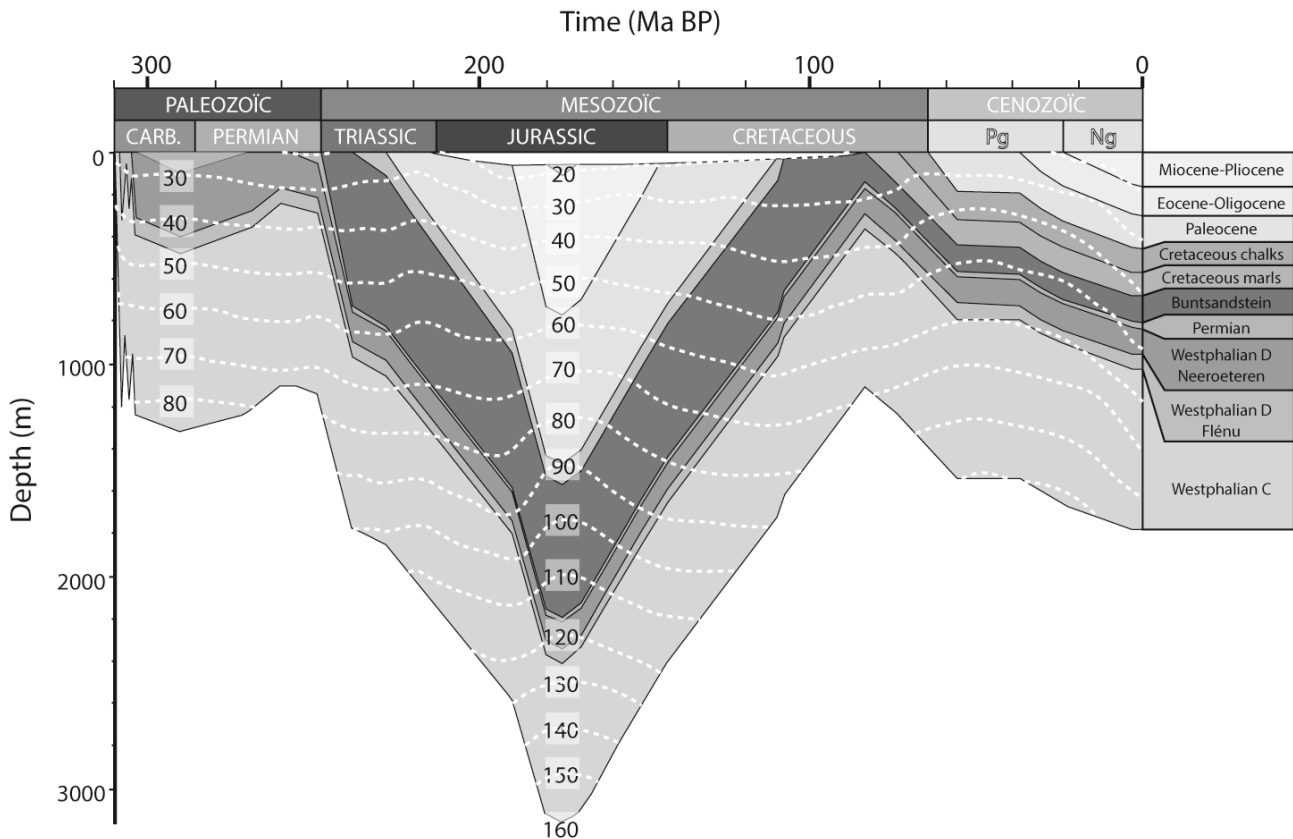


**Figure 3.** Burial history of well KB172. A constant heat flow of 82 mW/m<sup>2</sup> is assumed. Maximal burial is reached during the Jurassic and is followed by the erosion of 1990 m of Triassic to middle Jurassic sediments. Dashed white lines are isotherms.

**Table 1.** Properties of the Buntsandstein at the locations of the five sampled wells (Mus. = Muschelkalk Formation; C.U. = Cimmerian Unconformity; Cret. = Cretaceous; n.a. = not available; base refers to the base of the formation).

	KB64	KB98	KB169	KB172	KB201
Subcrop depth	605 m	782 m	739 m	682 m	806 m
Thickness	560 m incl. Röt	227 m	313 m	128 m	448 m
Overlain by	Mus., 70 m	C.U., Cret.	C.U., Cret.	C.U., Cret.	C.U., Cret.
Estimated $T_{\max}$	n.a.	n.a.	125 °C, base	95–115 °C	ca. 120 °C
Core quality	poor	poor	only base	good	good

permeability were acquired from 28 samples on 1.5 inch plugs by means of helium porosimetry and horizontal air permeability measurements.

To be able to refine the diagenetic processes that took place, 37 carbonate samples were analysed for their  $\delta^{13}\text{C}$  and  $\delta^{18}\text{O}$  isotopic composition. However, only in a few samples, pure one-phase carbonate generations could be micro-sampled, since carbonate phases are often intergrown or too small. The analyses were done at the University of Erlangen (Germany). The carbonate powders reacted with 100% phosphoric acid (density >1.9; Wachter & Hayes, 1985) at 75 °C using a Kiel III online carbonate preparation line connected to a Thermo Finnigan 252 mass spectrometer (Thermo Electron Corp., Waltham, MA, USA). All measured values are reported in per mill relative to V-PDB by assigning a  $\delta^{13}\text{C}$  value of +1.95‰ and a  $\delta^{18}\text{O}$  value of -2.20‰ to NBS19. Reproducibility based on replicate analysis of laboratory standards is better than  $\pm 0.03\%$  for  $\delta^{13}\text{C}$  and  $\pm 0.05\%$  for  $\delta^{18}\text{O}$  ( $1\sigma$ ). Because of the mixture of carbonate phases in most samples, the measured  $\delta^{18}\text{O}$  values could not be corrected for the fractionation related to the used extraction method. Calculated isotopic compositions of fluids are reported in V-SMOW.

A Linkam heating-cooling stage (Linkam Scientific Instruments, Tadworth, UK) was used for microthermometric analysis of fluid inclusions. The used preparation technique is described by Muchez & Viaene (1994).

The mineralogical composition of the clay fraction of 20 sandstones was determined by XRD-analysis of texturized clay fractions. Because of the large sizes of the clays, as observed with SEM, the analyses were performed on the <36  $\mu\text{m}$  fraction of the sandstones. The method described by Muchez et al. (1991) was used for the separation of the clay fraction. The oriented samples were prepared by the ‘glass slide method’ as described by Moore & Reynolds (1997), because of its ease of application when using relatively coarse clay fractions. Analyses were conducted on a Philips PW3710 diffractometer (PANalytical, Almelo, The Netherlands) with graphite monochromatised  $\text{CuK}\alpha$ -radiation. The working conditions were 45 kV and 30 mA, rotating sample holder and secondary monochromator with divergence and receiving slit of respectively  $1^\circ$  and  $0.1^\circ$ . A count time of 1 s was chosen and a step size of  $0.02^\circ 2\theta$ . The identification of the clay mineralogy followed the recommendations made by Thorez (1976), Moore & Reynolds (1997) and Hillier (2003).

The elemental compositions of carbonate and feldspar grains in 12 samples were quantified by means of electron probe micro-analysis (EPMA) on a JEOL JXA-8621MX (JEOL (Europe) B.V., Zaventem, Belgium). Beam conditions were 15

kV and 10 nA for energy and current, respectively. To avoid beam damage, the beam was defocused to a spot diameter of 5  $\mu\text{m}$ . Carbonate crystals were analysed by means of cross-sections consisting of non-overlapping points (up to 40). Single-point analyses were performed on smaller crystals. Standard and sample X-ray counting times were 50 s on the peaks and 20 s on the background. The standards used for measurements on carbonates were dolomite (Ca, Mg, Mn and Fe), calcite (Ca, for calcites) and hematite (Fe, for samples with higher than 1 mol%  $\text{FeCO}_3$ ). Sanidine, albite and plagioclase (An65) standards were used for measurements on feldspars. Data were processed using a ZAF-program, with  $\Phi\rho Z$  calculation of the absorption factor. The method proposed by Lane and Dalton (1994), whereby standards are represented as metal oxides was used for the ZAF corrections on carbonates. Accuracy and precision were tested on secondary standards and are better than 0.1 mol% for Ca, Mg, Fe, K, Si and Al, and better than 0.2 mol% for Na and Mn. Himax (SAMX, Saint Laurent Du Var, France) software was used to make qualitative maps of the concentrations of 11 elements (C, O, Na, Mg, Al, Si, S, K, Ca, Mn and Fe). Beam conditions for mapping were 15 kV, 10 nA and 1  $\mu\text{m}$  for energy, current and spot size, respectively. All maps were made on grids of 1 by 1  $\mu\text{m}$  and have sizes between  $512 \times 512 \mu\text{m}$  and  $2048 \times 2048 \mu\text{m}$ . Acquisition time was 2 ms per element per pixel.

## 6. Results

In this section, first the results from the clay mineralogy will be given since these results are of relevance for the petrography section that is subsequently given. Subsequently, information on stable isotopes, fluid inclusion microthermometry and electron probe micro-analysis are provided.

### 6.1. Clay mineralogy

Figure 4 shows air-dried, glycolated and heated X-ray diffractograms of a representative sandstone sample (<36  $\mu\text{m}$  fraction). Four main types of clay minerals were identified, i.e. kaolinite, illite, chlorite and smectite.

The clay fractions of the coarse-grained sandstones generally show more kaolinite relative to other clays than those of the fine-grained samples. All sandstones analysed with XRD contain kaolinite, although kaolinite was not always observed petrographically, likely due to the absence of its blocky (booklet) characteristics.

Illite was found in all samples, in varying quantities. Its content, relative to other clay minerals, is higher in the finer grained sandstones. In most samples, the air-dried oriented clay

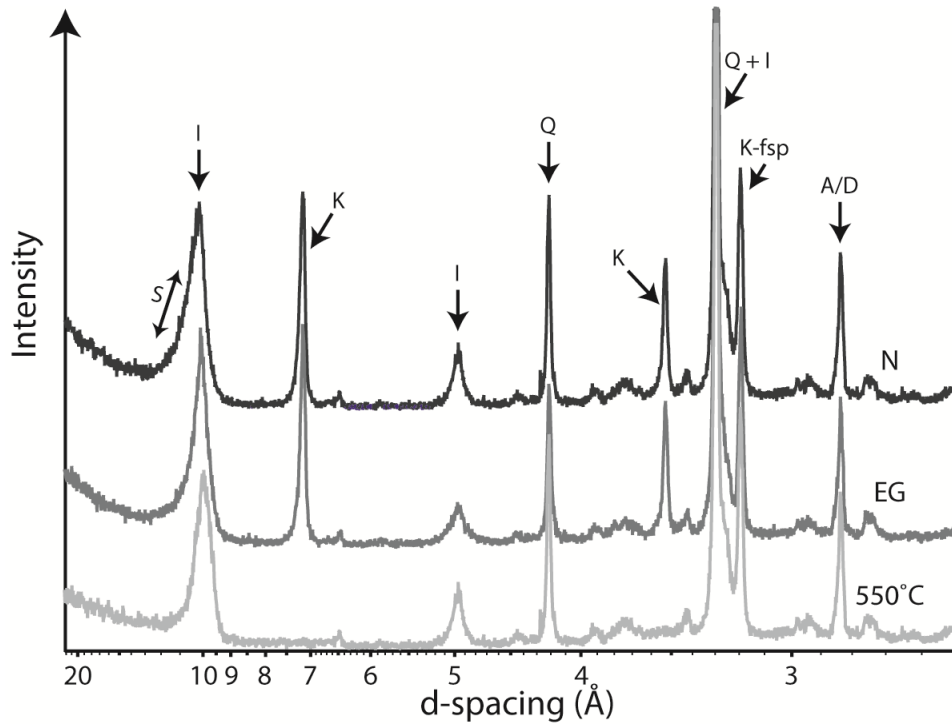


**Figure 4.** X-ray diffractograms of air-dried (N), glycolated (EG) and heated (550 °C) clay fraction (<36  $\mu\text{m}$ ) of a representative sample of the Buntsandstein (KB172 – 779.35 m). S = smectite; I = illite; K = kaolinite; Q = quartz; K-fsp = K-feldspar, microcline; A/D = ankerite/dolomite.

fraction shows an asymmetry of the 10 Å reflection of illite, towards higher d-spacings, i.e. 12–13 Å, which is most distinct in the fine-grained samples. The asymmetry is not present in ethylene glycol-solvated specimens, which indicates the presence of smectite interlayers in the illite crystal structures. The relatively low intensities and the positions of the illite ‘shoulder’ reflections (i.e., the sharp decreasing intensities from 10 Å towards 12–13 Å) indicate a high illite content within the illite-smectite mixed-layer clays. According to the differential  $2\theta$  (or d-spacing) measurements proposed by Środoń (1980), illite contents are well above 90% for the samples with the broadest 10 Å reflections.

Except for the smectite in the illite structures, the sandstones contain little smectitic clays, as no clear 17 Å reflections were observed in the ethylene-glycol saturated samples.

The analysed samples of the Buntsandstein show relatively sharp 7 Å reflections, no doubling of the 3.5 Å reflections and no clear 14.2 Å reflections. The 7 Å reflections completely disappear after heating, which means the amount of chlorite, if present at all, must be small (<1%).

## 6.2. Petrography

### 6.2.1. Detrital constituents

The selected Buntsandstein samples are mostly fine to medium-grained, well-sorted, sublithic arenites to subarkoses. Two samples have low lithic- and feldspar contents, and classify as quartz arenites (Table 2; Fig. 5). The coarse-grained strata generally have a bimodal sorting with larger grains or pebbles floating in a medium-grained matrix. These pebbles are usually well rounded, while for most of the fine to medium-grained sandstones the roundness of the grains varies from sub-rounded to well-rounded.

The main component of these rocks is quartz (Table 3; average 46.6%), which are mainly monocrystalline, but also metamorphic-derived polycrystalline grains (average 15.8%) exist. The quantity of microcrystalline grains is low in most samples (average 0.4%), except for one very coarse sandstone (KB201, 1191.7 m), containing 7.8% microcrystalline (chert) fragments.

The sandstones contain on average 8.2% of lithic fragments which are generally little affected by diagenesis including compaction. The bulk of them consists of coarse-grained siliciclastics (silt to sand-sized quartz grains), being fragments of sandstone, siltstones or psammites or their metamorphic equivalents of which the metamorphic grade is low (i.e. rank 0 to 2 according to Garzanti & Vezzoli, 2003). Other lithics are mainly fragments of pelitic to metapelitic rocks with similar low metamorphic grades. Some samples contain larger fragments (up to 5 mm) of relatively fine-grained sandstone, which are often tightly cemented by sparry calcite. The mineralogy of the less cemented fragments resembles Westphalian C sandstones (Bertier et al., 2008).

The Buntsandstein contains on average 5.3% of feldspars. Some samples, mainly those of well KB64, contain large

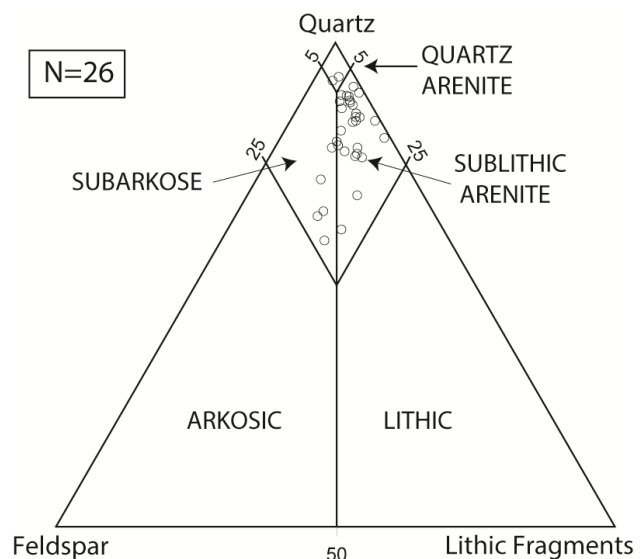


**Figure 5.** QFL plot (Folk, 1974) of the studied Buntsandstein samples. Most sandstones classify as sublithic arenites to subarkoses. A couple samples are quartz arenites. None of the analysed samples contains enough clay to be classified as a wacke.

**Table 2.** Mineralogical compositions of representative samples of the Triassic sandstones obtained by pointcounting (n = 1000). Porosity (%) and permeability (mD) values were measured by He-porosimetry and horizontal air permeability measurements.  
 (Qm = monocrySTALLINE quartz; Qp = polycrySTALLINE quartz; Ch = microcrystalline quartz; LF = lithic fragments; Fsp = feldspar; Musc = muscovite; Biot = biotite; Qa = authigenic quartz; Kaol = kaolinite; ill = illite; CM = other clay minerals; Feox = Fe-oxi/hydroxide rims; Ank = euhedral ankerite/dolomite; Sid = siderite; Cc = detrital carbonate fragments and oncoïd cement phases; Carb = clouded carbonates; Op = opaque phases; Por = porosity, point counted).

Well	Depth	Strat.	Sample n°	Point Counting (%)													Helium		Horizontal Air					
				Qm	Qp	Ch	LF	Fsp	Musc	Biot	Qa	Kaol	ill	CM	Feox	Carb	Sid	Ank	Cc	Op	Por	Other	Por. (%)	Perm. (mD)
KB64	764	Bree	64-rotem-A	24.7	14.4	0.0	14.8	12.7	2.9	2.5	3.6	3.9	1.5	4.5	0.2	0.5	0.2	5.9	0.1	1.3	6.2	0.1	-	-
KB64	771	Bree	64-rotem-B	27.5	16.1	0.0	11.8	14.4	1.4	1.5	4.1	0.5	3.4	2.3	0.5	2.5	0.0	5.4	0.0	0.0	8.1	0.5	-	-
KB64	789	Bree	64-rotem-C	24.1	15.7	0.3	14.1	16.3	1.9	0.8	3.2	0.7	0.7	2.6	1.4	0.1	0.3	9.5	0.1	0.0	8.1	0.1	-	-
KB64	800	Bree	64-rotem-D	25.2	13.5	0.5	10.8	14.5	0.4	0.0	5.2	1.1	1.3	1.2	0.5	1.8	0.2	4.7	0.0	0.1	19.1	0.0	-	-
KB172	762.25	Bullen	BS.03.01	26.8	21.9	0.6	7.3	6.7	0.1	0.0	3.2	0.0	2.3	1.9	12.4	11.3	0.0	0.0	0.0	0.1	5.4	0.0	16.45	40.21
KB172	770	Gruitrode	BS.03.02	33.5	10.0	1.1	6.1	2.0	0.4	0.0	0.7	0.0	0.3	1.8	29.5	10.4	0.1	0.1	2.4	0.0	1.6	0.0	7.82	0.03
KB172	771	Gruitrode	BS.03.03	37.9	11.1	0.6	2.5	2.3	0.4	0.0	2.0	0.1	0.1	1.5	11.6	16.8	0.1	0.0	9.2	0.2	3.6	0.0	11.58	4.14
KB172	773.15	Gruitrode	BS.03.04	33.3	12.1	0.7	7.2	2.1	0.0	0.0	3.2	0.0	0.0	0.1	9.5	15.6	0.0	3.1	8.4	0.0	4.5	0.2	12.27	24.49
KB172	779.35	Gruitrode	BS.03.05	31.2	12.1	0.2	3.7	2.1	0.3	0.0	3.1	0.0	0.2	1.9	9.9	10.5	0.0	13.0	0.2	1.5	10.1	0.0	16.08	90.25
KB172	791.25	Gruitrode	BS.03.06	37.2	13.6	0.3	5.0	2.3	0.1	0.0	6.1	0.1	0.1	1.1	8.9	11.5	0.1	3.3	0.1	0.1	10.0	0.1	13.21	105.21
KB172	795.4	Gruitrode	BS.03.07w	29.3	14.3	0.1	4.6	2.8	0.1	0.0	8.7	0.0	3.4	3.7	1.0	21.4	0.5	0.0	0.1	0.0	9.9	0.1	15.82	53.92
KB172	795.4	Gruitrode	BS.03.07r	33.5	10.7	0.1	5.2	3.4	0.2	0.1	7.8	0.0	0.7	2.1	9.5	17.6	0.0	0.0	0.0	0.0	9.1	0.0	15.82	53.92
KB172	799.6	Gruitrode	BS.03.08	41.9	11.5	0.3	6.9	2.4	0.2	0.1	11.1	0.0	2.5	1.5	0.3	12.2	0.3	0.0	0.9	0.1	7.7	0.1	14.12	46.49
KB172	809.3	Gruitrode	BS.03.09w	35.7	16.9	0.3	5.8	2.1	0.0	0.1	7.3	0.3	5.5	3.3	0.1	13.7	0.4	0.4	0.1	0.0	7.9	0.1	14.00	11.56
KB172	809.3	Gruitrode	BS.03.09r	28.1	19.2	0.0	2.5	1.7	0.1	0.0	3.3	0.9	0.3	3.2	2.5	31.0	1.7	0.0	4.3	0.0	1.0	0.2	14.00	11.56
KB169	1051.4	Gruitrode	BS.03.10	34.9	6.6	0.3	5.5	0.5	1.3	0.3	6.2	0.2	2.8	4.3	19.5	10.2	0.0	0.0	0.5	0.1	6.8	0.0	8.82	0.02
KB201	833.75	Bree	BS.03.11	36.4	16.9	0.0	8.1	5.7	0.4	0.0	6.0	0.2	9.6	0.7	0.1	5.9	0.0	0.0	0.2	0.1	9.6	0.1	20.15	296.41
KB201	882	Bree	BS.03.12w	33.1	20.8	0.0	8.3	8.3	0.0	0.1	3.9	0.3	8.6	0.5	0.0	3.0	0.0	0.0	2.0	0.0	9.5	1.6	19.12	42.50
KB201	882	Bree	BS.03.12r	34.7	19.2	0.0	8.7	7.5	0.4	0.0	3.8	0.0	4.9	1.0	2.9	1.9	0.3	0.9	1.6	0.0	12.1	0.1	19.12	42.50
KB201	869.55	Bree	BS.03.13	32.5	8.7	0.1	8.8	4.6	1.0	0.6	1.1	0.0	1.8	1.8	17.7	0.1	0.1	5.3	0.1	0.0	15.6	0.1	16.51	1.32
KB201	882.25	Bree	BS.03.14	24.6	17.1	0.0	14.1	8.3	0.6	0.2	4.7	0.7	3.3	2.1	7.9	9.1	0.1	0.0	0.1	0.0	7.1	0.0	18.17	11.78
KB201	918.75	Bree	BS.03.15	27.4	17.9	0.0	11.4	4.8	0.3	0.1	4.9	0.5	0.9	1.0	6.2	10.1	0.2	0.0	9.7	0.0	4.5	0.1	10.91	2.10
KB201	969.8	Bullen	BS.03.17	26.0	19.2	0.1	7.5	2.4	0.2	0.0	5.0	0.7	3.4	0.4	0.3	25.6	0.1	0.1	0.1	0.0	8.9	0.0	16.60	68.34
KB201	1016.25	Bullen	BS.03.18	32.0	21.3	0.3	7.9	3.1	0.1	0.0	0.9	0.3	3.7	1.4	0.3	18.3	0.0	0.0	3.9	0.0	6.5	0.0	12.84	26.25
KB201	1072.2	Bullen	BS.03.19	30.2	17.4	0.0	10.8	5.1	1.0	0.2	3.9	0.9	5.1	2.0	0.3	15.5	0.1	0.1	0.0	0.0	7.4	0.0	16.56	12.46
KB201	1099	Bullen	BS.03.20	24.9	18.8	0.0	10.3	4.7	0.3	0.0	8.5	0.5	1.0	1.1	4.8	17.0	0.0	0.0	0.8	0.0	7.2	0.1	16.93	96.24
KB201	1159.4	Bullen	BS.03.21	25.7	27.6	0.0	10.3	13.8	0.0	0.1	6.3	0.3	3.5	0.4	0.3	4.6	0.0	0.0	0.0	0.1	6.9	0.1	13.60	11.23
KB201	1181.7	Bullen	BS.03.22	32.3	23.9	0.3	10.4	7.4	0.2	0.2	2.7	0.0	10.3	0.0	0.1	4.5	0.1	0.1	0.0	0.0	7.5	0.0	13.50	23.47
KB201	1191.7	Bullen	BS.03.23	15.1	15.4	7.8	8.0	0.4	0.0	0.0	3.1	0.0	2.2	0.7	2.1	37.8	0.6	0.1	0.0	0.0	6.6	0.1	11.30	5.62
KB201	1220.7	Gruitrode	BS.03.24	41.5	16.2	0.0	7.2	2.4	0.1	0.0	5.4	0.0	1.8	0.4	0.4	20.8	0.3	0.0	0.1	0.1	3.3	0.0	5.29	0.05
KB201	1246.55	Gruitrode	BS.03.25	33.7	14.3	0.1	5.8	0.6	0.0	0.1	12.5	0.2	0.1	0.6	16.8	9.8	0.1	0.1	1.7	0.1	3.1	0.3	6.81	0.04
KB201	1254.9	Gruitrode	BS.03.26	31.4	12.1	0.1	11.1	0.7	0.0	0.0	2.6	0.0	0.2	0.7	8.7	9.1	0.0	19.5	1.8	0.0	1.9	0.1	5.37	0.02

**Table 3.** Average compositions (av.) and standard deviations ( $\sigma$ ) of the studied Triassic sandstones from point counting, He-porosimetry (He por) and horizontal air permeability analyses (Hor. Air Perm.).

	av.	$\sigma$
Quartz (monocryst.)	30.8	5.6
Quartz (polycryst.)	15.8	4.6
Quartz (microcryst.)	0.4	1.4
Lithic Fragments	8.2	3.2
Feldspar	5.3	4.6
Mica	0.7	1.1
Quartz (authigenic)	4.8	2.8
Kaolinite	0.4	0.7
Illite	2.7	2.7
Other Clay Minerals	1.6	1.2
Fe-oxi/hydroxides	5.8	7.3
Ankerite	2.2	4.5
Siderite	0.2	0.3
Other Carbonates	13.4	11.7
Coal Fragments	0.0	0.0
Opaque Minerals	0.1	0.3
Porosity	7.4	3.8
He Por (%)	13.67	4.06
Hor Air Perm (mD)	38.65	59.31

quantities of feldspars (max. 16.3%). CL revealed that they mainly consist of blue luminescent K-feldspar, with variable intensity and colour (Fig. 6A). Some grains are more greenish blue, which is typical for K-feldspars with higher Na content. Some feldspars have yellowish-green spots or zones, which suggests the presence of albite. The twinning patterns of the grains indicate the presence of orthoclase and microcline. The degree of alteration is variable but overall the alteration is limited.

Micas constitute a small percentage (average 0.7%). Both muscovite and biotite were identified.

Almost all Buntsandstein samples contain rounded, detrital micritic fragments (average 1.5%). Generally, they are recrystallised, replaced or cemented by later authigenic carbonates. All possess a faint red staining colour. The fragments are usually red brown in single polarised light, due to the presence of Fe-oxides/hydroxides in their matrices (Fig. 7A), and have dark luminescence colours, typical of formation in an oxidising environment.

Other phases that make up the detrital mineralogy are phosphate grains and detrital clays. Both are present in most samples, but only in very small quantities (<1%).

### 6.2.2. Red versus white sandstones: clay rims

White sandstones are coarser grained than red ones (Fig. 7E). However, their detrital composition is similar, though red horizons generally contain slightly more micas. The colour difference is often, but not always, strata-bound. In some samples coarser grained white and finer grained red layers alternate on mm-scale. Some red samples contain white spots, often with irregular shapes, and not always visually interconnected.

The framework grains in most samples are rimmed by a thin band of tangentially oriented clay particles. In the red sandstones, these clay rims are stained by Fe-oxi/hydroxides (Fe-O/H), resulting in the typical brownish-red colours (Fig. 6B). The clay rims are thicker in red samples (generally about 5 to 10  $\mu\text{m}$ , locally up to 50  $\mu\text{m}$ ) than in white samples (<1  $\mu\text{m}$  to a couple of  $\mu\text{m}$ ). In both, red and white sandstones, they are usually covered by authigenic clay coats (Fig. 6B, 6D). The staining by Fe-O/H in the red samples makes the rims easy to distinguish from the latter, whereas in the white sandstones,

optical distinction can only be made based on the preferential radial orientation of the clays on the grain surfaces. The thin clay rims in the white sandstones have striking bright yellow to white birefringence colours, typical of smectitic or illitic clays. In red sandstones the rims were quantified as Fe-O/H-rich rims (Table 2, average 5.8%), as they contain the bulk of the Fe-O/H in these samples. In the white samples, they were quantified as illite, because they are hard to distinguish from other illite phases.

Clay rims generally completely envelope the framework grains, a feature that is most obvious in the red sandstones, where rims are thicker. They are also present at grain contacts, where they are squeezed between grains and consequently they are thinner. In white samples, enclosure appears to be less complete. Around the less well-rounded grains, the clay rims exhibit wide variations in thickness. They are consistently thicker in depressions on the grain surfaces and commonly thinner close to grain contacts. The rims in the coarse sandstones, which are generally composed of well-rounded grains, are much thinner than those in fine-grained horizons, consisting of more angular grains.

Geopetal and meniscus fabrics were rarely observed. The rims do not span multiple grains, do not exhibit internal layering, and are not associated with root or burrow structures. They also do not coat any of the authigenic phases. They are commonly covered by diagenetic clays, and were observed between authigenic and detrital quartz (Fig. 6C) as well as K-feldspar (Fig. 6D), between carbonate clasts and carbonate cements, as outlines of replaced fragments in carbonate cemented zones and as clay shells (Fig. 9D) in secondary pores. The clay rims around heavily altered/dissolved feldspar grains do not invade the intragranular pores.

SEM-EDS petrography of broken rock chips showed grains covered by K, Fe and Mg-rich Al-silicates, which are often overgrown and intergrown with diagenetic clay coats, which were recognised by their delicate crystal habits (Figs 6B, 8B, 8C, 8D). The clay particles within the rims have irregular shapes and are oriented parallel to the grain surfaces (Fig. 8A, 8B), while those of the authigenic clays are generally perpendicular to the surfaces (Fig. 6B, 6C, 6E, 8C). Typically, grains are covered by rims consisting of mats of randomly oriented, overlapping flat fibres of illite, which appear to wrap the grains (Fig. 8D). This morphology suggests significant recrystallisation of the irregular clay particles. On some grains, small quartz outgrowths have broken through the clay rims, where on others the rims are largely covered by quartz overgrowths (Figs 9A, 6E).

EDS-analysis of the rims always revealed the presence of Fe, but in relatively low concentrations in comparison to K, Al and Si, even in the darkest brown-red samples. At high magnifications, small Fe-oxide/hydroxide needles, usually about 100 nm in thickness and a couple of  $\mu\text{m}$  long, could be observed between the clay platelets of the rims (Fig. 9B, 9C). Also, clusters occur of tabular, often pseudo-hexagonal, imperfect crystals of about 100 nm in thickness and < 5 by 5  $\mu\text{m}$  in the other dimensions (Fig. 9C).

The samples cover a wide range of transition colours between dark brown-red and white, with the darker coloured samples containing more Fe-O/H as confirmed by SEM petrography. Yet, even in the lightest coloured samples remnants of Fe-O/H are present, which are always found in clay rims that are separated from the ambient porosity by diagenetic cements. The red colour of the oxides is commonly present between authigenic quartz overgrowths (generally completely enveloping the grains) and detrital host grains (Fig. 6C), and around framework grains enclosed in carbonate cements. Grains enclosed in the latest generation of authigenic carbonate,

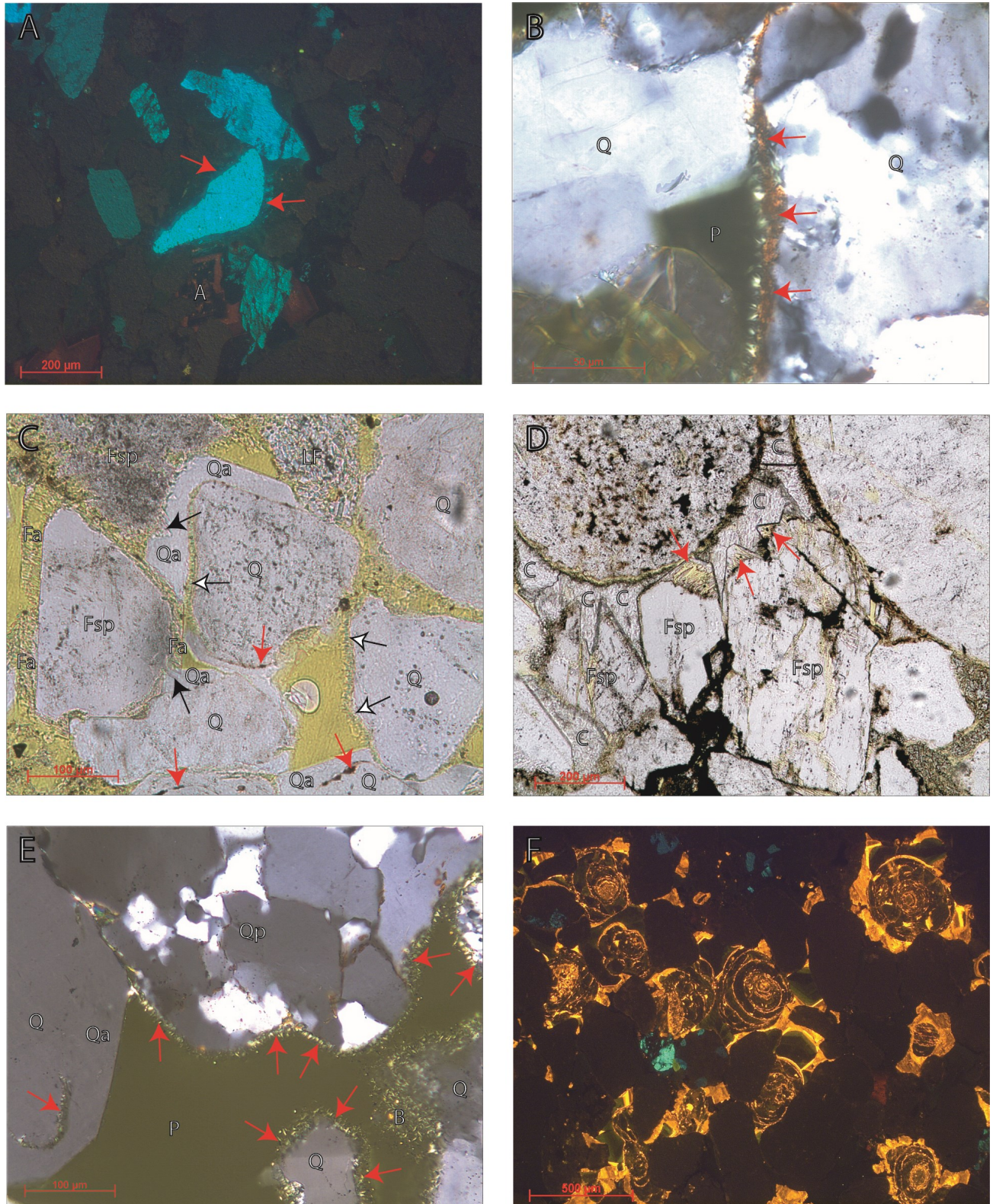


**Figure 6.** Photomicrographs of Buntsandstein samples. A. (Cathodoluminescence) Variations of luminescence colours of K-feldspar grains. K-feldspar overgrowths (arrows) are faint blue to non-luminescent (KB201 – 882.25m). B. Detail of a framework grain covered by a clay rim (arrows), which is stained red by Fe-oxides/hydroxides. The rim is covered by a diagenetic clay coat consisting of illite flakes and needles, which have bright yellow birefringence colours and are perpendicular to the grain surface (KB201 – 831 m). C. Clay rims (red arrows) and clay coats (open arrows), locally enclosed between detrital quartz grains (Q) and authigenic overgrowths (Qa). The left-hand side of the picture shows two K-feldspar grains (Fsp) covered by K-feldspar overgrowths (Fa), which are partly enclosed in authigenic quartz (black arrows) (KB201 – 833.75 m). D. Feldspar grains (Fsp) with large overgrowths (arrows), cemented by clouded dolomite (C). Clay rims are present between detrital and authigenic feldspar. The overgrowths are partly dissolved (porosity is filled with yellow-stained epoxy) (KB172 – 762.15 m). E. Illite coatings (arrows) covering framework grains (Q & Qp). Coating on the left is enclosed between quartz grain and overgrowth (Qa). In open pores (P) illite constitutes a boxwork texture (B) (KB201 – 1181.7 m). F. (Cathodoluminescence) Large spherulites with decentred core (centre). The dark zone is transected by thin rims filled with brighter cement. The latter resembles the orange cement between the oncoids (KB201 – 1016.25 m).

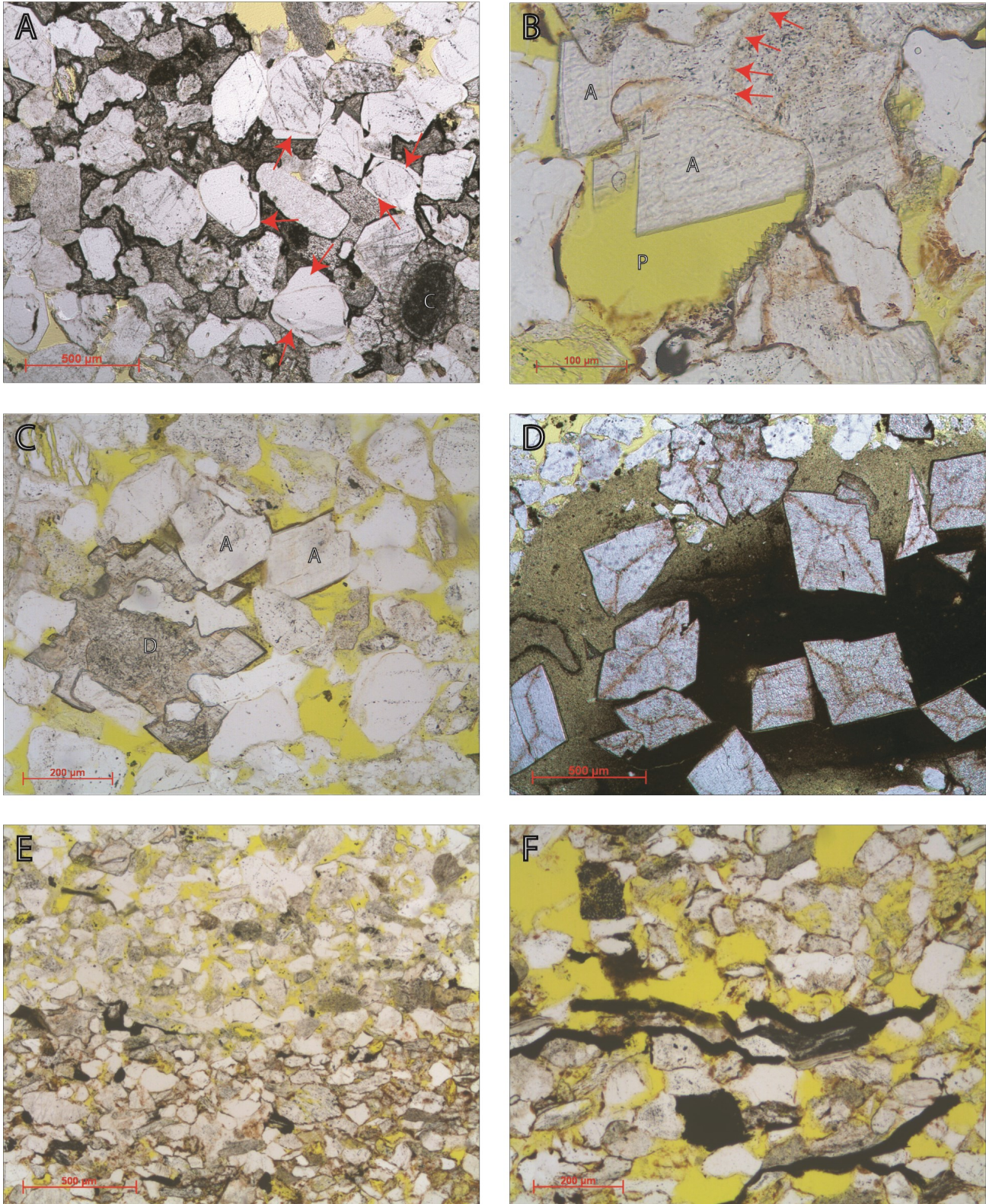


**Figure 7.** Photomicrographs of Buntsandstein sandstones. A. Concretion consisting of framework grains cemented by dolomite, which is heavily clouded by solid inclusions. Quartz grains in the concretion often have large overgrowths (arrows). The dolomite replaces enclosed framework grains, which is evident from their irregular outlines (KB201 – 833.75 m). B. Euhedral carbonate crystal (A) partly filling an open secondary pore (P). The clear carbonate is an extension of a more clouded carbonate, which replaced detrital grain. The outlines of the detrital grain are preserved as rims of hematite (arrows) (KB201 – 882.25 m). C. Clouded dolomite (D) and clear ankerite (A). Both phases are rimmed by a thin layer of siderite (KB201 – 1072.2 m). D. Ankerite crystals in a clast consisting mostly of illite. The crystals display an hourglass texture formed by hematite inclusions (KB172 – 799.6 m). E. Abrupt contact between a red and white zone. The red zone consists of smaller grains which are often elongated. Grain contacts in the red zone are significantly longer than in the white zone. The red zone in this sample constitutes a dissolution seam (KB201 – 869.55 m). F. Detail of a dissolution seam. Micas are aligned and bordered by partly dissolved framework grains. This part of the seams has a remarkably high secondary porosity (KB201 – 869.55 m).

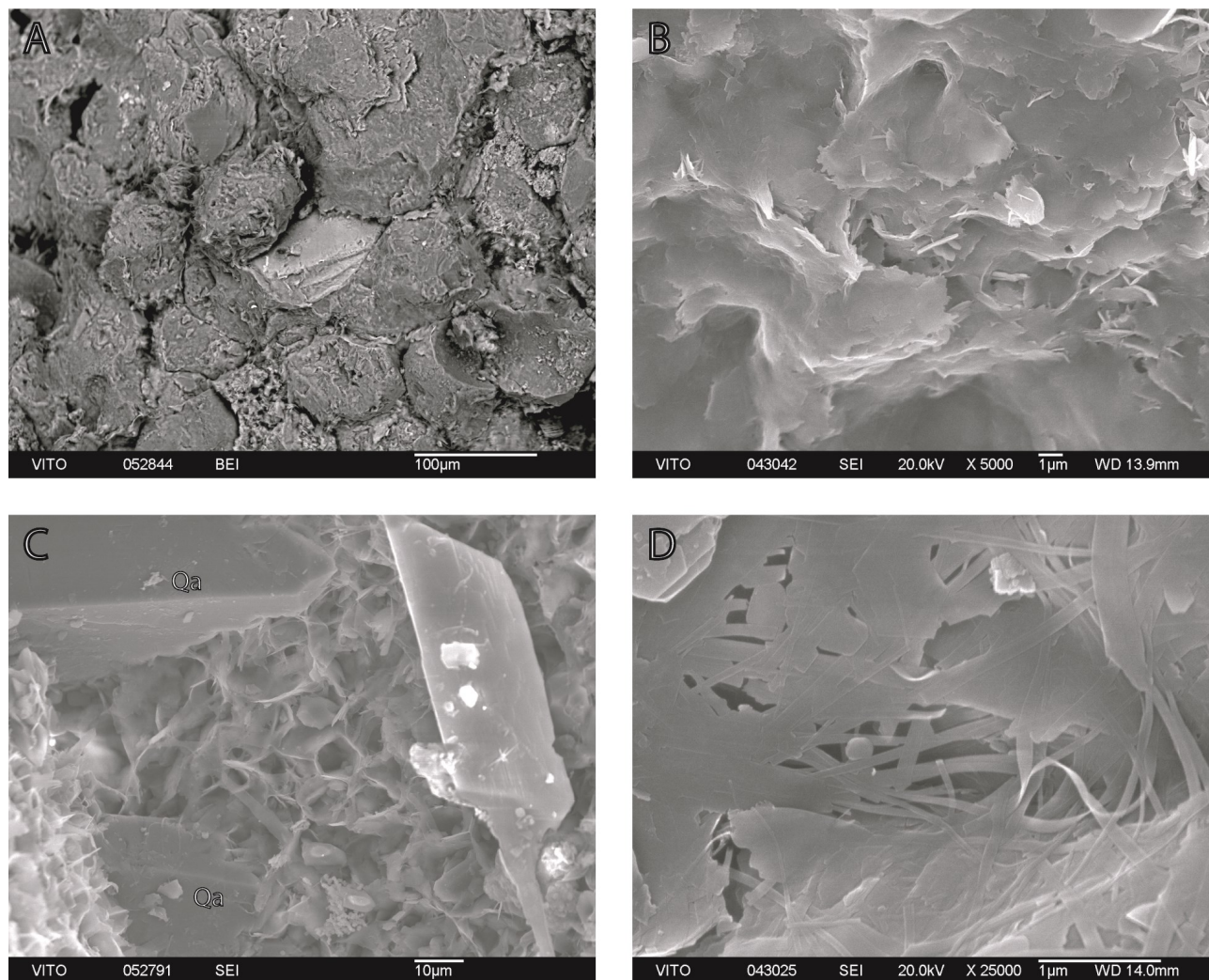


**Figure 8.** SEM images of Buntsandstein sandstones. A. Framework grains wrapped in thick clay rims. The lighter grain in the centre of the picture is a K-feldspar (KB201 – 869.55 m). B. Detail of the surface of a grain covered by a clay rim. The clay consists of irregular platelets which are more or less parallel to the grain surface (KB172 – 779.35 m). C. Detail of the surface of a grain covered by an illite coat. The illite crystals are oriented perpendicular to the grain surface and often constitute a honeycomb texture. The coating is partly covered by quartz overgrowths (Qa) (KB201 – 1181.7 m). D. Clay rim consisting of mats of randomly oriented, overlapping flat fibres of illite (KB172 – 869.55 m).

consisting of transparent, often saddle-shaped ankerite/dolomite, in the white samples are never stained by Fe-O/H.

### 6.2.3. Authigenic constituents and diagenetic alterations

#### 6.2.3.1. Authigenic K-feldspar

Almost all K-feldspar grains in the studied Buntsandstein samples are covered by authigenic K-feldspar overgrowths (AKF) (Fig. 6D). The size of the overgrowths is highly variable. The largest overgrowths (>100 µm) occur adjacent to primary pores. Detrital grains are in general almost completely enclosed by overgrowths, except at grain contacts (usually point contacts).

In red sandstones, red-stained clay rims are present between the detrital feldspar grains and diagenetic overgrowths (Fig. 6D). These rims are usually also present in the white samples but could not always easily be discerned. All AKF are altered. Typically, the overgrowths are better preserved than the detrital grains, but the opposite also occurs. Some grains, mostly those displaying the typical tartan-twinning pattern of microcline,

appear to be covered by several generations of K-feldspar overgrowths. The oldest, inner generations generally better resisted alteration. AKF are generally not covered by authigenic clay coats. Yet, these clay coats, in contrast to the rims, were also not routinely observed between authigenic and detrital feldspar. On BSEM (backscatter scanning electron microscopy) images overgrowths were, albeit rarely seen, enclosing small parts of diagenetic clay coats (Fig. 10A). Most feldspar grains enclosed in thick clay rims appear to have no authigenic overgrowths. In some samples, small authigenic feldspar crystals were observed between the clays constituting rims.

The AKF are often enclosed in early carbonate cements (Fig. 6D). The latter cements, however, do not enter the dissolution pores of altered overgrowths. Later carbonate generations tend to replace both authigenic and detrital feldspar, and are often found in alteration voids of both. The genetic relation between AKF and authigenic quartz (AQ) overgrowths is not entirely clear from petrography. Both phases were not seen replacing one another. Generally, quartz overgrowths end where it makes contact with feldspar overgrowths. Though, in some cases, AKF are partly enclosed in AQ (Fig. 6C).

K-feldspars overgrowths display a faint bluish luminescence

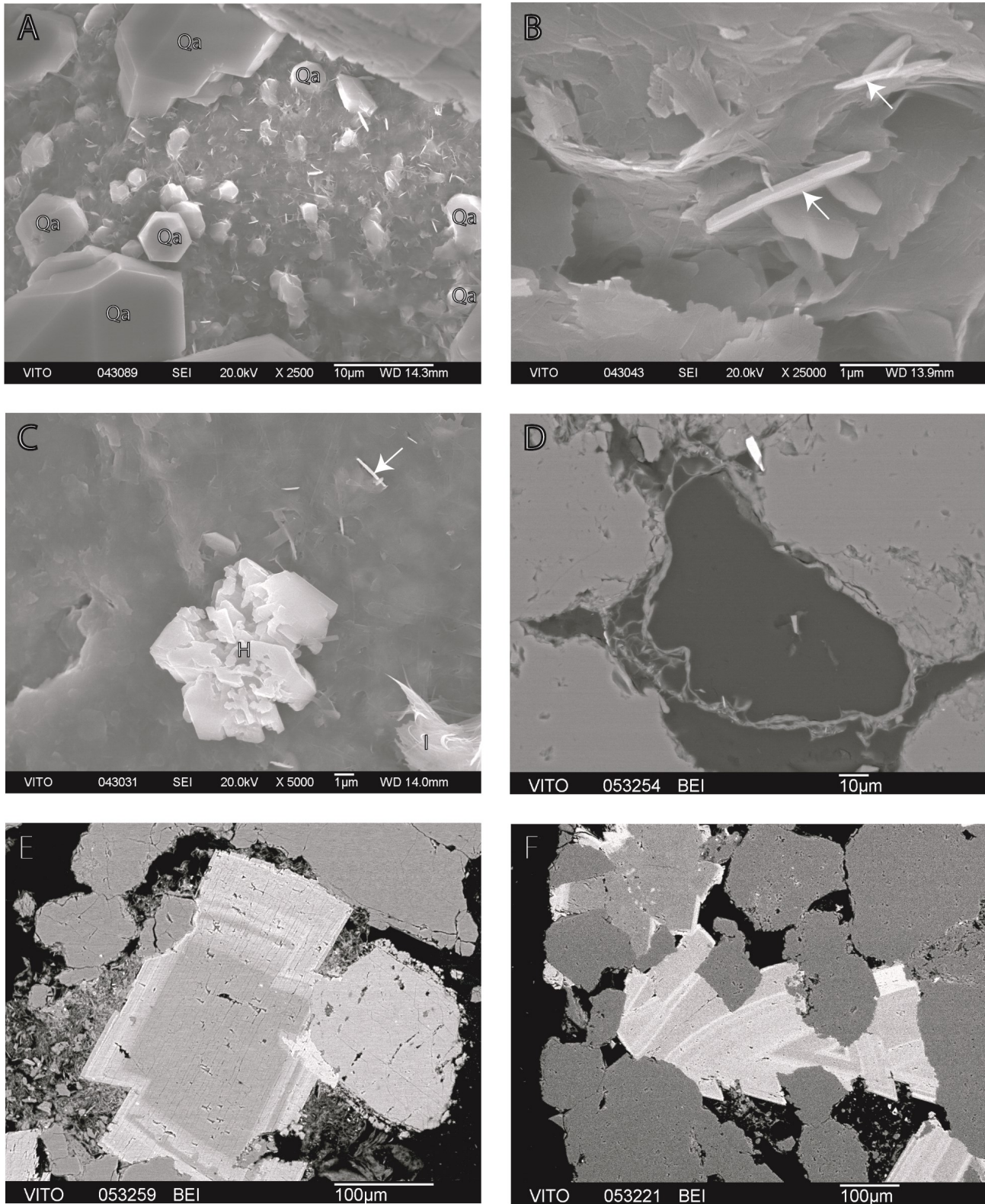


**Figure 9.** SEM and BSEM images of Buntsandstein sandstones. A. Small outgrowths of authigenic quartz (Qa) popping through a clay rim. Larger quartz overgrowths partly cover the clay rim (KB172 – 779.35 m). B. Hematite needles (arrows) on the surface of a clay rim (KB172 – 779.35 m). C. Detail of irregularly shaped, tabular hematite crystals (H) on the surface of a clay rim. Hematite is also present as needles (arrow). The rim is partly covered by authigenic illite (I) (KB172 – 779.35 m). D. Cross section of clay rim surrounding an open secondary pore. Hematite is present between the clay platelets of the rim as very small lighter coloured needles (KB172 – 779.35 m). E. Warped shape of ankerite crystal. The outer zones are richer in Fe (lighter coloured). The brighter grain on the right-hand side is a K-feldspar (KB172 – 779.35 m). F. Banded surfaces of ankerite crystal. Comparison with image E illustrates that the zoning of the ankerite does not display a constant pattern (KB172 – 779.35 m).

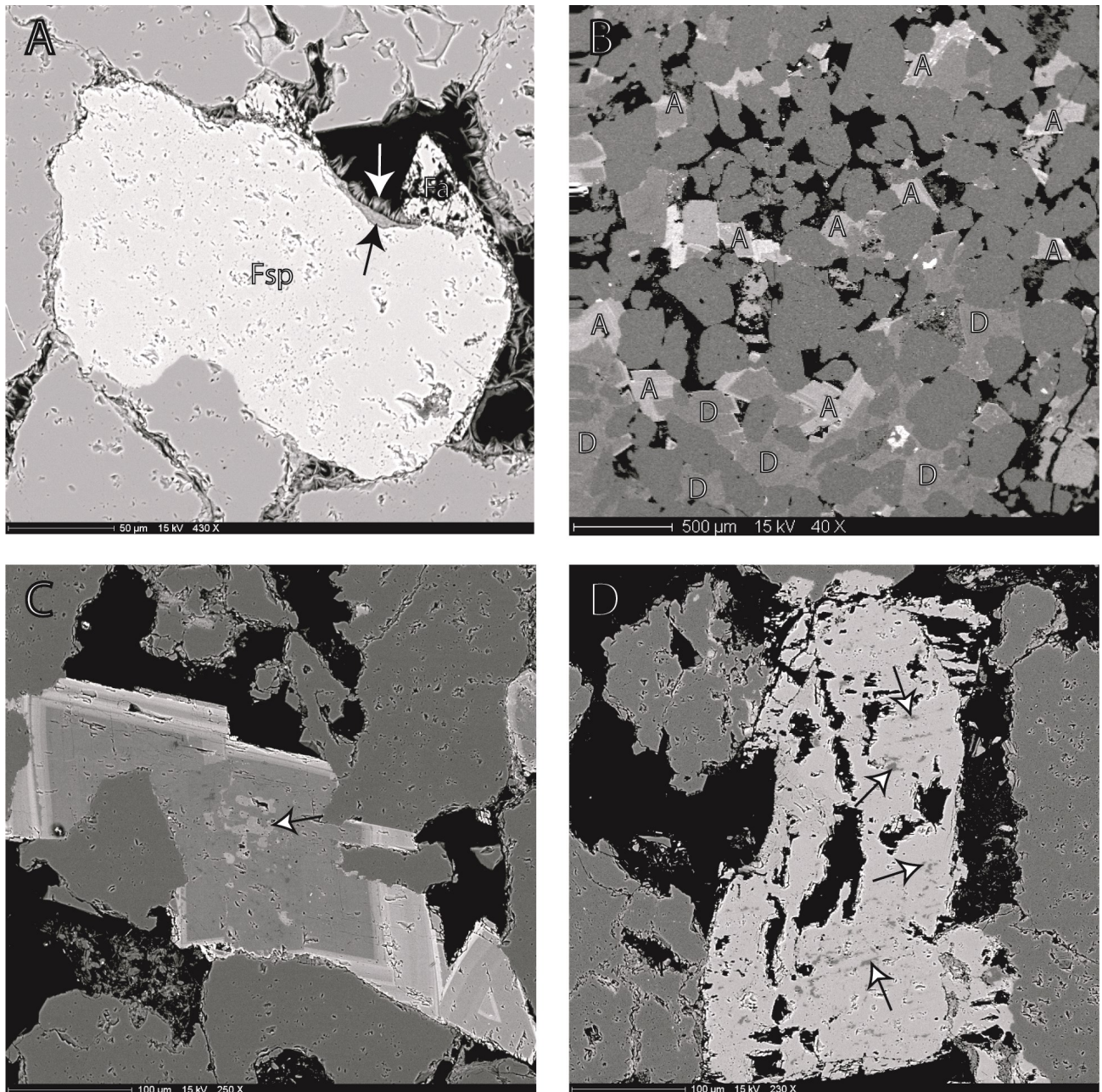


**Figure 10.** BSEM images of Buntsandstein sandstones. A. K-feldspar grain covered by clay rim (black arrow), clay coat (white arrow) and authigenic K-feldspar overgrowths (Fa). The large overgrowth in the upper right corner of the picture covers both the clay rim and coating (KB201 – 1181.7 m). B. Euhedral ankerite (A) as overgrowths on a dolomite (D) concretion and as individual crystals. The cores of the crystals also consist of dolomite (KB172 – 779.35 m). C. Zoning of an ankerite crystal. The outer growth zones are richer in Fe than the dolomitic core. The core of the crystal contains bright patches of calcite (arrow) (KB172 – 779.35 m). D. Altered K-feldspar grain containing darker speckles of albite (arrows) (KB201 – 882.25 m).

taken with long exposure times (Fig. 6A). They are dark in comparison to the bright greenish-blue luminescent detrital K-feldspar grains. Most detrital feldspars contain zones having the same dark bluish luminescence as the overgrowths. Albitisation, which can be clearly distinguished on BSEM images as dark spots, appears not to have affected the K-feldspar overgrowths.

#### 6.2.3.2. Clay coats

In many Buntsandstein samples, the clay rims wrapping framework grains are covered by diagenetic clay coats that consist of fibrous to needle-shaped crystals of about 10  $\mu\text{m}$  in length, which have bright yellow to white birefringence colours. They are oriented perpendicular to the grain surface (Fig. 6B).

Their delicate crystal habits, as observed with SEM, suggest an authigenic nature (Fig. 8C). In some samples, coated grains display honeycomb textures (Figs 6E, 8C). Such textures, and the birefringence colours of the crystals, are typical of illite derived from smectite (Ehrenberg & Nadeau, 1989). Near open primary pores, the illite needles often make up box-work textures.

The contact between clay rims and clay coats displays intense intergrown fabrics. Clay coats are more common in white than in red samples. Some red sandstones contain no coats at all (yet all of them consist of rimmed grains), while in all white samples some coated grains were observed.

The perpendicular clay coats are exclusively found on framework grains rimmed by parallel clay platelets and are

never present on other phases. They are also absent at grain contacts. They frequently occur between authigenic and detrital quartz, but rarely between K-feldspar grains and their overgrowths. Grains that are completely coated tend not to have overgrowths. Where grains are less completely coated or the clay coats are thinner, overgrowths cover parts of the framework grains. Cross-sections of coated grains revealed that overgrowths 'nucleated' on a small, uncovered grain surface and then extended laterally to cover the clay coats.

The genetic relationship between authigenic carbonate cements and clay coats is not always clear from petrography. Where coated framework grains make contact with carbonate crystals or cements, the clay coats are generally absent. In a few samples, parts of the coats seem to be enclosed in early carbonate cements. In some primary pores, displacive growth of euhedral dolomite/ankerite crystals with respect to box-work illite has taken place. SEM petrography showed that the surfaces of some of these euhedral carbonate crystals are partly covered by illite, whereby its orientation is different from that of the coats, i.e. it generally consists of randomly oriented fibres parallel to the carbonate surfaces.

#### 6.2.4. Carbonate spherulites

Some samples contain rounded, generally micritic carbonate grains that are surrounded by a rim of large radial calcite crystals (Fig. 6F), which show a cross-extinction pattern in double polarised light, which is typical of spherulitic structures. Their size ranges between 100 and 500  $\mu\text{m}$ . The cores, of which the diameter is often less than one-fifth of the total diameter, are not always in the centre of the spherulites. In the samples containing spherulites, few detrital carbonate grains without radial crystals were observed. In one sample the spherulites make up 9.7% (Table 2). Under plane polarised light the radial crystals sometimes appear to be composed of thin (1–10  $\mu\text{m}$ ) concentric laminae, which are discontinuous and tend to taper out. In red samples, the laminae are generally bordered by thin rims of Fe-O/H. In white samples, these rims are missing.

The size of the crystals constituting the rims, and the fact that they crosscut overlapping laminae is indicative of recrystallisation. CL-images of the spherulites generally show dull luminescent cores, surrounded by a thick zone (often 10x diameter of the core) of non-luminescent to faint yellowish-brown phase and an outer, thinner rim of mainly bright luminescent, zoned cement (Fig. 6F).

#### 6.2.5. Subhedral clouded dolomite

Some of the studied sandstones contain concretions of poorly crystallised, subhedral carbonate (Fig. 11B), which is generally heavily clouded by solid inclusions (Fig. 7A; Table 2, average 13.4%). In some samples clouded subhedral crystals are also present outside of the concretions, where they are commonly overgrown by later carbonate cements. These clouded carbonates were quantified as 'carb' in point counting.

The size of the concretions is highly variable (100  $\mu\text{m}$  to 1 cm). They commonly have a nodular shape, sometimes elongated parallel to the bedding. Most concretions contain recrystallised spherulites and remnants of detrital carbonate fragments, which in most cases are replaced by the clouded carbonate. The latter fragments can be recognised by hematite rims, which reveal their former outlines. Enclosed framework grains are always coated by hematite-stained clay rims, even in white sandstones (Fig. 7A). The clouded carbonate tends to replace enclosed quartz grains. Here again, hematite rims reveal the original outlines of the grains. The intergranular volume in the concretions is larger than in the rest of the sandstones and grain contacts in the concretions are generally less evolved, suggesting that they formed before the main compaction. In

numerous concretions, rather large quantities of AQ are present as well-developed circumgranular overgrowths.

Luminescence patterns of the concretions resemble those of the recrystallised spherulites. Detrital carbonate grains acted as nucleation sites for the nodules, as evidenced by the growth zones in the cement around them. The surrounding cement often consists of thin, bright, and non-luminescent zones, alternating on  $\mu\text{m}$ -scale, which are surrounded by a thick non-luminescent zone, a thin bright zone and a dull-luminescent cement making up the bulk of the concretions. The latter are often rimmed by large euhedral to subhedral carbonate crystals with dark, non-luminescent cores and faintly red luminescent outer growth zones. The crystal cores contain speckles of dull cement in the concretions. The outer growth zones are generally transparent under plane polarised light, i.e. they contain little or no solid inclusions. EDS analyses of the nodules revealed that they consist of Fe-poor dolomite. BSEM petrography showed the dolomite is rather homogeneous (Fig. 10B), with locally light patches of calcite, which are probably remnants of replaced carbonate grains. In some white sandstones, the nodules are corroded or partly dissolved, and surrounded by a rim of Fe-O/H.

#### 6.2.6. Euhedral Ca-Mg-Fe carbonates

Most samples of the Buntsandstein contain a late-diagenetic, transparent (no solid inclusions), zoned, Fe-rich, euhedral, saddle-shaped carbonate phase (Fig. 9E, 9F) which was quantified as 'dolomite/ankerite' (Table 2, average 2.2%). Point count results are an underestimation of the true volume because in many cases this carbonate can only be distinguished by BSEM and CL (Fig. 10B). It occurs as blue-stained overgrowths on the clouded dolomite in concretions and replaces other carbonate phases (Fig. 7B).

Where present as euhedral crystals in the matrix, it was recognised by the warped crystal shapes, presence of growth zones and absence of solid inclusions, which contrasts with the clouded dolomite. The crystal cores often do contain solid inclusions, suggesting replacement of clouded dolomite. These cores, which consist of Fe-poor dolomite (EDS), are non-luminescent, with dull and sometimes bright speckles. BSEM petrography, EDS analyses and EPMA element maps (Fig. 12) revealed the presence of calcite inclusions which are probably remnants of detrital carbonate grains. Fe-oxide inclusions often reveal the outline of replaced grains.

The outer growth zones are faintly red to orange on CL-images taken with extended exposure time, while the outermost growth zone is non-luminescent (Fig. 6A). The latter zone consists of a thin (<10  $\mu\text{m}$ ) siderite rim (Fig. 7C), which locally also occurs as thin growth zones. BSEM-EDS revealed alternating zones of ankerite (often Mg-rich) and dolomite (often Fe-rich) around a dolomite core of varying size with respect to the rest of the crystals (Figs 9E, 10C, 12). Fe-content increases non-systematically toward the edges of the crystals.

These carbonates post-date the other carbonate phases, as it commonly replaces them. In some samples, replacement of AQ occurs, yet in most samples the genetic relationship with AQ is not entirely clear from petrography. Carbonate crystals are regularly present in secondary pores (Fig. 7B). Sometimes they contain remnants of K-feldspar grains (and overgrowths). Feldspar relicts also are observed in open pores, indicating the carbonates postdate feldspar alteration. In secondary pores of which the well-rounded shape reveals the dissolution of detrital carbonate grains, perfectly shaped euhedral Fe-rich crystals were observed. The fact that these contain no inclusions of calcite, as observed in their counterparts in samples with limited secondary porosity resulting from carbonate dissolution, suggests they are formed after carbonate dissolution.

SEM petrography on rock chips showed a lot of these



**Figure 11.** Core photographs. A. Contact between finely parallel laminated red fine-grained sandstone and coarser grained bleached sandstone. B. Red fine-grained sandstone intercalated in bleached coarser grained white sandstone with small dolomite concretions. C. White sandstone with well-developed stylolites.

carbonate crystals are wrapped in thin sheets composed of strips and fibres of illite. The euhedral crystals were also regularly observed in large clay clasts consisting of illite (Fig. 7D). The carbonates locally make up more than half the volume of the clasts. The orientation and packing of the illite needles surrounding the carbonate crystals suggest displacive crystal growth. Many crystals in the clasts contain illite needles, which regularly display an interior hourglass texture, which is delineated by small reddish-brown solid, opaque, inclusions suggesting they partially consist of hematite. In most clay clasts the euhedral carbonates display similar luminescence as in the matrix, but some clasts have irregular-shaped patches of brighter orange cement in a matrix of dull brownish luminescent carbonate. The texture suggests intensive replacement by the

younger dull, Fe-rich (EDS) generation, which is also recognised in the outer growth zones of other euhedral carbonates outside of the clay clasts.

In a couple of samples, the outer, dull, Fe-rich growth zones partly replace the cores of the crystals, along cracks that fan out from contacts with adjacent, or partly enclosed, framework grains. These cracks transect the inner, brighter luminescent growth zones, suggesting that the euhedral carbonate was formed during an important phase of mechanical compaction.

#### 6.2.7. Authigenic quartz

Authigenic quartz (AQ) is one of the most voluminous diagenetic phases in the Buntsandstein (Table 3, average 4.8%, max. 12.5%). The bulk of the AQ constitutes of syntaxial

overgrowths on detrital quartz grains (Figs 6C, 6E, 7A). In most samples, the AQ are clearly discernible from the detrital grains, as dust rims which mostly consist of small reddish-brown hematite inclusions separate both phases. They are omnipresent in the red samples, but also quite common in white sandstones. Furthermore small idiomorphic quartz crystals were observed in primary and secondary pores in most samples, but in smaller quantities than the overgrowths.

White sandstones tend to contain more AQ than the red samples, respectively on average 5.4% ( $n = 17$ ) and 4.2% ( $n = 15$ ), however, the difference is only 1.2%. The highest quantities of AQ are found in the coarser samples and in samples where the clay-hematite rims and clay coats are less well developed, which are more typical of white than red samples. Grains without coats or clay rims always have well-developed, thick (recurrently  $>50 \mu\text{m}$ ) overgrowths. AQ also develop on grains with thin or discontinuous clay-hematite rims, usually enclosed between grain and overgrowth. Perpendicular clay coats were also less commonly seen between grains and overgrowths (Fig. 6C, 6E). Where clay coats are well developed, AQ occurs in small quantities as tiny outgrowths locally covering the coats (Fig. 9A). Locally clay coats were observed on AQ.

In samples with high quantities of AQ, several grains are completely enclosed by overgrowths. In general, these samples show few signs of pressure dissolution. Point contacts are the most prominent type of grain contacts, while concavo-convex contacts are rather rare. Furthermore, in samples with well-developed clay-hematite rims, AQ is sparse, while concavo-

convex grain contacts are omnipresent and sutured contacts are frequent. The latter occur dominantly in fine-grained red samples.

Well-developed AQ are also present in carbonate concretions, where grain packing is less dense than in the surrounding matrix (Fig. 7A). The clouded, subhedral dolomite commonly replaces the overgrowths. Replacement by the euhedral zoned Fe-rich carbonates was only in a few, rather indistinct, cases observed.

Quartz overgrowths occasionally enclose K-feldspar overgrowths around adjacent feldspar grains (Fig. 6C).

#### 6.2.8. Compaction

In some samples compaction is clearly manifested by the presence of dissolution seams which occur parallel to bedding (Fig. 11C), which often delineate the contact between red and white zones (Fig. 7E). They are made up of aligned micas and partly dissolved, elongated framework grains with sutured contacts (Fig. 7F). Framework grains in dissolution seams tend to be smaller than adjacent grains and dissolution seams always contain higher quantities of opaque matter than their surroundings. A part of this consists of Fe-O/H. Dissolution seams were only seen in and at the boundaries of fine-grained red zones, never in the coarse white sandstones. Often the areas around the seams have high secondary porosities (Fig. 7F). In one sample large voids border the dissolution seams, which probably are remnants of dissolved carbonate concretions. Their presence next to dissolution seams suggests the seams predate secondary porosity generation.

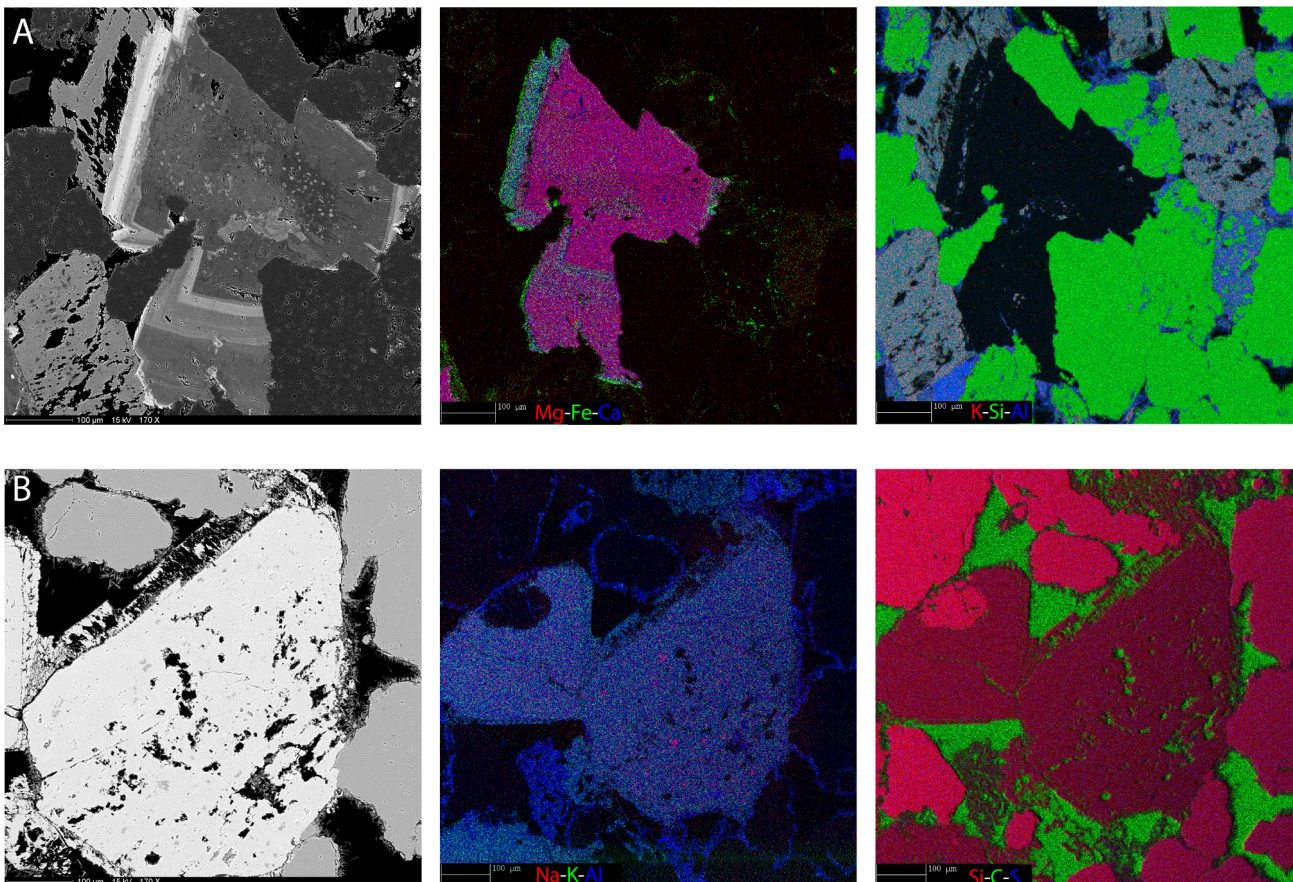


**Figure 12.** EPMA element maps of a typical dolomite/ankerite crystal (A) and feldspar grain (B) in the Buntsandstein. The Mg(red)-Fe(green)-Ca (blue) map shows the zoning pattern of the carbonate crystal. The bright spots in the centre of the crystal in the BSEM image are calcite (blue). The K (red)-Si(green)-Al(Blue) map reveals that the carbonate partly replaced a K-feldspar grain and still contains inclusions of it. The K(red)-Si(green)-Al (Blue) of the feldspar grain (B) shows small red albite inclusions, that are black on the BSEM image. The green colour on the Si(red)-C(green)-S(blue) is the epoxy used for the impregnation of the sample.

Grain contacts, indicative of compaction, are less evolved in the generally coarse, white than in fine-grained red samples (Fig. 7E). In the latter, concavo-convex contacts are ubiquitous and sutured contacts are quite common, while in the former point-contacts are omnipresent and concavo-convex contacts are exceptional.

In sandstones with high AQ content, grain contacts are less evolved. Many grains are completely enclosed by syntaxial overgrowths and seem to make no contact with adjacent grains (in thin sections). In red samples, the most evolved grain contacts are seen where the clay-hematite rims envelop the grains completely. Rim thickness with respect to grain size seems to have little effect on grain contacts. Samples with abundant (perpendicular) illite coats seem to have less evolved grain contacts, but this could not always be quantified.

Several of the observed euhedral Fe-rich carbonates have cracks that transect the cores and some zonations. The crack infill displays the same luminescence as the outer zonations of the crystals.

Secondary pores and dissolution voids generally reflect the rounded shapes of former grains and concretions. They show no signs of deformation (Figs 7B, 7F, 9D).

#### 6.2.9. Authigenic illite

Illite is the most abundant clay mineral (Table 3, average 2.7%). It occurs as clay rims and coats around framework grains and is present in, mainly primary, pores forming a boxwork texture (Fig. 6E). Thin straps and small needles of illite were often observed with SEM on altered feldspar grains and their authigenic overgrowths. This type of illite occludes only a small part of the secondary, intragranular porosity in the latter phases. Similar straps of illite were also observed on the surfaces of euhedral Fe-rich carbonate crystals.

#### 6.2.10. Authigenic kaolinite

The average kaolinite content is only 0.4% (Table 3). Most samples contain little or no kaolinite. Those which do contain kaolinite, generally also have relatively high mica contents. Here mica plates are often wedged apart by vermicular kaolinite booklets. Similar booklets were observed near altered lithic fragments.

#### 6.2.11. Feldspar alteration

The degree of feldspar alteration in the studied Buntsandstein is highly variable. Some samples contain only delicate relicts, while in others, feldspars are well preserved. Also, fresh grains are often observed next to secondary pores containing feldspar remnants. Non-altered feldspar grains are often covered by extensively dissolved overgrowths (Fig. 6D). The opposite, well-preserved overgrowths on relicts of grains, was also observed, though less frequently. Feldspar alteration generally resulted in open oversized porosity. In some samples, tiny illite needles were observed within largely dissolved feldspar grains. A few samples contain secondary pores with remnants of feldspars or carbonates, surrounded by clay-hematite rims. Occasionally such pores were seen in carbonate concretions. In general feldspar grains are heavily altered in samples containing large amounts of secondary pores.

#### 6.2.12. Albitisation

BSEM petrography revealed tiny, dark, speckles of albite in feldspar grains (Fig. 10D). Its composition was confirmed by EDX analyses and EPMA element mappings (Fig. 12). The speckles are often arranged along cleavage or twinning planes. Individual albite spots generally occur adjacent to holes or small fractures in the grains. They were not observed in AKF overgrowths. Albite was also recognised in CL-images of

K-feldspar grains, by its greenish colour. Many K-feldspar grains display zones of slightly different luminescence colours, always with greenish-blue shades (Fig. 6A).

#### 6.2.13. Siderite

Siderite was observed only in small amounts (average 0.2%, Table 3), mainly in the vicinity of altered micas, as small, often irregularly shaped crystals. Siderite is often enclosed in clouded dolomite or euhedral ankerite. In some samples, euhedral ankerite crystals are rimmed by siderite (Fig. 12).

### 6.3. Stable isotope geochemistry

The carbonate content of the studied Buntsandstein samples is dominated by detrital, mainly calcitic grains and authigenic dolomite/ankerite. The detrital grains are often overgrown (spherulites), cemented or replaced by pre-compactional calcite, which could not always be distinguished petrographically from the grains. The volume of the latter calcite phase is small in comparison to volume of the detrital carbonates. The grains and cements are intergrown and often replaced by dolomite, which itself is replaced and overgrown by ankerite and locally by a thin siderite rim. The latter three phases are not easily distinguishable by means of petrography. Therefore most of the stable isotopic compositions reported relate to bulk compositions. Only in a few samples pure carbonate phases, which mainly consisted of larger concretions and clasts, could be micro-sampled.

The  $\delta^{13}\text{C}$  and  $\delta^{18}\text{O}$  compositions (37 samples) are plotted in two graphs, one showing the relative amount of ankerite/dolomite in each sample and the other the relative content of detrital carbonate and calcite cements (Fig. 13). The samples containing ankerite/dolomite are scattered between -8 to -4‰  $\delta^{18}\text{O}_{\text{PDB}}$  and -7 to +1‰  $\delta^{13}\text{C}$  with 3 samples with significantly lower  $\delta^{13}\text{C}$ -values, i.e. -6.3‰  $\delta^{13}\text{C}$ . These low values are from the same sample containing large clasts consisting of euhedral ankerite/dolomite imbedded in clays. One of the larger clasts could be micro-sampled; the other two results are from bulk samples. They gave similar results.

In two samples larger nodules of dolomite clouded by solid inclusions could be micro-sampled, which are depleted in  $\delta^{18}\text{O}$ . Although all other samples contain dolomite and ankerite, which could not be quantified separately, the zoned, clear saddle ankerite is better developed and clearly more voluminous in certain samples. Yet, the isotopic compositions of the latter are scattered among the other results.

The isotopic compositions of samples containing detrital carbonates and early calcite cements plot in the same range as for ankerite/dolomite. No relationship between the content of detrital carbonate and calcite cement and isotopic composition is apparent from the plot (Fig. 13).

### 6.4. Fluid inclusion microthermometry

Few fluid inclusions in authigenic phases in the studied sandstones are large enough for reliable microthermometric analysis. Only in the clear saddle ankerite crystals enough measurable aqueous inclusions containing two phases, i.e. liquid and gas, were found. All inclusions were measured in the transparent, outer growth zones of the euhedral crystals. The measurements are given in Table 4.

The bulk of the homogenisation temperatures ( $T_{\text{h}}$ ) of the ankerite in the Buntsandstein range between 120 °C and 135 °C ( $n = 7$ ). Two inclusions have higher  $T_{\text{h}(\text{tot})}$ , and for one inclusion no homogenisation was observed below 180 °C. The latter observations might be indicative of stretching. One inclusion has a considerably lower  $T_{\text{h}(\text{tot})}$  of 85 °C, but similar  $T_{\text{e}}$  and  $T_{\text{m}(\text{ice})}$ . Homogenisation was clearly observed as the inclusion was rather large (10 by 6  $\mu\text{m}$ ) which makes it more vulnerable

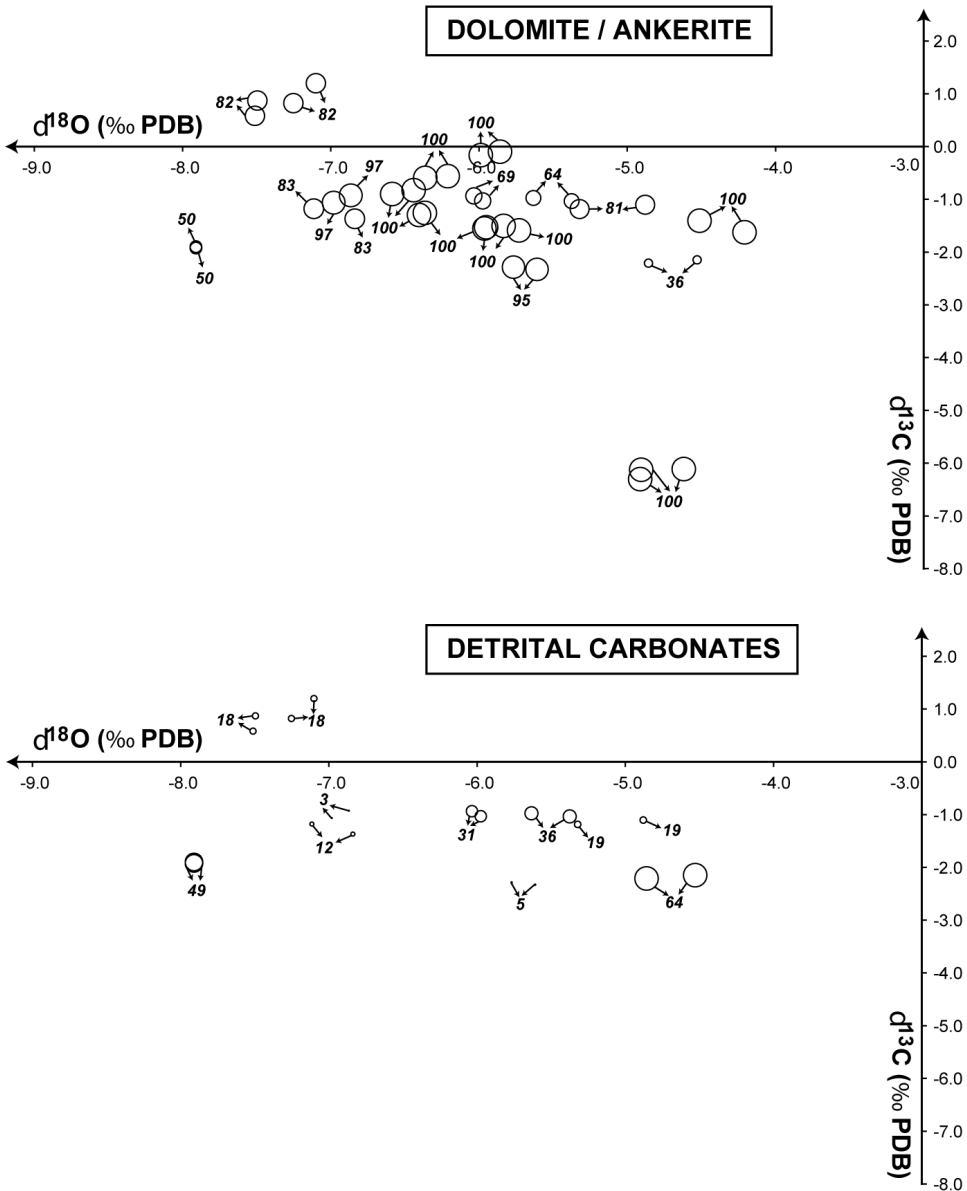


**Figure 13.** O and C stable isotopic compositions of the carbonates in the Buntsandstein sandstones. All values are plotted as circles of which the centre corresponds with the measurement and the size represents the percentage of the considered carbonate phase, relative to the total carbonate content of the analysed sample. These percentages, which are derived from point counting, are also given as labels next to or inside the circles.

to stretching, but this would result in a higher  $T_{h(\text{tot})}$ . The crystal cores usually show signs of replacement and recrystallisation. However, the distinction between core and outer growth zones cannot always be made without advanced techniques i.e. BSEM and CL. Therefore the low-  $T_{h(\text{tot})}$  inclusion could well represent a younger carbonate generation.

### 6.5. Electron probe micro-analyses (EPMA)

EPMA results are summarised in Figure 14. A total of 407 points on line transects of 4 detrital calcite grains and 15 authigenic ankerite/dolomite crystals in 5 samples were analysed. The detrital calcite grains consist on average of 92.4 mol%  $\text{CaCO}_3$ , 4.3 mol%  $\text{MgCO}_3$ , 2.7 mol%  $\text{FeCO}_3$  and 0.6 mol%  $\text{MnCO}_3$ . Only 14 analyses on these grains gave reliable results, as they consist of small micritic grains, which produce a rough surface. They also contain small Fe-oxide particles, which affect the Fe measurement. Euhedral carbonates cover a broad compositional range (47.1–58.6 mol%  $\text{CaCO}_3$ , average 53.1 mol%  $\text{CaCO}_3$ ; 10.7–51.2 mol%  $\text{MgCO}_3$ , average 37.6 mol%  $\text{MgCO}_3$ ; 0.9–35.5 mol%  $\text{FeCO}_3$ , average 8.4 mol%  $\text{FeCO}_3$ ; 0.1–3.4 mol%  $\text{MnCO}_3$ , average 0.9 mol%  $\text{MnCO}_3$ ). They generally have relatively pure dolomitic cores which are surrounded by more ankeritic growth zones. The Fe content increases outward and the outer growth zone often consists of siderite. The Ca

content shows little variation within the same crystal but tends to differ between crystals/samples. All line transects, across the dolomite/ankerite part of the crystals, show broadly the same Fe/Mg ratio (0 to 4), sometimes the upper limit of this ratio is lower (i.e.  $\pm 3$ ). These crystals generally do not have sideritic outer rims. In some crystals, the dolomite cores contain relicts of replaced calcite grains, which often are smaller than the spot size of the analysis (5  $\mu\text{m}$ ). Measurements consequently produced intermediate results (not accounted in the calculation of the average composition). All measurements with Ca content higher than 58 mol%  $\text{CaCO}_3$  are from spots partly covering calcite inclusions. The outer siderite rim around some crystals was also thinner than the spot size, resulting in bulk compositions. All analyses with  $\text{FeCO}_3 > 30$  mol% and  $\text{CaCO}_3 < 50$  mol% are from spots partly covered by siderite. In some cases, pure siderite compositions could be measured, which plot around 80 mol%  $\text{FeCO}_3$ , 10 mol%  $\text{CaCO}_3$  and 10 mol%  $\text{MgCO}_3$ . A few of the analysed crystals contained small siderite inclusions, apart from the outer rim. A strong negative correlation ( $r^2 = -0.93$ ) exists between the Mg and Fe content in the euhedral dolomite/ankerite crystals. Also, Mn correlates negatively with Mg ( $r^2 = -0.68$ ). Consequently, a positive correlation exists between Fe and Mn ( $r^2 = 0.66$ ).

BSEM pictures and element maps show that the zonation of

**Table 4.** Results (°C) of the microthermometric study of fluid inclusions in ankerite crystals of the Buntsandstein ( $T_{h(tot)}$  = homogenisation temperature,  $T_c$  = temperature of first melt,  $T_{m(ice)}$  = final melt temperature). Samples originated from the Gruitrode member.

n°	Buntsandstein		
	$T_{h(tot)}$	$T_c$	$T_{m(ice)}$
1	147.1	-	-21.2
2	118.5	-40.2	-
3	143.8	-47.3	-23.9
4	122.1	-	-
5	-	-47.0	-26.2
6	121.1	-	-
7	125.2	-	-20.0
8	85.6	-49.7	-25.5
9	129.4	-45.2	-24.3
10	124.2	-41.2	-23.6
11	127.2	-42.2	-24.9
av.	124.3	-44.7	-23.7

the dolomites/ankerites is consistent within each sample. Zones with identical composition are present in the same sequence in different crystals, but the size (width) of the zones varies between crystals. Crystals in different samples show different zoning patterns. In some samples, the ‘outer’ siderite zone is covered by a thin Mg-rich ankerite zone.

## 7. Discussion

The discussion starts with a description of the major diagenetic processes that affected the reservoir quality of the Buntsandstein. These processes are arranged chronologically in a paragenetic sequence that was linked to the burial history of the formation (Fig. 15). A summary figure is given in Figure 18 where the contrast between red beds and bleached beds is shown. Subsequently, effects on reservoir quality are addressed.

### 7.1. Eodiagenesis

#### 7.1.1. Inherited clay rims stained by Fe-O/H

The clay-coated framework grains (Figs 6, 8, 10) in the Buntsandstein constitute ‘inherited clay rims’ (ICRs), a term proposed by Wilson (1992) to describe coats of detrital clay on framework grains where clays were present on the grains prior to their arrival at the site of deposition. The distribution, texture, and composition of ICRs allow distinguishing them from other types of detrital and neoformed clays. Wilson (1992) provided a detailed description of the characteristics identifying ICRs. Differentiation of the rims in the Buntsandstein sandstones from other types of clay coats was based on: (i) presence at point contacts between the framework grains; (ii) their widely varying rim thickness; (iii) increased thickness in embayments in framework grains, especially within finer grained sandstones where these depressions are more common; (iv) absence on the surfaces of diagenetic components.

Wilson (1992) states that ICRs originate from recycling of coated grains. The latter can be formed by four different mechanisms, i.e. (i) biogenic reworking; (ii) in situ degradation of smectitic clay or mud intraclasts; (iii) mechanical infiltration as suspended load in surface waters and (iv) adhesion on wetted grain surfaces. Busch et al. (2020) recently compiled additional controlling factors on the presence and extent of grain coats. Because framework grains with inherited clay rims represent recycled material, the specific origin(s) of the clays coating the grains is difficult and, in most cases, impossible to constrain. Clay rims are mainly found in shelf and eolian environments. In

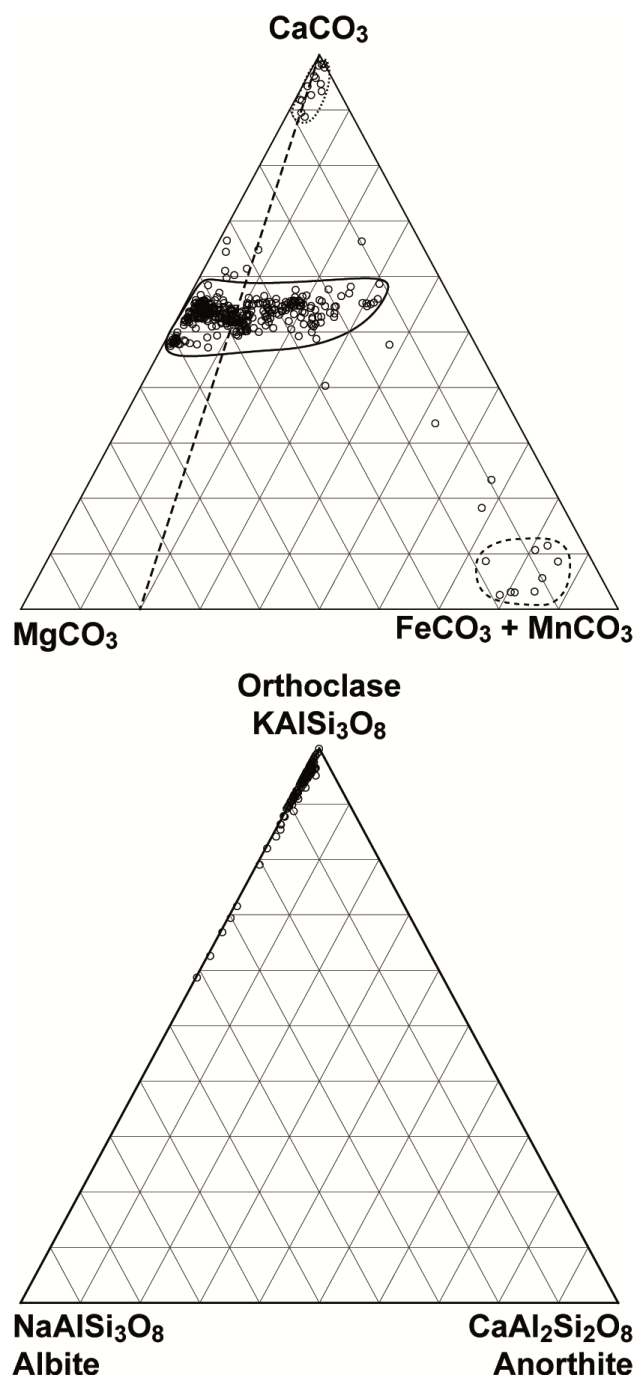


**Figure 14.** Ternary plots of EPMA-analyses on carbonate phases and feldspar grains of the Buntsandstein. The dashed line in the upper diagram delimits the ankerite(left)/dolomite(right) fields.

the latter, clays are introduced into sand debris primarily by adhesion on wetted surfaces and by infiltration through invasion by surface waters, processes that occur predominantly in low-lying sabkha, interdune and desert-floor environments. Framework grains with ICRs generated in these environments can be recycled into a variety of eolian deposits and may also occur in fluvial deposits, like in the Buntsandstein in the Campine Basin. These sediments were deposited within a dryland river system, in which sabkha or playa environments occurred abundantly. The fact that ICRs are omnipresent in all sampled reservoir horizons implies that the clay-coating mechanisms must have been efficient, widespread, and that these environments were recurrently recycled, i.e. eroded by the river system. The high detrital carbonate content of many

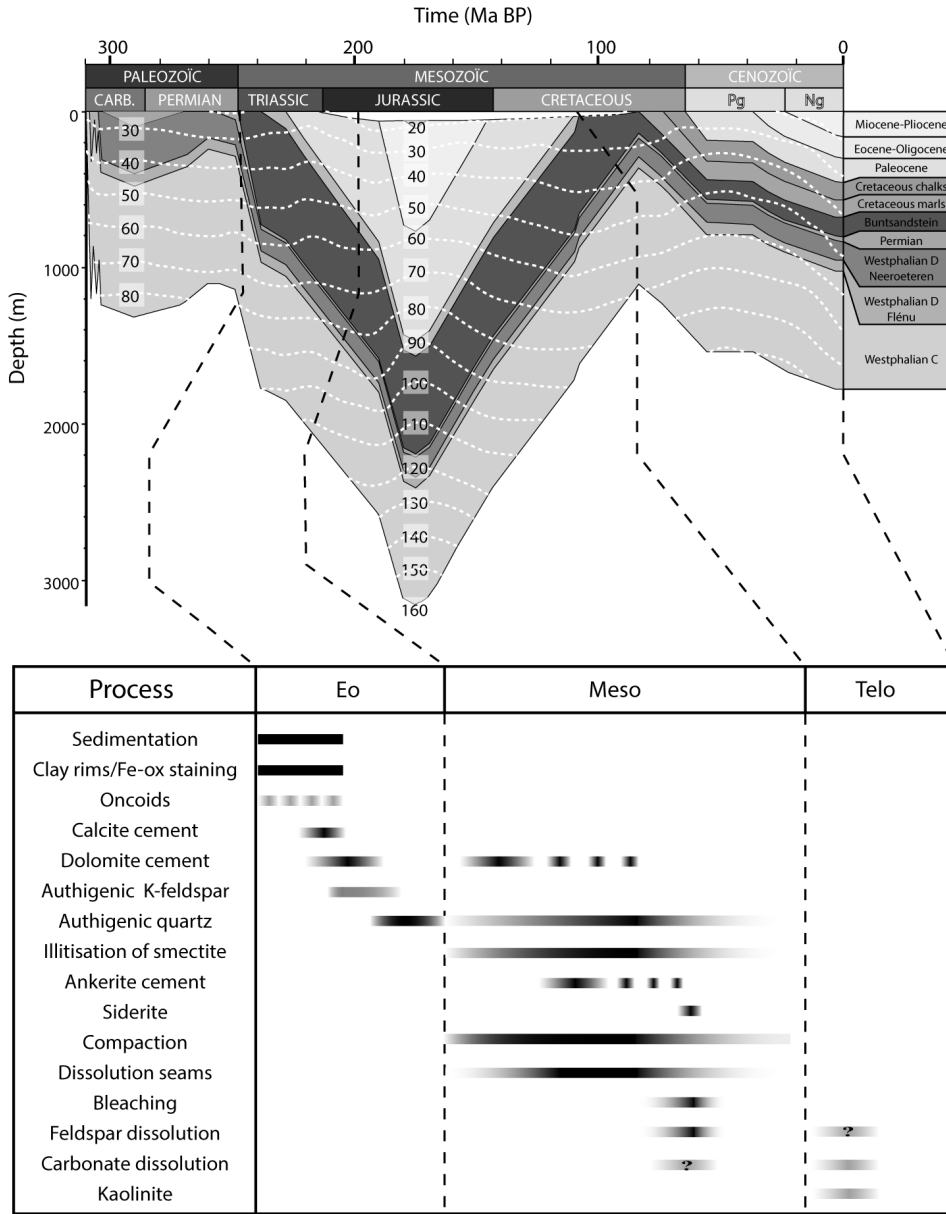


**Figure 15.** Paragenetic sequences of the Buntsandstein sandstones, coupled to the burial curve of KB172. The burial history was divided into five consequent periods, which correspond to the specific diagenetic regimes that are mentioned in the text. The colours of the bars representing the diagenetic processes are a measure of the intensity or impact on the reservoir (darker = larger impact).

samples supports the recycling of playa lake environments, in which often carbonate layers are formed, which must have been common in this Triassic fluvial system. Also of importance is that the clay coats are well developed and display good grain coverage, features that have been recognised in both fluvio-aeolian and estuarine sandstones (e.g. Wooldridge et al., 2017; Molenaar & Felder, 2018).

Many of the more fine-grained sandstones contain pellets or peloids. Faecal pellets are common in playa lakes, where they are excreted by sediment-feeding organisms (Flügel, 2004). Filter-feeding organisms, on the other hand, form pellets that consist primarily of clay. The studied pellets (or peloids) consist of micrite and clays. Many are brown-coloured by the presence of Fe-O/H, others are opaque, due to high hematite content. Pellet-forming organisms typically cause burrowing activity, which is according to Wilson (1992) another major mechanism by which ICRs are formed.

The Fe-O/H that are concentrated in the ICRs (Fig. 6B) originate from weathering, typically in soils, of Fe-silicates (amphiboles, pyroxenes, ...) and are transported in rivers as ferric hydroxide colloids in dilute suspension, or adsorbed on the surfaces of clay minerals (Pettijohn et al., 1987). After deposition, the ferric hydroxides spontaneously dewater to form

Fe-O/H or, if complete dehydration occurs, hematite. The red-brown staining is caused by the presence of ferric iron (Fe<sup>3+</sup>) of which little (about 0.3%, Muchez et al., 1992) is required to produce significant colouring. Colour variations reflect the total oxi/hydroxide content and composition. Red beds, i.e. sandstones stained red by Fe-O/H, are common in arid continental environments.

**7.1.2. Spherulites**

Spheroidal carbonate-coated grains in the Buntsandstein typically resemble deformed ooids but are referred to as spherulites because they are not always spherical and their cortex is formed by non-concentric, partially overlapping laminae (Fig. 6F), with characteristic cross extinction pattern. Their nuclei always consist of carbonate grains. Despite that, some features also have been recognised in recently extensively studied so-called “pre-salt spherulites”, of which the biotic (bacterial) or abiotic origin is still debated (Scherer et al., 2015; Catto et al., 2016), the internal texture of Buntsandstein spherulites differs from the latter.

Spherulites are known from recent and ancient marine as well as freshwater environments. Marine oncoids, which resemble the spherulites typically have marine bioclast

fragments as nuclei. In the studied sandstones, the nuclei consist of micritic or partly micritised carbonates. Non-marine spherulites are generally attributed to fluvial channels and bottom lags of ponds (Flügel, 2004). Here, spherulite growth is favoured by high carbonate input and the contribution of calcite-supersaturated water. Radially arranged micro-cracks, as observed, seem to be a common feature of freshwater spherulites, but it is not entirely clear how they are formed (Flügel, 2004).

The studied spherulites generally exert little control on the sandstone reservoir quality, as they only occur locally and in low quantities. Where they are abundant, they appear to have acted as preferential nucleation sites for carbonate cements. This confirms the existence of carbonate-saturated ponds and reworking by fluvial channels of the sediment, which is evident from overlapping and crosscutting spherulite laminae.

### 7.1.3. Eogenetic carbonate cements: origin

The studied spherulites are often overgrown by calcite cements with intricate CL-zoning (Fig. 6F). The latter are in most samples intergrown or partly replaced by dolomite, which often consist of subhedral crystals that are heavily clouded by solid Fe-O/H inclusions. Both phases form concretions that enclose framework grains (Figs 7A, 10B, 11). The intergranular volume in these concretions is visibly larger than that of the surrounding non-cemented areas, which implies they formed before significant compaction took place.

In some samples, also dolomite cement is complexly zoned, which generally typifies early eogenetic cements. These likely formed close to a water table, where subtle variations in pore water composition occur caused by various degrees of mixing between phreatic and vadose waters (Morad et al., 2000). The calcite and dolomite cements are non-ferroan, which is another characteristic of early carbonates. Hot, dry, continental environments are highly oxidising and have a paucity of reducing organic matter. Therefore all iron remains in the ferric state. Carbonate minerals that precipitate here are thus iron-free (Worden & Burley, 2003).

Eogenetic carbonate cements in arid continental settings have either a pedogenic or a phreatic origin (Morad, 1998; Worden & Burley, 2003; Schmid et al., 2006; Scorgie et al., 2021). The bulk of the studied cements display characteristics typical for groundwater cements (Pimentel et al., 1996), rather than pedogenic cements. The latter normally occur in low permeability horizons and are typically associated with more stable surfaces on floodplains, while phreatic cements are also present in permeable lithologies. In our case, they are typically associated with drainage channels, playas, and lake deposits. Pedogenic cements are usually finely crystalline, while phreatic cements show a wider range of crystal sizes, like the studied cements. In addition, typical pedogenic fabrics, such as rhizocretions, biologically induced structures (burrows, root traces), glaebules, vadose features like pendant cements, etc. are not common in the Buntsandstein. Moreover, dolomite is not a common pedogenic carbonate (Spötl & Wright, 1992; Schmid et al., 2006). Yet, it cannot be excluded that a small part of the cement has a pedogenic origin since the earliest cements surrounding spherulites and peloids sometimes resemble meniscus or pendant fabrics. Also, some fragments might have a pedogenic origin.

The spatial distribution of phreatic carbonate cements in dry continental environments is related to mineral water interaction during regional groundwater flow from proximal to distal settings and to evaporative ionic concentration of pore waters. However, the presence of clay coats may inhibit eogenetic carbonate cementation (Lai et al., 2019). Groundwater in permeable, proximal fluvial sandstones adjacent to uplifted

areas has elevated Ca/Mg ratios, and hence commonly forms phreatic calcrete (Garcia et al., 1998). Groundwaters in the distal deposits have high Mg/Ca ratios, due to the calcite precipitation in the proximal facies and evaporative concentration, which favours dolomite precipitation (Spötl & Wright, 1992).

In playa-lake environments, calcrete and more often dolocrete layers form by the interaction of groundwater with lake brines during periods of strong evaporation and lake-level lowering (Colson & Cojan, 1996). Erosion and reworking of these cemented layers produce carbonate intraclasts. Their presence may result in carbonate recementation at the bases of fluvial channels (Burley, 1984), like those of the Buntsandstein. The phreatic concretions are most abundant in samples with high amounts of carbonate fragments.

### 7.1.4. Eogenetic carbonate: stable isotopes

Although some concretions could be micro-sampled, the stable isotope results (Fig. 13) seem not to reveal much information on their genesis. Both  $\delta^{18}\text{O}$  (-4 to -8‰ V-PDB) and  $\delta^{13}\text{C}$  values (+1 to -2‰, with three outliers from the same sample with values around -6‰) plot in a relatively narrow range. Yet, all concretions contain carbonate fragments and most of them consist of both calcite and dolomite cements. Many are overgrown or partly replaced by later Fe-rich dolomite and ankerite. The stable isotope plots show no significant correlations between ankerite/dolomite or detrital content and isotope signatures. Also, the  $\delta^{18}\text{O}$  and  $\delta^{13}\text{C}$  values lack any sort of trend (e.g., inverted J-trend pointing towards some pedogenic influences; Allen & Matthews, 1982).

The relatively narrow O and especially C isotopic range of the analysed bulk samples with varying ankerite/ dolomite/ calcite contents suggests that the different carbonate phases have similar isotopic compositions, possibly in relation to some resetting. Assuming that the bulk of the cements consist of dolomite which precipitated in equilibrium with unmodified early-Triassic meteoric water ( $\delta^{18}\text{O} = -6\text{‰}$  V-SMOW; Knox et al., 1984) displaying a  $\delta^{18}\text{O}$  range between -8 and -4‰ V-PDB, this results in precipitation temperatures between 27 and 47 °C, using the fractionation equation of Land (1983) (Fig. 16A). These values are rather high for phreatic water in a hot dry continental environment. Moreover, to produce the ionic concentration needed for dolomite precipitation from groundwater, a considerable degree of evaporation is required, which causes the enrichment of the water in heavy oxygen. Assuming dolomite precipitation in equilibrium with water enriched in  $^{18}\text{O}$  by evaporation (e.g. -3‰ V-SMOW), this results in unrealistic (near-surface) temperatures (42–63 °C; Fig. 16A). This suggests that part of carbonate cements equilibrated with evolved water during deeper burial. Muchez et al. (1991) studied the Buntsandstein of borehole KB201 in the Campine Basin. They succeeded in taking pure isotope samples of eogenetic concretions, referred to as glaebules, from three palaeosol horizons. They report that the analysed glaebules consist solely of calcite, although they also mention replacement by later diagenetic dolomite in other samples. These authors consider all dolomite in the Buntsandstein as mesogenetic. Such replacement of calcite by dolomite could explain the large intergranular volume in the concretions, but not the intricate CL-zoning of some of the dolomite cements. The concretions they analysed have an average  $\delta^{18}\text{O}$  of -2.2‰ V-PDB, which is considerably less depleted than any of our analyses. They calculated, assuming a precipitation temperature of 20 °C, that the glaebules formed from water with a  $\delta^{18}\text{O}$  of -1.6‰ V-SMOW. The latter value is significantly higher than the  $\delta^{18}\text{O}$  of -6.0‰ V-SMOW of the Triassic meteoric water in the region (Knox et al., 1984), which they, logically, attribute to

evaporation.

With regard to the  $\delta^{13}\text{C}$  values, most values indicate a system where the contribution of depleted carbon (e.g. soil-derived  $\text{CO}_2$ ) is limited. The carbonate signature seems to be buffered between +1 and -2‰. The three outliers, with depleted  $\delta^{13}\text{C}$  signature varying around -6‰, best can be explained by the involvement of an organic-derived C-source, e.g. soil-derived  $\text{CO}_2$ . The eogenetic carbonates in the studied sandstones are remarkably similar to those of the Triassic Sherwood Sandstone Group of the Corrib Field in the Slyne Basin (Fig. 17) on the continental shelf, offshore western Ireland. These sediments, which were described in detail by Schmid et al. (2003, 2004, 2006a, 2006b), were deposited contemporaneously with the Buntsandstein Formation (Scythian) in a similar sedimentary setting. Predominant carbonate cement in the Sherwood Sandstone Group of the Corrib Field is non-ferroan dolomite, which is associated with minor calcite and ferroan dolomite/ankerite. The quantities of late diagenetic ferroan dolomite/ankerite, which also forms rims around the eogenetic dolomite, are lower than in the studied Buntsandstein. The Sherwood dolomite  $\delta^{13}\text{C}$  values range between -3.2 and +2.1‰, which is broadly similar to the Buntsandstein (-2.3 to +1.2‰). Carbonates in both formations have a pedogenic/phreatic origin with few exceptions of three soil-derived cements with  $\text{CO}_2$ -depleted  $\delta^{13}\text{C}$  values.

Schmid et al. (2006b) argued that the highest  $\delta^{13}\text{C}$  values measured in the Sherwood Sandstone (Fig. 17) relate to carbonate formation in periods of reduced rainfall, minimised biological activity (vegetation) and high evaporation. During such periods the dominant C-source was atmospheric carbon, possibly enriched in heavy C due to evaporation, with a low contribution of biological, light C resulting in  $\delta^{13}\text{C}$  values around +2‰. Conversely, the lightest  $\delta^{13}\text{C}$  values represent carbonates formed in periods with more precipitation and subsequently larger vegetation cover and a lower degree of evaporation. During such periods, the dominant C-source for carbonate precipitation was still atmospheric  $\text{CO}_2$ , but the input of biologically derived, light C was more substantial, which resulted in  $\delta^{13}\text{C}$  values around -2‰ and even somewhat lower.

The gradual  $\delta^{13}\text{C}$  variations of the carbonates in the stratigraphical record of the Corrib Field thus reflect transitions from arid to less arid conditions and vice-versa and can be interpreted as a proxy for the palaeoenvironment and palaeoclimate. Schmid et al. (2006b) strengthened these findings by correlation with other indicators of the palaeoenvironment/climate, such as depositional facies and abundance of carbonate cement. They also demonstrated that C-isotope records of different wells in the Corrib Field provide a tool for stratigraphic correlation. They also plotted the  $\delta^{13}\text{C}$  values of the Buntsandstein of KB201 (Muechez et al., 1992) versus depth, and observed a trend that is similar to those of the Corrib Field. As these locations are located nearly 1200 km apart from one another, Schmid et al. (2006a) suggested that the palaeoclimate evolution signal in the Lower Triassic sandstones of the Corrib Field records a major sub-continent scale event.

The isotopic results presented in this study corroborate the trend observed by Schmid et al. (2006a) (Fig. 17) except for the four samples at the top 100 m of the reservoir (806–904 m depth below surface). Their  $\delta^{13}\text{C}$  values plot between -1 and 0‰, and are rather inconsistent with the observed trend of gradually more negative values towards a depth of around 900 m, which Schmid et al. (2006a) seem to consider as the top of the Buntsandstein. Schmid et al. (2006b) used an easily recognisable playa horizon, locally known as C1, which occurs in all the core sections of the Corrib Field as stratigraphic marker. On a depth scale normalised to this playa horizon, the  $\delta^{13}\text{C}$  trends of the boreholes they studied, coincide nicely.

As this playa horizon evidently did not stretch to the Campine Basin, there is no means of correlating the trend in KB201 with those of the Corrib Field. Schmid et al. (2006a) based their suggestion of a sub-continent scale palaeoclimate controlling event on the fact that the trends in the Corrib Field and KB201 are similar in shape and reach maximum  $\delta^{13}\text{C}$  values about 150 m below the top of the Triassic sandstone formations. Yet, this top in KB201 lies about 100 m higher than they were considering it to be. Furthermore, the top of the Buntsandstein in KB201 consists of an erosive contact with the Cretaceous and therefore cannot be used for chronostratigraphic correlation.

Besides the samples of KB201, also the isotopic composition of 17 samples of KB172 was analysed. Unfortunately, these do not cover the sampled depth range densely enough to observe any trend. Yet, all values, except three, are in the same  $\delta^{13}\text{C}$  range as for KB201. The three outliers have a  $\delta^{13}\text{C}$  of around -6‰. They come from the same sample, which contains dolomite concretions overgrown and partly replaced by ankerite. The relative ankerite content of this sample seems quite high.

The observed  $\delta^{13}\text{C}$ -depth trend in the Campine Basin holds important implications concerning the diagenetic history of the Buntsandstein and might be useful for intrabasinal stratigraphic correlation, which is currently rather provisionally based on the occurrences of evaporites and shales. This could provide insight in the depositional setting and the architecture of the Buntsandstein, which is complicated by post-Triassic tectonics.

#### 7.1.5. Eogenetic carbonates: implications for geological $\text{CO}_2$ sequestration

The fact that  $\delta^{13}\text{C}$  compositions of carbonate cements in the Buntsandstein vary smoothly with the stratigraphy, and most likely yield a palaeoclimatic signal, implies that diagenesis in the reservoir was isochemical with respect to  $\text{CO}_2$  or dissolved carbonate. The observed trend reflects therefore a primary, eogenetic signal. Such signals are normally obscured by later, generally mesogenetic influxes of  $\text{CO}_2$  with different  $\delta^{13}\text{C}$  signatures. The Westphalian coal-bearing sequences, underlying the Buntsandstein, have generated vast quantities of  $\text{CO}_2$  during their burial history (Van Keer, 1999; van Tongeren et al., 2000).  $\text{CO}_2$  generated by organic matter, such as coal, typically has distinctly negative  $\delta^{13}\text{C}$  values (e.g., < -20‰ V-PDB; Irwin et al., 1977). As the primary  $\delta^{13}\text{C}$  signal in the Buntsandstein was not affected by this influx, this implies that these sandstones were non-reactive towards the released  $\text{CO}_2$ , or that the  $\text{CO}_2$  did not pass through the reservoir in sufficient quantities to affect the  $\delta^{13}\text{C}$  composition. Yet, most of the studied sandstones contain a late diagenetic ankerite. As this phase has a mesogenetic origin, this matter will be discussed further on.

#### 7.1.6. K-feldspar authigenesis

Authigenic K-feldspar (AKF) occurs as overgrowths on detrital K-feldspar grains (Fig. 6A, 6C). The total AKF content is strongly related to the detrital K-feldspar content. Samples with high detrital content have the highest AKF content (estimated volume <2%). Yet the effect of AKF on the reservoir properties is minimal, as the bulk of the overgrowths are heavily affected by, most likely late-diagenetic, alteration and dissolution.

Petrographic observations indicate an early eogenetic AKF origin. The overgrowths postdate the clay rims, predate the eogenetic clouded dolomite and seem to have grown partly contemporaneous with an early generation of authigenic quartz. They often completely enclose detrital grains and, elsewhere, contacts of host grains with adjacent grains are point-contacts, i.e. indicative of a pre-compactional genesis. Such an early formation of AKF is also in line with for example Bjørlykke et al. (1986).

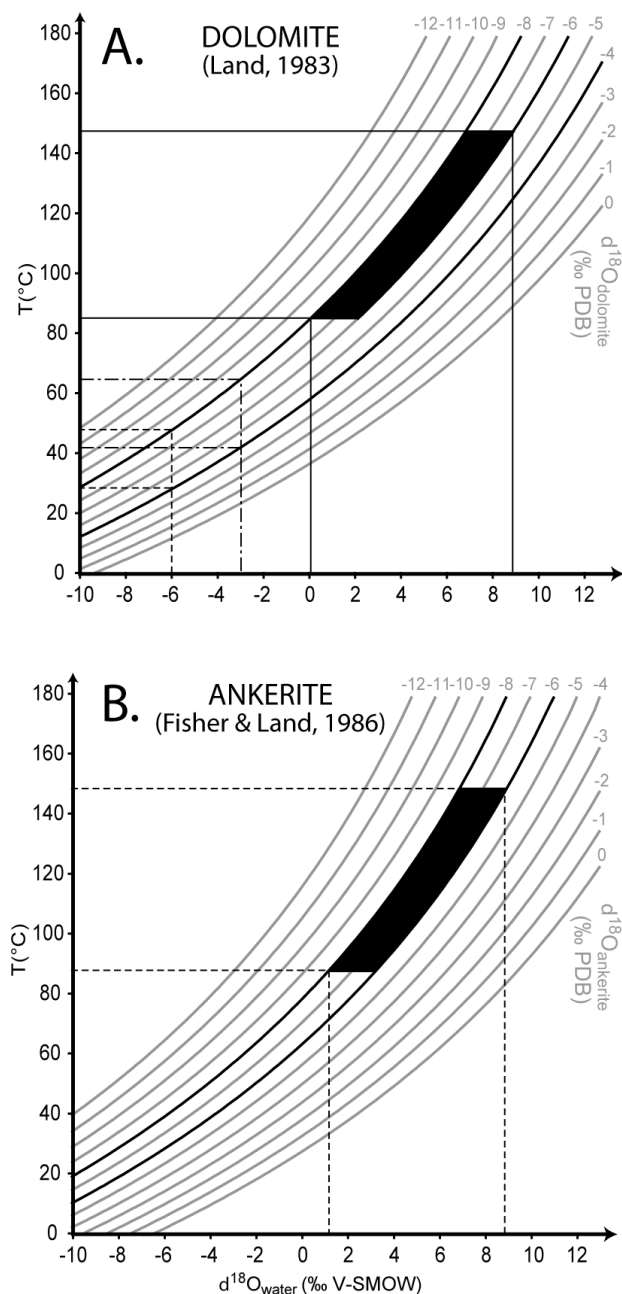


**Figure 16.** Oxygen isotopic fractionation of dolomite (A) and ankerite (B) as a function of the  $\delta^{18}\text{O}$  of the ambient water and temperature. The measured isotopic compositions of the eogenetic carbonate concretions in the Buntsandstein range between  $-8$  and  $-4$ ‰ V-PDB. Assuming that the bulk of the cements consists of dolomite which precipitated in equilibrium with unmodified early-Triassic meteoric water ( $\delta^{18}\text{O} = -6$ ‰ V-SMOW; Knox et al., 1984), yields precipitation temperatures between  $27$  and  $47$  °C, using the fractionation of Land (1983) (Dashed line in diagram A). Assuming that the dolomite precipitated in equilibrium with water enriched in  $\delta^{18}\text{O}$  by evaporation (e.g.,  $-3$ ‰ V-SMOW), results in surface temperatures of  $42$ – $63$  °C (Dotted-dashed line in diagram A). The analysed mesogenetic dolomite/ankerite has  $\delta^{18}\text{O}$  values between  $-8$  and  $-6$ ‰ V-PDB. Fluid inclusions in these phases have homogenisation temperatures between  $86$  and  $147$  °C. Using the fractionation equation of Land (1983) this corresponds to water compositions of  $0$  to  $+8$ ‰ V-SMOW (full line diagram A). The ankerite fractionation equation of Fisher & Land (1986) yields slightly higher compositions (diagram B).

Eogenetic K-feldspar is a common phase in red beds (Worden & Rushton, 1992; Morad et al., 1994; Rossi et al., 2002; Schmid et al., 2004; Henares et al., 2014; Mahmic et al., 2018). The crystallisation of AKF requires an interstitial supply with K, Al and Si, of which several sources have been discussed in the literature. Rossi et al. (2002) suggested that the AKF in the TAGI sandstones (Algeria) related to refluxed residual brines derived from overlying evaporites. However, these authors came also to the conclusion that evaporites could never supply the necessary Si and Al. A more commonly proposed source is the alteration (hydrolysis) of unstable Al-silicates. Walker et al. (1978) suggested that the hydrolysis of hornblende, pyroxene and plagioclase grains by intrastratal alteration provided the ions for AKF in the Cenozoic desert alluvium of SW-USA and NW-Mexico. Such grains might have been present in freshly deposited Buntsandstein sands. Dissolution voids might have been destroyed by later compaction. They could also have supplied Fe to the red coats. But no hard evidence supports their former presence. Moreover, whether these phases could provide the necessary K is unclear. Several authors (Kastner & Siever, 1979; Ali & Turner, 1982; De Ros et al., 1994; Rossi et al., 2002) added volcanic fragments to the series of dissolved grains which could provide the K. But they are not expected to have constituted a sufficient part of original Buntsandstein mineralogy. Patterson & Tatsumoto (1964) compared the Pb isotopic composition of detrital K-feldspar grains and their overgrowths and found them to be similar. This made them conclude that detrital K-feldspar can be an important source of ions for AKF. The presence of Ba in the AKF, in the Triassic Bromsgrove Sandstones in Central England, and alkali feldspar being the only obvious Ba source, brought Ali & Turner (1982) to the same conclusion.

The observations that K-feldspar simultaneously dissolves and precipitates pose an intriguing thermodynamic predicament. Ali & Turner (1982) suggested that certain K-feldspar grains, e.g. those with compositional or structural variation, are preferentially dissolved. They did not measure systematic compositional differences between detrital and authigenic feldspar, but did observe an optical discontinuity between orthoclase or microcline host grains and their overgrowths, which was not present in sanidine host grains. This made them conclude that the overgrowths they studied consist of sanidine, and that the preferential dissolution of detrital grains is related to differences in the Al/Si ordering rather than to differences in composition. The conclusions of Ali & Turner (1982) were adopted by numerous authors addressing eogenetic AKFs (e.g., De Ros et al., 1994; Rossi et al., 2002; Schmid et al., 2004). These authors name detrital K-feldspar as an important source of ions for K-feldspar authigenesis, but did not go into detail on the mechanism of preferential dissolution and reprecipitation. Simultaneous dissolution of less stable K-feldspar polymorphs and precipitation of more stable polymorphs is thermodynamically possible, yet requires specific chemical conditions. Considering the slow dissolution kinetics of K-feldspar, it is not likely that the chemical conditions, in the presumed phreatic environment where the overgrowths formed, remained constant long enough to dissolve one polymorph and precipitate significant quantities of another polymorph knowing that these processes are likely to be extremely slow. The kinetics of feldspar dissolution are obviously controlled by the saturation state of the fluid.

Maraschin et al. (2004) proposed a model for K-feldspar authigenesis whereby detrital K-feldspar dissolves in proximal areas of the basin, where undersaturated meteoric recharge dominates over evaporation, and precipitation of overgrowths occurs further along the groundwater pathways throughout the basin. K-feldspar authigenesis (i.e. precipitation) here is driven

## Offshore west of Ireland

## Campine Basin

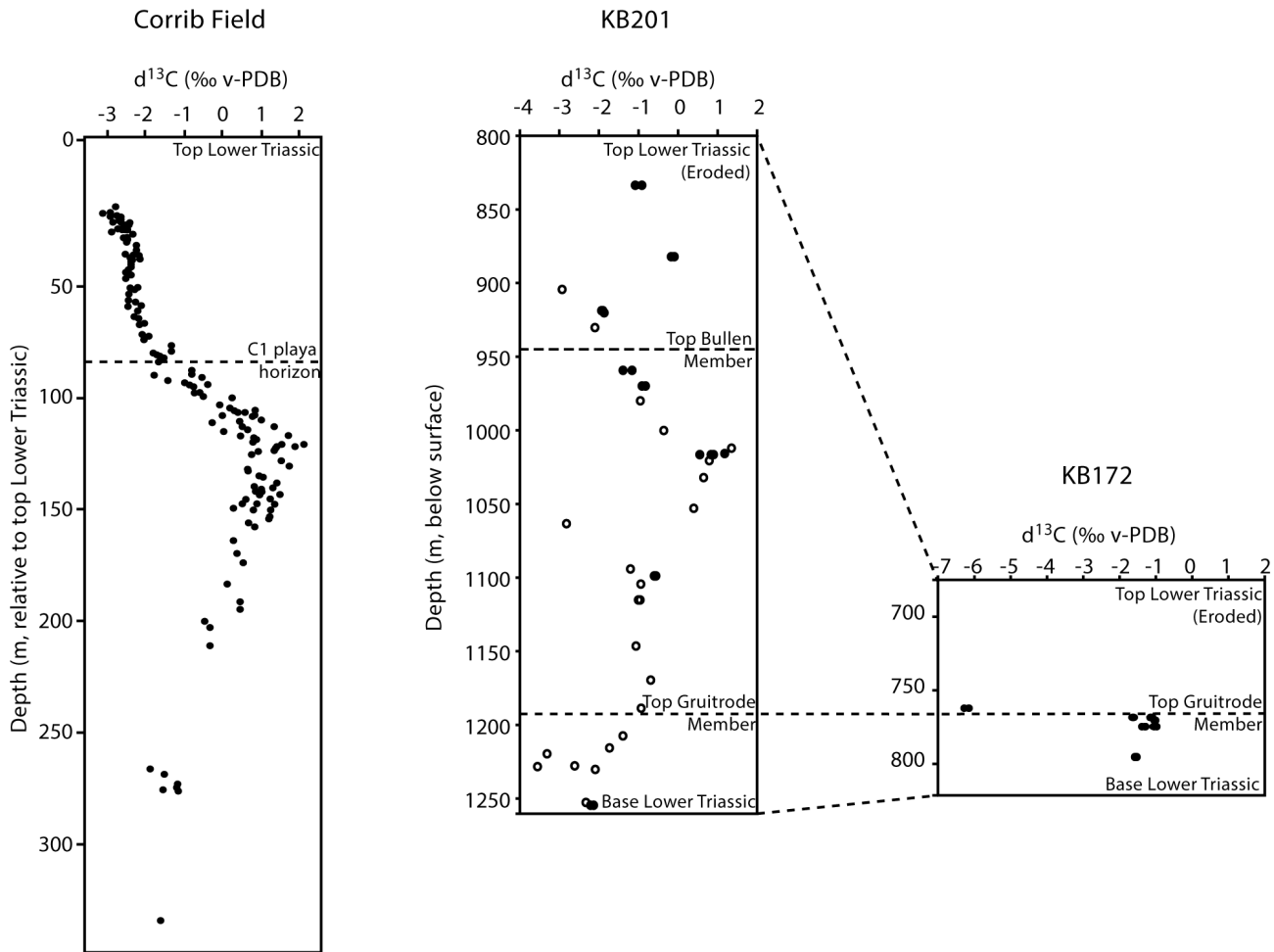


**Figure 17.** The stratigraphic trend in C-isotopes observed in the Triassic Sherwood sandstone of the Corrib Field (Offshore west of Ireland) observed by Schmid et al. (2006a) corresponds relatively well to the depth trend observed in the Buntsandstein of borehole KB201 (open circles: Muchez et al., 1992; full circles: this study). Schmid et al. (2006a) attribute this trend to a gradually changing climate. In the Campine Basin, a couple of points deviate from the trend. These are samples with relatively high mesogenetic carbonate content. The interval available from KB172 does not cover a sufficient depth range to reflect a trend. Most values, however, plot in the expected range.

by evaporative concentration, much like phreatic carbonate genesis in arid continental environments. This model parries the thermodynamic issues by laterally separating the dissolution and precipitation environments, which also makes the preferential dissolution of less stable polymorphs superfluous. Such a model requires mass transfer over long distances, from the source (dissolution) area to the horizons where K-feldspar authigenesis takes place. Al and Si are fairly immobile at surface temperatures and would likely precipitate along the groundwater pathways as kaolinite or smectitic clays before K-feldspar saturation is reached (by evaporation). Maraschin et al. (2004) observed these phases in the Açú Formation (Potiguar Basin, NE-Brazil), on which their model is based.

Part of the smectite, of which the clay rims were originally composed in the Buntsandstein, was probably formed by a similar mechanism. The clay rims, however, predate the K-feldspar overgrowths, and formed in several phases of reworking of the sediments before final deposition of the sand. Reworking is the only process that can produce a complete envelopment of grains by clay rims. Consequently, the smectite of the clay rims is not likely to have had a phreatic origin. Furthermore, kaolinite is sparse in the studied strata.

K-feldspar authigenesis in the Buntsandstein most likely took place by a mechanism similar to that of Maraschin et al.

(2004) but operating on a smaller scale. Evaporative concentration is the most obvious drive for supersaturation and resulting precipitation in a desert-like environment like that of the Buntsandstein. K-feldspar grains were an important source of ions, together with other unstable Al-silicates. Dissolution of these phases is suggested to have taken place in near-surface environments, like those where the smectite coats formed. The omnipresence of eogenetic AKFs throughout the Buntsandstein implies that the groundwater was most of the time during deposition near K-feldspar saturation, which is supported by the fact that the overgrowths consist of single, continuous, large crystals. Such overgrowths are formed at low degrees of supersaturation (Worden & Rushton, 1992; De Ros et al., 1994; Lee & Parsons, 2003). Dissolution is suggested to have taken place in both vadose and phreatic zones, due to episodic infiltration of undersaturated meteoric water during wet periods. Short periods of extensive runoff and infiltration of meteoric water are typical for dry river systems and are recognised in the sedimentological structures making up the bulk of the Buntsandstein (i.e. sheet flood deposits, broad shallow channels, playa lakes, etc.). Mixing of groundwater (and vadose water) with those meteoric waters temporarily causes undersaturation of K-feldspar and consequent dissolution. Evidently, less stable feldspars will be dissolved faster during such periods.



This process appears to be important in coarse sediments, in arid regions, scarce of vegetation, like the depositional environment of the Buntsandstein. Evidently phreatic evaporation is more significant in areas with shallow water tables. However, Scanlon et al. (2003) demonstrated the importance of evaporation of phreatic water more than 20 metres below surface. Anyhow, evaporation at or directly above the water table would also lead to evaporative concentration in the phreatic zone, if recharge and groundwater flux are restricted. Another argument Kelly et al. (2007) state to validate the vadose origin of the syntaxial quartz cements they studied is the homogeneity of the  $\delta^{18}\text{O}$  values of the analysed overgrowths. If circulating ground waters in the phreatic zone precipitated quartz cements, they expect the variations in temperature and water composition to result in more variable  $\delta^{18}\text{O}$  values. In the Buntsandstein case, however, the abundance of AKFs and phreatic dolomite cements indicates a groundwater system with restricted recharge and circulation. In such a non-dynamic flow system, compositional variations, caused by the mixing of water from different sources, should be minimal and temperature will be depth related. Consequently, the  $\delta^{18}\text{O}$  values of the eogenetic overgrowths are expected to be rather homogeneous. The stable isotopic compositions were not analysed though, as the results would most likely be obliterated by the  $\delta^{18}\text{O}$  signatures of the mesogenetic AQs.

## 7.2. Mesodiagenesis

### 7.2.1. Illitisation of smectitic clays

The smectite to illite transformation process is manifested in the Buntsandstein by the cornflake and honey-comb morphologies of clay rims (Fig. 8). XRD analyses reveal that the bulk of the clay consists of illite (Fig. 4). Remnants of smectite interlayers in this illite disclose its origin from precursor smectitic clays.

Although the maximum temperatures attained during burial of these sandstones are relatively low ( $\sim 125\text{ }^\circ\text{C}$  for the base of the formation), smectite was almost completely transformed into illite. Several factors may increase the rate of illitisation during burial. The most important control on the transformation rate, besides temperature, is the availability of potassium (McKinley et al., 2003). The relatively high K-feldspar content of the Buntsandstein provided a generous K-supply. Also, the fairly high porosity, permeability and good interconnectivity between the sandstone layers positively affected the rate of the illitisation process. McKinley et al. (2003) also mention the effect of the smectite composition and origin on the rate of illitisation. Authigenic smectite is intrinsically more stable and less susceptible to illitisation than detrital smectite, as it is formed during diagenesis and therefore is closer to equilibrium conditions during burial. The smectite in the Buntsandstein, however, was formed during deposition, as it occurs in inherited clay rims. The geochemical conditions of smectite authigenesis are assumed to have been closer to a 'weathering environment' (which produces detrital smectite) than a diagenetic environment. The composition of smectite is mainly determined by the host lithology it originated from (by weathering). Felsic rocks tend to produce dioctahedral smectite, while Fe and Mg-rich mafic lithologies alter to trioctahedral smectite. The former is much easier (i.e., faster) transformed to illite and therefore presumed to have been the dominant type in the Buntsandstein.

The illite being part of clay coats, consisting of crystals perpendicular to the grain surface, most likely resulted from the conversion of smectite in the clay rims it covers. Yet, it is not entirely clear why this type of coats occurs in certain, mostly white but also some red samples while they are absent in others. The samples where these coats occur are typically coarse-grained sandstones with relatively high feldspar contents and

porosity. In such samples a higher illitisation rate can be expected, which might result in more crystalline illite, like the hairy, whiskery, or platy illite constituting the coats. Where they occur, the coats often expand to boxwork illite filling intergranular porosity and impairing the permeability.

The smectite to illite conversion generally produces carbonate and quartz cements. In our case, it probably sourced part of the cations incorporated in the euhedral ankerite, as discussed further on. The direct contribution of this process to the total quartz cementation in the Buntsandstein is likely less important. The conversion reaction probably did have a significant indirect effect on the quartz cementation. Besides preventing quartz nucleation like the clay rims they originated from, coats consisting of perpendicularly arranged illite also counteract pressure dissolution, unlike clay rims, which tend to enhance it.

### 7.2.2. Chemical compaction and quartz cementation

Chemical compaction is evidenced in the Buntsandstein by the presence of dissolution seams (Fig. 11C) and by the concavo-convex grain contacts in some samples. Both features are much more common and distinct in red than in white sandstones. The latter, however, contain considerably more quartz cement, of which a significant part presumably resulted from chemical compaction. These observations can be attributed to the dual role of illitic clays in controlling quartz cementation. Inherited clay rims prevent nucleation of pore-filling quartz overgrowths on detrital quartz grains, but illitic clays, like micas, at grain contacts act as a catalyst for chemical compaction and concomitant release of silica for quartz cementation (Bloch et al., 2002; Monsees et al., 2020).

The role of clay rims and coats in retarding quartz cementation by blocking potential nucleation sites for overgrowths on detrital quartz 'seed-grains' was identified decades ago (Heald & Larese, 1974 and references therein) and has since been invoked to explain heterogeneous distribution of quartz cements in various sandstones (e.g. Molenaar, 1986; Moraes & De Ros, 1990; Pittman et al., 1992; Wilson, 1992; Bloch et al., 2002; Heidsiek et al., 2020 and many others). The effectiveness of grain coats or rims in preventing quartz cementation is a function of their completeness, as well as of their thermal history, the grain size of the sandstone and the relative abundance of quartz grains.

The effect of illite and mica on pressure dissolution was recognised a long time ago and was first thoroughly described by Heald (1955). The mechanism behind illite-mica-induced dissolution (I-MID) is still not completely understood and is subject of much debate (Walderhaug et al., 2004; Sheldon et al., 2004; Bjørlykke et al., 2017). The I-MID mechanism was inferred from petrographic observations of dissolution textures at illite/mica-quartz interfaces and of the predominance of quartz dissolution at such interfaces over dissolution at quartz-quartz contacts in quartzose sandstones (Heald, 1955, 1959; Dewers & Ortoleva, 1991; Walderhaug, 1994, 1996; Oelkers et al., 1996, 2000; Renard et al., 1997, 2000; Fisher et al., 2000; Walderhaug et al., 2000; Walderhaug & Bjørkum, 2003; Weber & Ricken, 2005; Cyziene et al., 2006; Baron & Parnell, 2007; and many others). Bjørkum (1996) determined that I-MID requires negligible stress, by means of theoretical calculations of the mechanical properties of observed micas at surfaces of which 'pressure dissolution' of quartz grains irrefutably had taken place but where they were not deformed, though not supported by adjacent grains. In the literature, it was suggested that dissolution may result from electrostatics interaction between quartz and clay/mica surfaces (e.g. Walderhaug et al., 2000, 2004), but this has yet to be demonstrated unambiguously. The point of controversy is that the I-MID mechanism invokes a

local chemical effect to drive grain contact dissolution and diffusion of the resulting aqueous silica, which, according to some researchers, cannot induce a persistent gradient in chemical potential, and therefore cannot provide a driving force for chemical compaction (Sheldon et al., 2003, 2004). A more classic view of pressure dissolution calls upon the inhomogeneous distribution of normal stress over grain surfaces to provide a persistent gradient in chemical potential, and hence a persistent driving force for chemical compaction (Tada & Siever, 1989; Renard et al., 1999, 2000; Sheldon et al., 2003). The supporters of the I-MID mechanism succeeded in constructing predictive quantitative models explaining the distribution of quartz cement in sandstones, based on the assumption that the silica source of cement is quartz surfaces adjoining mica and/or clay grains (Oelkers et al., 1996, 2000; Walderhaug, 1996; Walderhaug et al., 2000). These models are in close agreement with field observations, and experimental studies (Bjørlykke et al., 2017) which evidently strengthens the idea that chemical compaction is controlled by I-MID.

Petrographic observations suggest that the enhanced chemical compaction of the red Buntsandstein horizons can be attributed to the I-MID mechanism. Although the average mica content in these sandstones is rather low, red horizons contain significantly more micas than their white counterparts (average 1.0% vs. 0.3%). Mica flakes are generally surrounded by elongated quartz grains (or remnants of grains) which have long contacts with the flakes, suggesting preferential partial dissolution. In many red samples, micas, surrounded by partially dissolved grains, are aligned along stylolite-like structures. Some samples contain thicker, continuous stylolites (or dissolution seams) filled with micas, clays (mostly illite), remnants of quartz and residual grains, which often constitute the contact between red fine and white coarse-grained zones. They closely resemble the I-MID stylolites described in the literature (Bjørkum, 1996; Oelkers et al., 1996; Cyziene et al., 2006). Zones of intense chemical compaction are easiest to recognise in samples containing high quantities of micas, which tend to be aligned. Yet, in many samples dissolution seams, consisting of elongated rimmed grains with long, often sutured contacts were observed which show that the clay rims effectively induced or enhanced pressure dissolution. This pressure dissolution is the most important source of mesogenetic quartz in the Buntsandstein.

Why these zones of intense chemical compaction are mainly restricted to the red Buntsandstein horizons can be attributed to several factors. First grain size could have played a role. The red horizons are typically fine- to medium-grained, while the white sandstones are generally coarser grained. Empirical studies of the relationship between grain size and intergranular pressure dissolution show that finer grained sandstones are more susceptible to intergranular pressure dissolution (Houseknecht, 1984; Tada & Siever, 1989). This is attributed to the relative thermodynamic instability of mineral surfaces relative to mineral interiors which results in Ostwald ripening, i.e. the preferential dissolution of small grains and reprecipitation of the dissolved silica as a contribution to larger grains (Worden & Morad, 2000). In the Buntsandstein, however, grain size is probably indirectly related to chemical compaction. In the finer grained, red sandstones the mica content is higher and the inherited clay rims are better developed. The higher mica content is related to hydrodynamic sorting in the depositional environment. Mica flakes are, due to their shape, deposited in lower energy environments and thus associated with finer grained clastics. Better development in finer grained sands is also an inherent characteristic of inherited clay rims, which are more complete and generally thicker than those in coarse-grained lithologies since they formed in less energetic

environments on generally more angular grains and thus suffer less from abrasion during deposition (Wilson, 1992).

A result of these well-developed rims is that the framework of the red sandstones, during compaction, was almost exclusively supported by illite-quartz contacts, which enhance pressure dissolution. A yet even more important effect of the completeness of the rims is the inhibition of quartz cementation. The complete coverage of detrital quartz grains by clay leaves no nucleation sites for the silica released by pressure dissolution. In the white Buntsandstein horizons, grain coverage is much less complete, which allows nucleation and growth of overgrowths. AQ overgrowths restrained chemical compaction in the latter horizons in multiple ways. They support the framework, i.e. reduce the effective stress by increasing the surface on which the pressure is applied (assuming that stress plays a role in chemical compaction; Oye et al., 2018). They also reduce the number of clay/quartz contacts, at which compaction is enhanced, by enclosing (incomplete) clay rims. This increases the relative amount of quartz/quartz contacts, at which chemical compaction requires higher stress.

The white Buntsandstein horizons contain significantly more AQ than the red ones, while considerably more silica was sourced by chemical compaction in the red sandstones. A part of this AQ has an eogenetic origin, which formation was in the red sandstones inhibited by the clay rims, and likely also contributed to the retardation of pressure dissolution in the white horizons. Still, a significant part of the AQ in the white horizons resulted from chemical compaction in the red horizons, though this is not irrefutably clear from the petrography of the overgrowths. Yet, the silica released in the red horizons had to end up somewhere but large-scale fluid flow is doubtful because of the low solubility of silica, requiring huge volumes of water. It is more likely to take place in the nearby white, more permeable levels which thus acted as silica sinks, while the finer grained, clay- and mica-rich, red sandstones acted as silica exporters. Such facies-selective transfer of silica has already been reported (e.g. Trewin & Fallick, 2000; Weber & Ricken, 2005; Cyziene et al., 2006; Morad et al., 2010). It is driven by diffusion, due to the establishment of a dissolved silica gradient between dissolution and precipitation sites, and operates at millimetre to metre scales (Morad et al., 2000). This mechanism eventually leads to extensive cementation of clean (mica and rim-free) horizons, while clayey and mica-rich sandstones, where the chemical compaction takes place, end up retaining some porosity (Bloch et al., 2002). In our case, this advanced scenario has not been reached, due to the relatively shallow burial.

The burial model for KB172 (Fig. 3) shows a maximum overburden load of ~1600 m for the top of the reservoir and ~2100 m for the base, corresponding to about 90 and 120 °C, respectively. Typically reported minimum temperatures for the initiation of significant AQ cementation sourced by chemical compaction are between 90 to 130 °C (McBride, 1989; Worden & Morad, 2000; Giles et al., 2000; Baron & Parnell, 2007). Besides temperature also residence time, during which the sandstones are exposed to a certain temperature, is an important control (Morad et al., 2000). Long periods of relatively low temperatures can result in the same amount of AQ as short-lived hot periods. As it is not possible to distinguish mesogenetic from eogenetic quartz in the Buntsandstein, conclusions on the maximum burial temperature and residence time here would be rash. However, assuming the presented burial history (and heat flow) is accurate, the AQ content of certain horizons of the Buntsandstein is rather high (up to 12.5%, Table 2) considering its relatively shallow maximum burial, compared to other sandstone reservoirs in the North Sea area (e.g. McBride, 1989; Walderhaug, 1994; Worden & Morad, 2000; Weber & Ricken,

2005; Baron & Parnell, 2007; Niazi et al., 2019) and compared to the underlying Westphalian C and D sandstones (Bertier et al., 2008).

### 7.2.3. Illitisation of K-feldspar

SEM observations of feldspar grains covered with illite give the misleading impression that these were illitised. In thin sections, however, it is clear that this illite resulted from the conversion of smectitic clay rims. Illite covering K-feldspar overgrowths, however, most likely originated from the 'direct' illitisation of K-feldspar grains. The impact of this process on the reservoir quality of the Buntsandstein sandstones appears to be low. The illitisation of K-feldspar requires a source of acid, a sink for the released  $K^+$ , and does not take place as long as kaolinite or smectite is present (Bjørlykke & Aagaard, 1992). Kaolinite is sparse in these sandstones and approximately all smectite is illitised, so the presence of these clays cannot have restrained the illitisation of K-feldspar. Bleaching of the currently white sandstones shows that a source of acid must have been present, at least some time during burial, as will be addressed below. Consequently, the illitisation of K-feldspar was likely restrained by the high aqueous  $K^+$  activity during mesodiagenesis. The omnipresence of eogenetic, phreatic, AKF suggests that the  $K^+$  activity in the Buntsandstein formation water was already high upon entering the mesodiagenetic realm. Also, the paucity of mesogenetic albite can be explained by high K concentrations.

### 7.2.4. Bleaching and secondary porosity generation

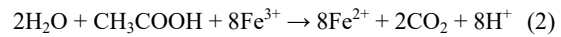
The process causing decolouration of red beds (Fig. 11A), by reduction of ferric iron that produces the typical reddish colours, is commonly referred to as bleaching (Glennie et al., 1978; Walker et al., 1978; Burley, 1984; Muechez et al., 1992; Parry et al., 2004; Haszeldine et al., 2005; Xie et al., 2021). Bleaching has been attributed to various kinds of reducing fluids, such as  $CO_2 - H_2S$  mixtures resulting from bacterial (Kirkland et al., 1995) or thermal sulphate reduction (Haszeldine et al., 2005), hydrocarbons (Surdam et al., 1993; Weibel & Friis, 2004; Schöner & Gaupp, 2005), methane (Ormö et al., 2004; Sundal et al., 2017; Xie et al., 2021), organic acids (Surdam & Crossey, 1985) and carbon monoxide (Haszeldine et al., 2005). Bleaching fluids generally need to contain only small quantities of the reductant (Ormö et al., 2004). Yet, the mobilisation of soluble  $Fe^{2+}$  is not strictly necessary for the decolouration of the sediment. Bleaching is generally controlled by flow paths.

Isolated, white reduction spots in some Buntsandstein red beds are attributed to the presence of organic matter, deposited with the sediment, which created small reducing settings and thus prevented reddening caused by precipitation of iron oxides (Weibel, 1998; Weibel & Friis, 2004 and references therein). All of them contain organic-rich clay or micrite clasts in their centres.

The bulk of the bleached Buntsandstein sandstones occurs in thick beds (several metres), which are often overlain by fine-grained, clayey layers. They make up about one-third of the reservoir in KB201, where the most complete section was cored. Compared to red reservoir sandstones, white horizons generally consist of coarser and more porous sandstones (Fig. 11A), features that were also recently described from Triassic fluvial red beds from southern Germany (Schmidt et al., 2020a). Apart from thick bleached beds and isolated reduction spots, also sections consisting of alternating coarser white and finer red layers were observed. All white sandstone horizons in the Buntsandstein are considered to be the bleached products of originally red sediments which is evident from numerous observations in white samples, of relics of red coats between quartz overgrowths and their host grains, and in carbonate cemented zones. These cements shielded the Fe-O/H in the

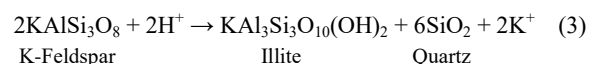
coats from the reducing pore fluids, thus inhibiting the bleaching process.

Bleaching in the studied Buntsandstein was most likely caused by organic acids generated by burial-related, thermocatalytic degradation of kerogen within the underlying Westphalian coal beds and organic-rich shales (Muechez et al., 1992) since most of the other mentioned reducing fluids do not originate within the Campine basin. The reactions (2), whereby organic acids (represented here by acetic acid) acted as electron donors for the reduction of ferric iron, produce  $CO_2$  and protons (Surdam & Crossey, 1985; Muechez et al., 1992).



The organic acids involved, and the  $CO_2$  and protons released in the bleaching reaction can result in secondary porosity generation by dissolution of feldspars or carbonates. Feldspar alteration induced by these reactions does not necessarily result in clay authigenesis, as even moderate concentrations of organic acids can increase the solubility of Al in brines, depending on the type of acid (Surdam & Crossey, 1985). Migration of organic acids through the Buntsandstein could thus explain the observed, considerably large, open intragranular porosity of K-feldspar grains. Creation of secondary porosity by carbonate dissolution, directly associated with the bleaching process, was less important. The  $CO_2$  produced by the redox reactions should dissociate in the formation water and increase the bicarbonate activity, thus enhancing carbonate stability with respect to other proton sinks such as feldspars. A redistribution of carbonate phases or recrystallisation to more stable carbonates can nevertheless be expected. Bleaching evidently causes the  $Fe^{2+}$  activity in the brine to rise, which increases the stability of Fe-carbonates with respect to calcite or dolomite (see discussion below).

The amount of iron oxides present in the red-coloured Buntsandstein sandstones of well KB201 averages 0.26 wt% (Muechez et al., 1992). The same authors made a reasonable estimate of the amount of organic acids produced by the maturation of organic matter in the Westphalian strata of the Campine Basin. A mass balance calculation illustrated that the organic acids had the potential to reduce vastly more ferric iron than the observed amount (Muechez et al., 1992). These calculations also show that not all the organic acid was consumed in the bleaching process and the  $CO_2$  and protons generated by the redox reactions had sufficient potential to create the observed secondary porosity by means of feldspar alteration. Muechez et al. (1992) considered the K-feldspar to alter to kaolinite, but at the burial conditions during which the bleaching took place, i.e. at higher temperatures and restricted flushing ( $K^+$  removal), K-feldspar is more likely to alter to illite (reaction 3).



Neither of both clays is present in sufficient quantities to account for the amount of presumably dissolved feldspar, implying that at least a considerable part of the Al released by feldspar dissolution was carried off by the bleaching fluids. Besides Al, evidently also Si and most likely K is released by feldspar dissolution. The Si could have precipitated as AQ, while the latter forms highly soluble ions, which easily have been carried away.

As mentioned before, organic acids can greatly increase the solubility of Al through the formation of Al-organic ligands, which decreases the required volumes of water to leach Al. Besides, it also explains the preferential leaching of feldspar

with respect to carbonates (which dissolve kinetically much faster and could thus neutralise the acids before significant feldspar dissolution takes place). The formation of Al-complexes also indirectly enhances the dissolution of feldspar, as it decreases the activity of  $\text{Al}^{3+}$  in solution. In addition, organic acids directly enhance feldspar dissolution by a ligand-mediated mechanism. The latter involves the adsorption of ligands to Al sites on the feldspar surface, the formation of Al-organic complexes at these sites, and the subsequent leaching of Al into solution. This mechanism was inferred from experimental work (Ullman & Welch, 2002). It appears to be specific to the type of organic acid and is not yet completely unravelled.

Bleaching was mainly restricted to the nowadays white horizons because of their better flow properties. Secondary porosity generation, on the other hand, appears not to have been restricted to the latter horizons. Many of the studied red samples have abundant secondary porosity, though they were not bleached. Yet, both processes are assumed to have been caused by the same fluids.

The two 'organic-acid consuming processes', i.e. feldspar dissolution and bleaching, are likely to have interacted. Evidently, the organic acid oxidised in the bleaching reaction (reaction 2) loses its complexation capacity. The  $\text{Fe}^{2+}$  released in the bleaching reaction could reduce the free-ligand activity (depending on the type of organic acid) and thus decrease the rate of feldspar dissolution, Al solubility and mobility.

The observation of secondary porosity in red sandstones suggests that mainly the bleaching capacity of the migrating fluids was restrained. Migration of acid-bearing fluids, maximal bleaching and depletion of the bleaching capacity occurred preferentially in the presently white horizons. The bleaching process cannot have consumed all the organic acids, as this would have seriously decreased the Al-leaching capacity of the fluids and consequently have resulted in clay authigenesis. Inhibition of bleaching by the formation of Al-organic ligands is also unlikely, as this would also halt feldspar dissolution. A more likely explanation is that the bleaching reaction itself (reaction 2) approached equilibrium due to the rising activity of its reaction products ( $\text{CO}_2$ ,  $\text{Fe}^{2+}$  and  $\text{H}^+$ ). This fluid, in equilibrium with  $\text{Fe}^{2+}$ , could then have leached the feldspar from the red sandstones without significant additional bleaching. This would also explain the occurrence of late diagenetic ankerite in red sandstones.

### 7.2.5. Mesogenetic carbonate cementation

Most of the studied samples contain euhedral, often saddle-shaped, carbonates. Genetic relations of these crystals with other diagenetic phases suggest a mesogenetic origin. EPMA mappings showed that these crystals generally have a relatively pure dolomitic core surrounded by ankeritic growth zones with an outward increasing Fe/Mg-ratio (Fig. 9E, 9F) and an outer sideritic rim. The cores of these carbonates often contain calcite inclusions, which are considered to be remnants of replaced grains. Also, the replacement of eogenetic dolomite was observed. BSEM petrography and EPMA element maps showed that the Fe-rich zones are better developed in bleached sandstones though they also occur in red sandstones. This is not reflected in the point counting data because the distinction could not always be made by means of transmitted light microscopy.

The mesogenetic origin is confirmed by fluid inclusion measurements, with an average homogenisation temperature of 124 °C and melting temperatures indicative of brines with high divalent cation content (Table 4). These carbonates could not be individually sampled for stable isotope analysis. Bulk rock isotope analyses seem not to correlate with the relative ankerite/dolomite content of the analysed samples (Fig. 12), which either

means that mesogenetic and eogenetic carbonates have similar isotopic compositions, or that the mesogenetic isotope signal is masked by the signature of the eogenetic carbonates, which are the dominant phase.

Bleaching of red beds in the Buntsandstein by organic acids expelled from the Westphalian (reaction 2) is a likely source of bicarbonate for the precipitation of mesogenetic carbonates. The measured C-isotopes are more or less compatible with an origin from organic acids (cf. Haszeldine et al., 2005), though generally slightly heavy (except the sample with highly depleted signature of -6.3‰). The observed depth trend in the C-isotopes (Fig. 17), however, cannot be explained by migrating bleaching fluids. The trend supports that the C-signatures are controlled by eogenetic carbonates. Measurements that deviate from the depth trend always have lower  $\delta^{13}\text{C}$ , which can be attributed to a contribution of more depleted carbon from oxidised organic acids.

Illitisation of smectitic clays, which originally constituted grain rims, was an important source of Ca and Mg for dolomite precipitation. This illitisation process likely took place at relatively low temperatures since the favourable K-supply and permeability of the sandstones. As the smectite was formed in the highly oxidising depositional Buntsandstein setting, its ferrous iron content must have been low. Illitisation consequently released dominantly Ca and Mg, which is reflected in the composition of the cores of the carbonate crystals.

The bleaching process was the main source of Fe for carbonate precipitation. The outwards increase of the Fe-content of the growth zones in the mesogenetic carbonates consequently reflects the relative importance of the latter process with respect to smectite conversion as cation source. The reduction of ferric iron likely was caused by the migration of organic acids, which could have induced carbonate dissolution, which extent was limited, as the contemporary oxidation of organic acids produced bicarbonate, thus decreasing the chemical affinity of carbonate dissolution reactions. Besides, the dissolution would have taken place contemporaneously with the precipitation of dolomite and ankerite. Therefore mainly calcitic phases are considered to have been susceptible to dissolution. Local dissolution of calcitic micrite clasts and pellets, and reprecipitation as dolomite or ankerite, offer an adequate explanation for the observed preservation of eogenetic C-isotopic signatures.

Oxygen isotopes are, in contrast to carbon isotopes, quite sensitive to temperature fractionation. The measured bulk  $\delta^{18}\text{O}$  values are rather low for carbonates formed in equilibrium with meteoric water enriched in heavy oxygen by evaporation. This suggests a significant contribution of isotopically lighter, mesogenetic carbonate to the measured bulk signatures. The mesogenetic signatures cannot be much lower than the lower range of the bulk measurements, as mesogenetic euhedral crystals are the dominant carbonate phase in some of the analysed bulk samples. Assuming that the mesogenetic dolomite has a  $\delta^{18}\text{O}$  between -8 and -6‰ V-PDB and precipitated at temperatures between 86 and 147 °C, water compositions would vary between 0 and +9‰ V-SMOW, using the fractionation equation of Land (1983). Precipitation of ankerite with the same isotopic composition, at the same temperatures, requires fluids with  $\delta^{18}\text{O}$  between +1 and +9‰ V-SMOW (fractionation equation of Fisher & Land, 1986; Fig. 16B). These signatures are reasonable for the expected brines, though the upper values are slightly high. Mesogenetic fluids in sedimentary basin are typically enriched in heavy oxygen due to advanced water-rock interactions, like the illitisation of smectite.

### 7.3. Telodiagenesis

Few telogenetic alterations were observed in the studied Buntsandstein samples. Yet, in four of the five studied wells, the top Buntsandstein corresponds to the erosional surface of the Cimmerian Unconformity (i.e., KB98, KB169, KB172 and KB201; Fig. 1). Bertier et al. (2008) showed that telogenetic alterations in the Westphalian sandstones, in wells where the Buntsandstein was eroded, correlate with the latter unconformity. Therefore also the Buntsandstein sandstones were exposed to surface-controlled conditions during the Mesozoic uplift.

The reason why few telogenetic alterations were observed is that the top of the Buntsandstein was not cored in any of the studied wells, and could consequently not be sampled. The impact of telogenetic processes is generally restricted to the first few metres or tens of metres below the erosional surface, as infiltrating waters tend to rapidly reach saturation with the major aqueous species (Shanmugan, 1990; Worden & Burley, 2003; Worden & Morad, 2003). The extent and spatial distribution of telodiagenesis is mainly controlled by the water flow through the exposed sediments, the long duration of the exposure, the warm and humid climate, and the gradual uplift and lowering of water table, while the very limited erosion likely relates to the gradual sea-level rise during the Cretaceous. The mineralogical composition of the strata suggests that the exposed sandstones had a relatively high buffering capacity for infiltrating meteoric fluids.

The upper 81 metres of the Buntsandstein in KB172 could not be sampled. The drilling report of this borehole mentions red to pinkish sand and poorly consolidated sandstone, for the top 66 metres (Dusar et al., 1987a). The poor consolidation of these sediments, in comparison to the underlying sandstones, resulted probably from telodiagenetic alteration. Most of the sediments directly underlying the Cimmerian Unconformity in the Campine Basin seem to be poorly consolidated (cf. the Neeroeteren Sandstone, Bertier et al., 2008).

In the upper two samples of KB172, limited dissolution of mesogenetic carbonates was locally observed. SEM petrography also revealed small, single kaolinite platelets, situated between the hairy authigenic illite of grain coats. These kaolinites are considered to have a telogenetic origin because of their occurrence on illitic coats and the fact that they are unaffected by illitisation. In borehole KB201, the upper 25 metres (806–831 m) of the Buntsandstein could not be sampled. Down to 813 m, partly bleached and decomposed sand was observed, overlying much less weathered fine-grained red sandstone, with again more weathering with increasing granulometry. No information is available on the nature of the sediments constituting the top of the formation at this location. The studied samples from the core top do not show clear telogenetic alterations, except for insignificant amounts of kaolinite seen by SEM. In the studied samples of the other wells, KB64, KB98 and KB169, no telogenetic alterations were observed as no rocks decomposed by Cretaceous meteoric alteration were cored.

The diagenetic history described in sections 7.1. to 7.3. is summarised in Figure 18.

### 7.4. Open versus closed system diagenesis

In the literature, the discussion as to whether porosity can be increased or not through dissolution of rock constituents (detritals and/or cements) during burial diagenesis is still ongoing (Schmidt & McDonald, 1979, 1980; Bjørlykke, 1984; Surdam et al., 1984; Surdam & Crosse, 1985; Burley, 1986; Gluyas & Coleman, 1992; Milliken et al., 1994; Giles & Marshall, 1986; Giles, 1997; Land, 1997; Wilkinson et al.,

1997; Burley & Worden, 2003; Bjørlykke, 2011; Bjørlykke & Jahren, 2012; Worden et al., 2018; Quandt et al., 2022). The critical question here is whether secondary porosity is redistributional (without real gain in total porosity) or enhanced (i.e., with a real increase in total porosity). One of the problems here is that differentiation between these two types of secondary porosity cannot be based on petrography alone, since the samples studied are not Representative Elementary Volumes (REV) and it is often not possible to accurately quantify the volume of phases dissolved at grain contacts, along stylolites or along thin clay rims, that at other places may cause cementation. Recognition of moldic intragranular secondary porosity, however, is easy, but inferring the amount of intergranular secondary porosity is often subjective. Also, as in the case presented here, it is often also difficult to quantify the volume of burial-related cement, since these cements formed in the eogenetic as well as in the mesogenetic realm.

Mesogenetic secondary porosity development was recognised in the studied strata, within the bleached as well as red-coloured strata. The latter lithologies were more affected by chemical compaction as testified by the more frequent existence of stylolites. This led to a net export of dissolution products such as silica, that was redistributed to other surrounding sandstones, such as the coarser grained bleached sandstones that acted as a sink, since this mesogenetic AQ cement type is more common in these sandstones. As stated above, based on mass balance calculations, Muchez et al. (1992) calculated that the released amount of fluids with dissolved organic acids was more than enough for explaining the observed iron-reduction, even without taking the intercalated organic Westphalian shales into account (see also Vandewijngaerde et al., 2016). Part or all of the released ferric iron was incorporated into the mesogenetic zoned ankerite and siderite, indicating that the system with regard to Fe acted as a (partly) closed system. These organic-rich fluids also can explain the leaching of feldspars. Since no vast amounts of mesogenetic authigenic clays were identified, the system acted as an open system exporting feldspar-related constituents. Some authors (e.g., Bjørlykke, 2011; Bjørlykke & Jahren, 2012) argue that open diagenetic systems do not exist in the burial realm often relying on data acquired from hydrocarbon reservoir systems that by their nature indeed can be considered as closed systems. The studied Buntsandstein, however, testifies of the interaction of large volumes of diagenetic reactive fluids that have passed through the sandstones, bleaching some of them and leaching specific minerals, like the feldspars. Some components gave rise to new cement phases, but others likely were exported, taking the huge fluid flux through the system into account. This study thus reports on a contrasting setting where the sandstones are not sealed by impermeable lithologies. That is likely one of the major reasons why the diagenetic system was partly open with regard to enhanced secondary porosity development. The bleached/non-bleached nature of the sandstones also testifies to a preferential and channelized fluid flow enriched in organic acids.

### 7.5. Reservoir Quality

The porosity (5.3–20.2%, average 13.7%) and permeability (0.02–296.4 mD, average 38.7 mD) of the studied sandstones were analysed on 26 samples, of which the mineralogy was quantified by means of point counting (Table 2). The acquired porosity and permeability values are in the same order of magnitude as unpublished results (Blyskowska & Vankerk, 1986; Corelab, 1990). This dataset, combined with previous results, was used to draw some conclusions on the effect of diagenesis on the Buntsandstein reservoir properties in the Campine Basin. Since the latter is a potential target for

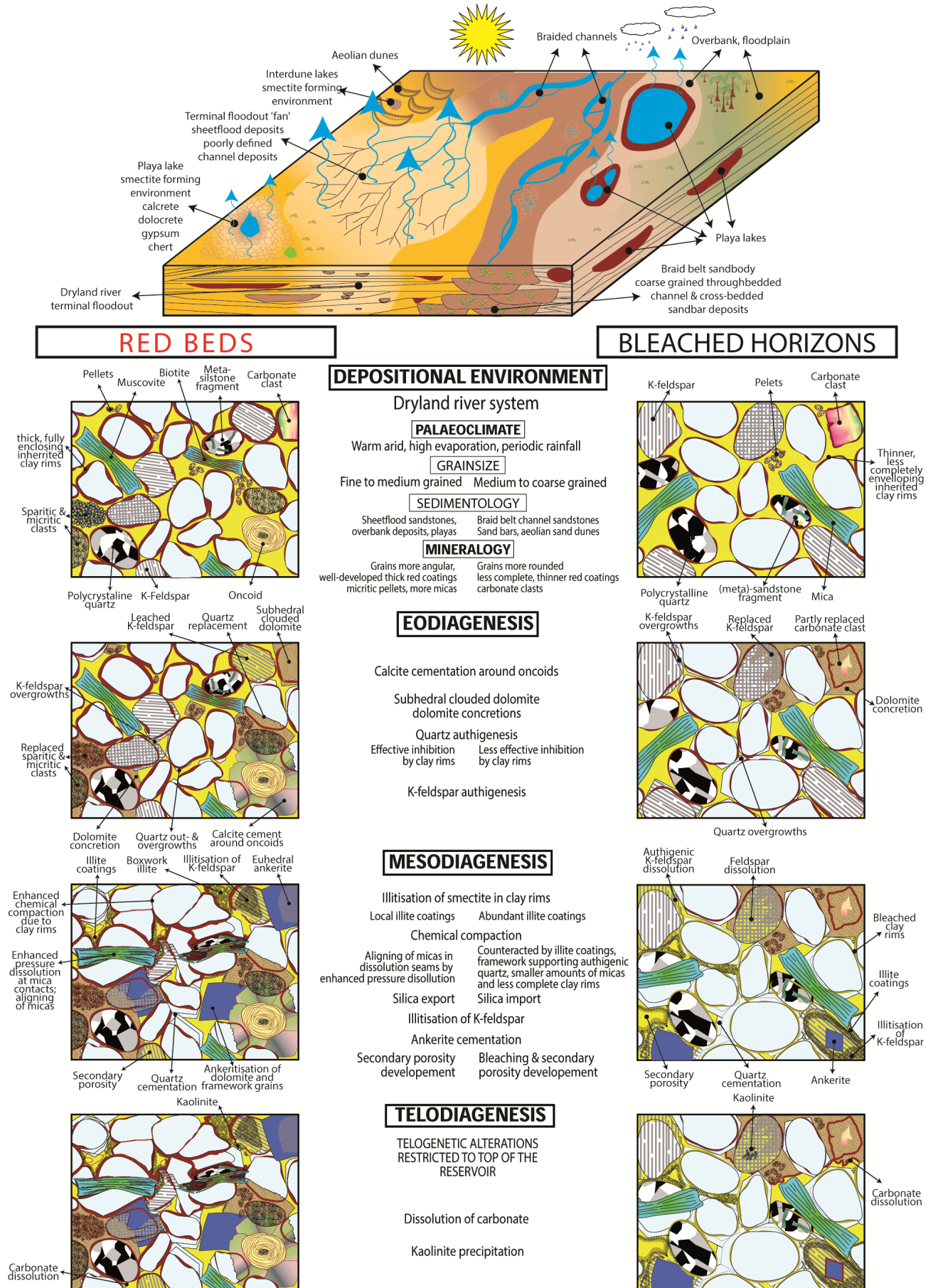


Figure 18. Schematic summary of the diagenetic history of the Buntsandstein in the Campine Basin.

underground sequestration of CO<sub>2</sub> and/or geothermal energy (and possibly also as hydrocarbon reservoirs in small structural-sedimentary traps in the Roer Valley Graben), also the reactivity of the reservoir will be addressed.

### 7.5.1. Porosity

The total carbonate content of the studied sandstones may amount up to 37%, of which the major part relates to eogenetic cloudy dolomite. Yet, the total carbonate content in the studied samples does not correlate with their He-porosity (Fig. 19). The clouded dolomite replaces both detrital and eogenetic calcite phases and is replaced by mesogenetic ankerite. The latter is an important porosity-occluding phase relative to the dolomite, however, only in a few samples. The bulk of the dolomite is found in nodules or cemented zones, of which the minus cement porosity is visibly larger than that of the adjacent sandstone matrix implying that the dolomite, and the bigger part of the ankerite that replaces it, occupies porosity that otherwise would have been destroyed by compaction. The porosity filled by carbonate cements is in samples with less carbonate taken in by framework grains, which disturbs the expected negative correlation between porosity and carbonates.

Also, the AQ content does not correlate with the He-porosity of the studied samples (Fig. 19). Here a similar explanation can be invoked. Petrography revealed that a considerable part of the AQ is eogenetic, which implies that the pore space it occupies would have been destroyed by compaction if it were not there. In addition, eogenetic AQ exerts a framework-stabilising effect since it increases the mechanical strength of the sandstone matrix, making it less susceptible to compaction. Hence, less primary porosity is destroyed by compaction, which compensates for the porosity occluded by the quartz cement. The absence of a positive correlation between AQ and porosity contrast with results recently published by Schmidt et al. (2020b), Busch et al. (2022) and Quandt et al. (2022).

No distinction was made between primary and secondary porosity in point counting. Secondary porosity is present in some mainly red samples as well-rounded pores. These pores have the size of the framework grains and do not contain any alteration products that could reveal their origin. The rounded shape, however, suggests that they might result from the dissolution of detrital carbonates. The bulk of the secondary pores in the studied samples result from feldspar alteration as evidenced by relicts in pores and the abundance of open dissolution voids in feldspar grains and their overgrowths. But this is not reflected in a negative correlation between feldspar content and He-porosity (Fig. 19). Conversely, feldspar content correlates positively with porosity, which suggests that the impact of feldspar dissolution was limited. Samples with high primary feldspar content still contain most of that original feldspar population, though the grains have significant intragranular porosity. Quandt et al. (2022) also reported that secondary porosity predominantly originated from K-feldspar dissolution.

Red sandstones have lower porosities than their coarser grained white counterparts. They contain more clay, thicker coats, often more carbonate and are more affected by chemical compaction. Yet, the lower porosity is also partly a primary effect. The red Buntsandstein horizons generally correspond to finer grained lithologies. Notice, however, that red sandstones also can have good poroperm characteristics. The effect of grain size with coarser grained lithologies possessing better reservoir quality has been reported by several authors from Buntsandstein and other red beds (e.g., Kunkel et al., 2018, Scorgie et al., 2021, Busch et al., 2022, Quandt et al., 2022).

There is no clear correlation between porosity of the

analysed samples and their depth, which underlines the limited impact of mesogenetic processes on porosity. Also, the depth beneath the Cimmerian Unconformity does not correlate with porosity (with the abstraction made of the top subcrop weathering zone associated with the Cretaceous palaeosol). Such a correlation would be expected where telogenetic alterations controlled porosity. Unfortunately, no cores from the top of the reservoir were available for analysis.

There is also no clear correlation between point-counted porosity and He-porosity (Table 2). This feature has also been noticed by Quandt et al. (2022) and their explanation, namely the contribution of heterogeneous occurrence of microporosity, is likely also valid in our study. Indeed microporosity is not visible using standard thin-section microscopy. Therefore porosity determined by point counting likely will be underestimated (Schmidt et al., 2020b).

### 7.5.2. Permeability

None of the point counting phases correlates well with permeability, suggesting that several processes, of which none has a dominant effect, control permeability. Samples with abundant and thick clay rims and coats generally have low permeabilities and samples in which the latter are less abundant tend to have higher permeabilities (Fig. 20). Nevertheless, some samples with low amounts of rims/coats also have low permeabilities. Petrography showed that the rims/coats obstruct pore throats. Although the rims are more abundant, the effect of the coats (radial illite crystals, extend to boxwork illite in bigger pores) is probably more devastating for the permeability. The coats are more abundant in white than in red sandstones. This is not reflected in the permeability results because the white samples often have high primary porosities. The AQ content of the samples does not correlate well with their permeability. Some samples with low permeability have high AQ contents, others low. Most samples with high permeabilities have relatively high AQ contents, which can be attributed to the framework stabilising effect of the eogenetic quartz, but also to the fact that white, coarse-grained samples contain more AQ. Also, the carbonate content consisting of eogenetic concretions does not correlate with permeability. Their restricted spatial distribution limits their effect on permeability.

The petrographic study revealed the presence of a lot of bedding parallel dissolution seams, which are located mainly in the finer grained red sandstones. They were attributed to mica-illite-induced dissolution, at the contacts of clay rims and muscovite flakes with quartz grains. The clays/micas accumulate in the dissolution seams, to form stylolite-like bedding parallel layers. These are likely to be far less permeable than the sandstone matrix and therefore contribute to vertical permeability barriers in the finer grained layers within the reservoir. This effect is not reflected in the permeability dataset, which only contains horizontal measurements.

In the case of CO<sub>2</sub> storage, a minimal permeability of 0.1 mD (10<sup>-16</sup>m<sup>2</sup>) is required for efficient injection (Bachu et al., 2007). For the studied sandstones this corresponds to a porosity of about 8%. The bulk of the analysed samples have higher permeabilities than this threshold. All samples with lower permeabilities are fine-grained red sandstones, mainly present at the base of the formation (Gruitrode Member).

### 7.5.3. Reactivity

The reactivity of the mineral assemblage of reservoir sandstones towards CO<sub>2</sub>-saturated, acidic brines is an important parameter in the evaluation of the suitability of a reservoir for underground disposal of CO<sub>2</sub>. Fast dissolution of minerals near CO<sub>2</sub> injection wells can cause well instability, while mineral precipitation near an injection point can decrease the efficiency of such injection.

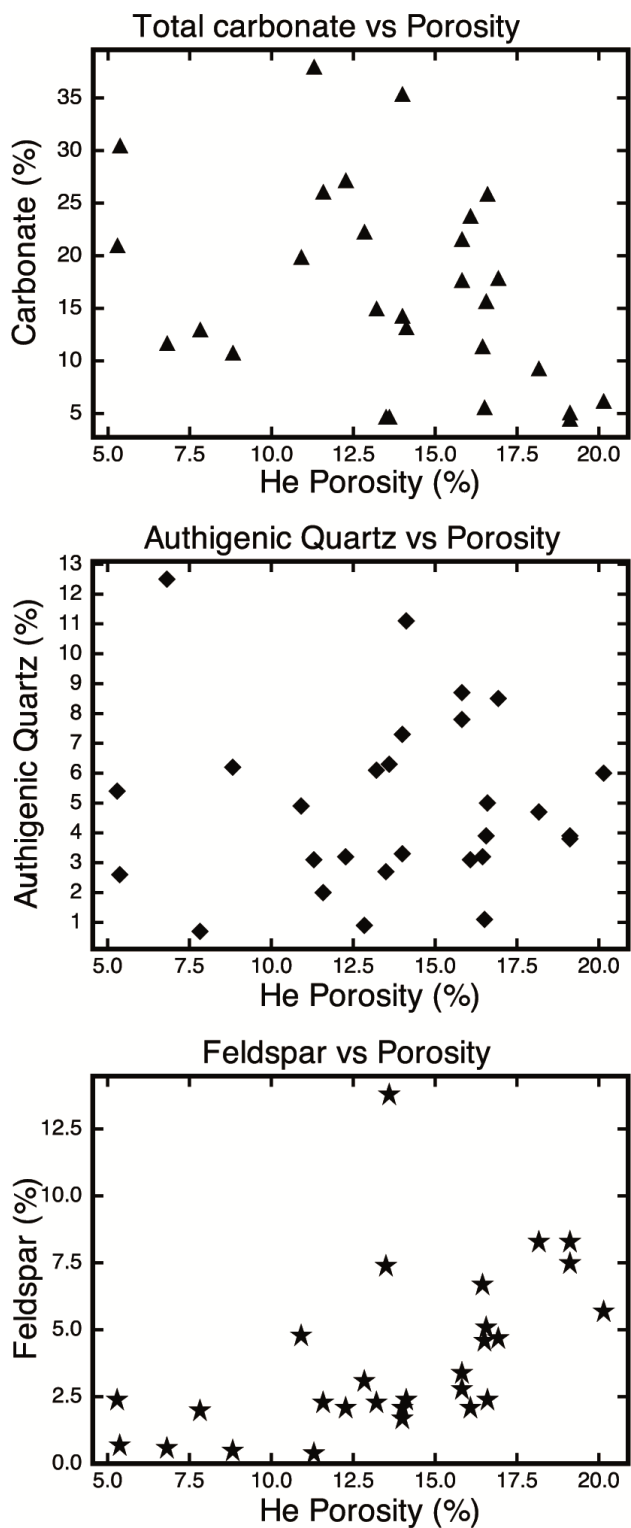


**Figure 19.** Plots of carbonate, authigenic quartz and feldspar contents versus porosity. Petrography shows that carbonate cements and authigenic quartz are important porosity occluding phases in the Buntsandstein, yet these are clearly not the major controls on the porosity of the reservoir. The feldspar content shows a positive correlation with porosity. Feldspar grains were partly leached by fluids containing organic acids. The resulting secondary porosity makes up a substantial part of the total porosity. The correlation reflects the fact that samples with high primary feldspar contents still contain high amounts of feldspars, though the intragranular secondary porosity from feldspar leaching is substantial.

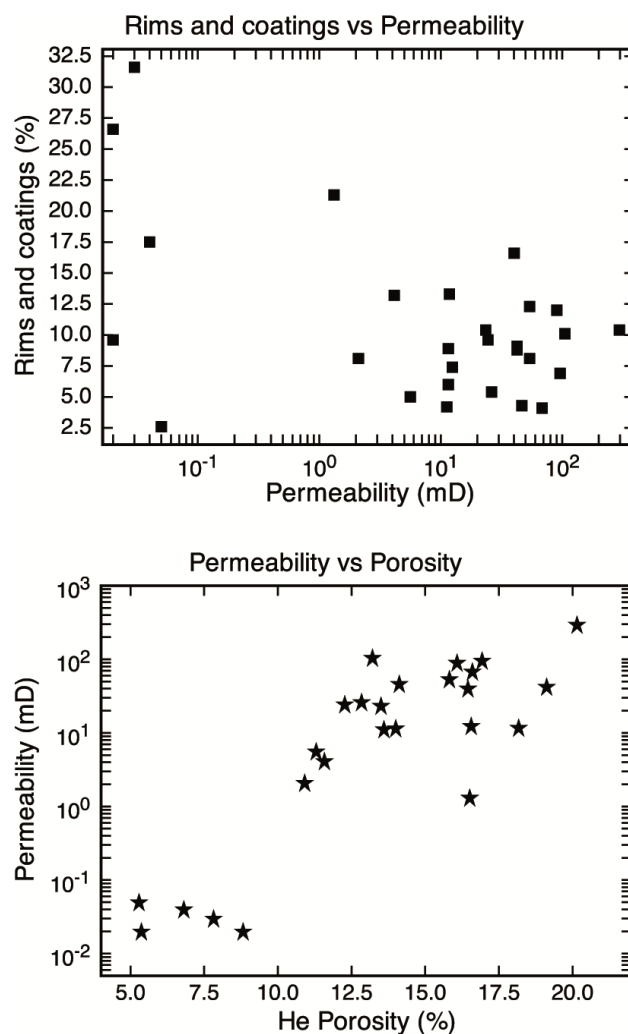


**Figure 20.** Plots of the amount of clay rims/coats and porosity versus permeability. Rims and coatings affect permeability, but samples with low permeability do not necessarily have high amounts of grain rims/coatings. The porosity/permeability plot shows that the bulk of the analysed samples has permeabilities above the threshold value for CO<sub>2</sub> storage of 0.1 mD.

In the long term, mineral alterations induced by CO<sub>2</sub> injection could lead to carbonate precipitation, which is a stable mechanism for long-term containment of the injected gas in a reservoir.

Short-term reactivity, which could affect injection, requires fast mineral reaction kinetics. In the studied Buntsandstein, carbonates are the only constituents that are likely to react sufficiently fast. The sandstones contain on average 15.8% of carbonate, of which the bulk constitutes eogenetic dolomite concretions. These carbonates clearly formed before compaction, as the framework of these concretions is barely grain supported and their quartz grains are partly replaced by the carbonate cement. In extreme cases, when the flow of CO<sub>2</sub>-saturated water is high, e.g., near an injection point, the concretions could be leached, which might lead to local framework collapse and mechanical instability. Overall, dissolution of mesogenetic carbonates has far less effect on the mechanical stability of the rocks, since these phases are present in primary and secondary pores, which are presumed to be framework supported because they formed after the main phase of compaction. Carbonate dissolution would create extra porosity but is not considered to have a substantial effect on permeability, as the bulk of the carbonate is locally concentrated

in concretions.

The studied sandstones contain substantial amounts of feldspars (average 5.3%). EPMA showed these are chiefly K-feldspars, with minor amounts of diagenetic albite. Since no anorthite is present, feldspar alteration is not a source of divalent cations for mineral trapping of injected CO<sub>2</sub>. Alteration of alkali feldspars in acidic CO<sub>2</sub>-saturated water would release K<sup>+</sup> and Na<sup>+</sup> ions, since at low K<sup>+</sup>/H<sup>+</sup> activities the main alteration product would be kaolinite. Such alteration could substantially enhance the ionic trapping capacity of the reservoir brine. Both proton consumption by the alteration reaction and the release of the monovalent cations increase the stability of aqueous bicarbonate species with respect to dissolved CO<sub>2</sub>. Given the present reservoir temperature, at which the mobility of aqueous Al and Si are low, the feldspar alteration products will mostly precipitate in situ and thus have little effect on permeability.

The overall potential for mineral trapping of the studied reservoir likely is low, due to the lack of non-carbonate mineral sources of divalent cations for carbonate precipitation. The clay content mostly consists of illite, which is rather unreactive in CO<sub>2</sub>-saturated brines and also contains only small amounts of divalent cations compared to other clays like smectites. The Fe-O/H content of the sandstones offers some potential for mineral trapping, but that would require reduction of the ferric iron, and thus the presence of a reducing agent. Pyrite dissolution could supply reduced sulphur species, which could reduce the Fe<sup>3+</sup>, but the pyrite content is low.

## 8. Conclusions

The effect of diagenesis on the Buntsandstein (Early Triassic) reservoir quality in the Campine Basin (NE Belgium) was assessed from a petrographic study complemented with fluid inclusion microthermometry, stable isotope, X-ray diffraction, electron microprobe analyses, and porosity-permeability measurements.

The following conclusions can be drawn:

- the sandstones of the Buntsandstein in the Campine Basin were deposited within a dryland river system, in a warm, mostly arid climate with episodic rainfall and high evaporation rates.
- during wetter periods feldspars and other less stable constituents were (partially) dissolved.
- strong evaporation during dry periods led to reprecipitation of the dissolved species as K-feldspar and quartz overgrowths, smectite and calcite/dolomite. Carbonates precipitated as nodules, which had little effect on the reservoir since they mainly fill primary porosity that would otherwise have been destroyed by compaction.
- reworking of the sediment in the depositional environment resulted in coats of the framework grains by inherited clay rims. These rims are better developed (thicker and more completely enveloping the grains) in finer grained sheet flood sandstones, overbank, and playa-lake deposits, than in the coarser grained sediments from braided belt channels, sandbars, and aeolian dune environments.
- the typical red colour of the sandstones arises from the presence of small amounts of Fe-oxide/hydroxides in the inherited clay rims.
- the original smectite composing the rims converted to illite during burial.
- the tangential orientation of the clay platelets in the rims led to illite-mica-induced dissolution during burial/compaction, which is manifested as bedding parallel dissolution seams. The latter are most prominent in the finer grained sediments, where the rims were better developed and effectively

inhibited precipitation of framework supporting authigenic quartz.

- the dissolution seams are filled with clay and micas and thus constitute important barriers to the vertical permeability of the reservoir.
- the silica released from the illite-mica-induced dissolution of quartz grains did not precipitate in the red sandstones but was exported (at mm to dm scale) to nearby bleached horizons, where nucleation inhibiting clay rims are less well developed.
- migration of fluids rich in organic acids, expelled from the underlying Carboniferous coal-bearing strata, resulted in local bleaching of sediments. This bleaching mainly affected the coarser grained horizons, which were more susceptible because of their lower Fe-oxide/hydroxide contents and higher intrinsic permeability. In the finer grained sediments, the original red colour was mostly preserved, which suggests that the reductive capacity of the fluid was limited.
- the bleaching reaction produced CO<sub>2</sub> or bicarbonate, which is not clearly reflected in the isotopic signatures of the carbonate cements. The latter show a clear eogenetic depth trend, which was attributed to climate changes during deposition.
- leaching of feldspar grains by the organic acids responsible for the bleaching, resulted in substantial amounts of open grain dissolution porosity.
- tectogenetic alteration in the studied sandstones was minor, however the critical intervals below the Cimmerian Unconformity could not be sampled.
- the porosity (5.3–20.2%, average 13.7%) and permeability (0.02–296.4 mD, average 38.7 mD) of the Buntsandstein make it a suitable reservoir for CO<sub>2</sub> storage or other geo-energy options (e.g., geothermal energy). The best reservoir properties are found in the bleached horizons. In these, the primary porosity was better preserved due to eogenetic framework supporting quartz cements, which counteracted mechanical compaction. In addition, the bulk of the secondary porosity is situated in the white beds.
- the reactivity of the Buntsandstein with CO<sub>2</sub>-rich brines is considered to be low.

## Acknowledgements

This work was supported by a research grant to P. Bertier by VITO, the Flemish Institute of Technological Research. Sample material was kindly provided by the Geological Survey of Belgium (Dr M. Dusar). Stable isotope analyses were carried out at the Institute of Geology and Mineralogy in Erlangen (Germany) by Prof. M. Joachimsky. We would like to thank Herman Nijs, who skilfully prepared the studied thin sections, and Dirk Steeno, for his invaluable technical assistance. P. van Tongeren is thanked for the stimulating discussions. We also thank the reviewers, Dr Michiel Dusar, Dr Richard Worden, and an anonymous reviewer for their constructive remarks. Dr Reinhard Gaupp is also thanked for reviewing a former version of the manuscript.

## Author contributions

The concept of this study was perceived by RS and RD. PB performed the optical petrography, the XRD-diffraction and geochemical analyses under supervision of RS, BL and RD. PB and RK did the SEM petrography and electron microprobe measurements. Data was interpreted by PB, RS and BL. PB and RS wrote the manuscript.

## Data availability

All studied samples are stored in the core repository of the Geological Survey of Belgium. Thin sections are stored in the collection of the Geology department of KU Leuven.

## References

- Ajdukiewicz, J.M. & Larese, R.E., 2012. How clay grain coats inhibit quartz cement and preserve porosity in deeply buried sandstones: Observations and experiments. *American Association of Petroleum Geologist Bulletin*, 96, 2091–2119. <https://doi.org/10.1306/02211211075>
- Ali, A.D. & Turner, P., 1982. Authigenic K-feldspar in the Bromsgrove Sandstone Formation (Triassic) of Central England. *Journal of Sedimentary Petrology*, 52, 187–197. <https://doi.org/10.1306/212F7F09-2B24-11D7-8648000102C1865D>
- Allan, J.R. & Matthews, R.K., 1982. Isotope signatures associated with early meteoric diagenesis. *Sedimentology*, 29, 797–817. <https://doi.org/10.1111/j.1365-3091.1982.tb00085.x>
- Bachmann, G.H., Geluk, M.C., Warrington, G., Becker-Roman, A., Beutler, G., Hagdorn, H., Hounslow, M.W., Nitsch, E., Röhling H.-G., Simon, T. & Szulc, A., 2010. Triassic. In Doornenbal, H. & Stevenson A. (eds), *Petroleum Geological Atlas of the Southern Permian Basin Area*. European Association of Geoscientists and Engineers Publications, Houten, 149–173.
- Bachu, S., Bonijholly, D., Bradshaw, J., Burruss, R., Holloway, S., Christensen, N.P. & Mathiassen, O.M., 2007. CO<sub>2</sub> storage capacity estimation: Methodology and gaps. *International Journal of Greenhouse Gas Control*, 4, 430–443. [https://doi.org/10.1016/S1750-5836\(07\)00086-2](https://doi.org/10.1016/S1750-5836(07)00086-2)
- Baron, M.J. & Parnell, J., 2007. Relationships between stylolites and cementation in sandstone reservoirs: Examples from the North Sea, U.K. and East Greenland. *Sedimentary Geology*, 194, 17–35. <https://doi.org/10.1016/j.sedgeo.2006.04.007>
- Bertier, P., Swennen, R., Lagrou, D., Laenen, B. & Kemps, R., 2008. Palaeo-climate controlled diagenesis of the Westphalian C & D fluvial sandstones in the Campine Basin (north-east Belgium). *Sedimentology*, 55, 1375–1417. <https://doi.org/10.1111/j.1365-3091.2008.00950.x>
- Bjørkum, P.A., 1996. How important is pressure in causing dissolution of quartz in sandstones? *Journal of Sedimentary Research*, 66, 147–154. <https://doi.org/10.1306/D42682DE-2B26-11D7-8648000102C1865D>
- Bjørlykke, K., 1984. Formation of secondary porosity: How important is it? In McDonald, D.A. & Surdam, R.C. (eds), *Clastic Diagenesis*. American Association of Petroleum Geologist, Tulsa, Memoir, 37, 277–286. <https://doi.org/10.1306/M37435C16>
- Bjørlykke, K., 2011. Open-system chemical behaviour of Wilcox Group mudstones: How is large-scale mass transfer at great burial depth in sedimentary basins possible? A discussion. *Marine and Petroleum Geology*, 28, 1381–1382. <https://doi.org/10.1016/j.marpetgeo.2011.01.009>
- Bjørlykke, K. & Aagaard, P., 1992. Clay minerals in North Sea sandstones. In Houseknecht, D.W. & Pittman, E.D. (eds), *Origin, Diagenesis, and Petrophysics of Clay Minerals in Sandstones*. SEPM Special Publication, 47, 65–80. <https://doi.org/10.2110/pec.92.47.0065>
- Bjørlykke, K. & Egeberg, P.K., 1993. Quartz cementation in sedimentary basins. *American Association of Petroleum Geologist Bulletin*, 77, 1538–1548. <https://doi.org/10.1306/BDFF8EE8-1718-11D7-8645000102C1865D>
- Bjørlykke, K. & Jahren, J., 2012. Open or closed geochemical systems during diagenesis in sedimentary basins: Constraints on mass transfer during diagenesis and the prediction of porosity in sandstone and carbonate reservoirs. *American Association of Petroleum Geologist Bulletin*, 96, 2193–2214. <https://doi.org/10.1306/04301211139>
- Bjørlykke, K., Aagaard, P., Dypvik, H., Hasting, D.S. & Harper, A.S., 1986. Diagenesis and reservoir properties of Jurassic sandstones from the Haltenbanken area, offshore mid Norway. In Spencer, A.M. et al. (eds), *Habitat of Hydrocarbons on the Norwegian Continental Shelf*. Graham & Trotman, London, 275–286.
- Bjørlykke, K., Line, L.H., Jahren, J., Mondol, N.H., Aagaard, P. & Hellevang, H., 2017. Compaction of Sand and Clay – Constraints from Experimental Compaction, Chemical Reactions and Fluid Flow During Burial – an Overview. *AAPG online journal* [https://www.searchanddiscovery.com/documents/2017/51449bjorlykke/ndx\\_bjorlykke.pdf](https://www.searchanddiscovery.com/documents/2017/51449bjorlykke/ndx_bjorlykke.pdf), accessed 15/09/2022.
- Bloch, S., Lander, R.H. & Bonnel, L., 2002. Anomalously high porosity and permeability in deeply buried sandstone reservoirs: origin and predictability. *American Association of Petroleum Geologist Bulletin*, 86, 301–328. <https://doi.org/10.1306/61EEDABC-173E-11D7-8645000102C1865D>
- Blyskowska, E. & Vanker, R., 1986. Unpublished Labofina report for the Belgian Geological Survey.
- Burley, S.D., 1984. Patterns of diagenesis in the Sherwood Sandstone Group (Triassic), United Kingdom. *Clay Minerals*, 19, 403–440. <https://doi.org/10.1180/claymin.1984.019.3.11>
- Burley, S.D., 1986. The development and destruction of porosity within Upper Jurassic reservoir sandstones of the Piper and Tartan fields, Outer Moray Firth, North Sea. *Clay Minerals*, 21, 649–694. <https://doi.org/10.1180/claymin.1986.021.4.14>
- Burley, S.D. & Worden R.H., 2003. *Sandstone Diagenesis: Recent and Ancient*. Oxford, Blackwell Publishing Ltd., 649 p. <https://doi.org/10.1002/9781444304459>
- Busch, B., Hilgers, Ch. & Adelman, D., 2020. Reservoir quality controls on Rotliegend fluvio-aeolian wells in Germany and the Netherlands, Southern Permian Basin – Impact of grain coatings and cements. *Marine and Petroleum Geology*, 112, 112104075. <https://doi.org/10.1016/j.marpetgeo.2019.104075>
- Busch, B., Adelman, D., Herrmann, R. & Hilgers, C., 2022. Controls on compactional behavior and reservoir quality in a Triassic Buntsandstein reservoir, Upper Rhine Graben, SW Germany. *Marine and Petroleum Geology*, 136, 105437. <https://doi.org/10.1016/j.marpetgeo.2021.105437>
- Colson, J. & Cojan, I., 1996. Groundwater dolocretes in a lake-marginal environment: an alternative model for dolomite formation in continental settings (Danian of the Provence Basin, France). *Sedimentology*, 43, 175–188. <https://doi.org/10.1111/j.1365-3091.1996.tb01466.x>
- Corelab, 1990. Unpublished report from 12 July 1990 for the Belgische Geologische Dienst.
- Catto, B., Jahner, R.J., Warren, L.V., Varejao, F.G. & Assine, M.L., 2016. The microbial nature of laminated limestones: lessons from the Upper Aptian, Araripe Basin, Brazil. *Sedimentary Geology*, 341, 304–315. <https://doi.org/10.1016/j.sedgeo.2016.05.007>
- Choquette, P.W. & Pray, L.C., 1970. Geologic nomenclature and classification of porosity in sedimentary carbonates. *American Association of Petroleum Geologist Bulletin*, 54, 207–250. <https://doi.org/10.1306/5D25C98B-16C1-11D7-8645000102C1865D>
- Cyziene, J., Molenaar, N. & Sliupa, S., 2006. Clay-induced pressure solution as a Si source for quartz cement in sandstones of the Cambrian Deimena Group. *Geologija*, 53, 8–21.
- De Ros, L.F., Sgarbi, G.N.C. & Morad, S., 1994. Multiple authigenesis of K-feldspar in sandstones; evidence from the Cretaceous Areado Formation, Sao Francisco Basin, central Brazil. *Journal of Sedimentary Research*, 64, 778–787. <https://doi.org/10.1306/D4267EBF-2B26-11D7-8648000102C1865D>
- Dewers, T. & Ortoleva, P., 1991. Influences of clay minerals on sandstone cementation and pressure solution. *Geology*, 19, 1045–1048. [https://doi.org/10.1130/0091-7613\(1991\)019<1045:IOCMOS>2.3.CO;2](https://doi.org/10.1130/0091-7613(1991)019<1045:IOCMOS>2.3.CO;2)

- Dickson, J.A.D., 1966. Carbonate identification and genesis as revealed by staining. *Journal of Sedimentary Research*, 36, 491–505. <https://doi.org/10.1306/74D714F6-2B21-11D7-8648000102C1865D>
- Dufour, F.Ch. & Heederik, J.P., 2019. Early Geothermal Exploration in the Netherlands 1980 – 2000. *European Geothermal Congress 2019*, Den Haag, The Netherlands, 11-14 June 2019, 10 p.
- Dusar, M., Bless, M.J.M., Borremans, G., Bouckaert, J., Burger, K., Lie, S.F., Muech, P., Paproth, E., Piérart, P., Somers, Y., Streef, M., Van Looy, J. & Viaene, W., 1987a. De steenkoolverkenningboring Gruitrode - Muisvenner Bemden (Boring 169 van het Kempens Bekken). *Belgische Geologische Dienst, Professional Paper*, 228, 107 p.
- Dusar, M., Bless, M.J.M., Borremans, G., Burger, K., De Loose, J., Fairon-Demaret, M., Felder, P.J., Gullentops, F., Lie, S.F., Muech, P., Paproth, E., Piérart, P., Rossa, H.G., Smolderen, A., Somers, Y., Steurbaut, E., Streef, M., Viaene, W., Witte, H. & Wouters, L., 1987b. De steenkoolverkenningboring Gruitrode - Ophovenderheide (boring 172 van het Kempens Bekken). *Belgische Geologische Dienst, Professional Paper*, 230, 235 p.
- Dusar, M., Langenaeker, V. & Wouters, L., 2001. Permian-Triassic-Jurassic lithostratigraphic units in the Campine basin and the Roer Valley Graben (NE Belgium). *Geologica Belgica*, 4, 107–112. <https://doi.org/10.20341/gb.2014.047>
- Ehrenberg, S.N. & Nadeau, P.H., 1989. Formation of diagenetic illite in sandstones of the Garn Formation, Haltenbanken area, mid-Norwegian continental shelf. *Clay Minerals*, 24, 233–253. <https://doi.org/10.1180/claymin.1989.024.2.09>
- Feist-Burkhardt, S., Götz, A.E., Szulc, J., Borkhataria, R., Geluk, M., Haas, J., Hornung, J., Jordan, P., Kempf, O., Michalik, J., Nawrocki, J., Reinhardt, L., Ricken, W., Röhling, H-G., Ruffer, T., Török, A. & Zühlke, R., 2008. Triassic. In McCann, T. (ed.), *The Geology of Central Europe. Volume 2: Mesozoic and Cenozoic*. Geological Society, London, 749–821. <https://doi.org/10.1144/CEV2P.1>
- Fermont, W., Jegers, L. & Dusar, M., 1994. A model study of coalbed methane generation in well Peer (KB206) Belgium. *Rijks Geologische Dienst, Haarlem, internal paper*, 67 p.
- Fisher, Q.J. & Land, L.S., 1986. Diagenetic history of the Eocene Wilcox sandstones, South-Central Texas. *Geochimica et Cosmochimica Acta*, 50, 551–561. [https://doi.org/10.1016/0016-7037\(86\)90104-3](https://doi.org/10.1016/0016-7037(86)90104-3)
- Fisher, Q.J., Knipe, R.J. & Worden, R.H., 2000. Microstructures of deformed and non-deformed sandstones from the North Sea: implications for the origins of quartz cement in sandstones. In Worden, R.H. & Morad, S., *Quartz Cementation in Sandstones*. Blackwell, Oxford, Special Publication of the International Association of Sedimentologists, 29, 129–146. <https://doi.org/10.1002/9781444304237.ch10>
- Flügel, E., 2004. *Microfacies of Carbonate Rocks: Analysis, Interpretation and Application*. Springer, Berlin, 976 p. <https://doi.org/10.1007/978-3-662-08726-8>
- Folk, R.L., 1974. *Petrology of Sedimentary Rocks*. 2nd ed. Hemphill Press, Austin, TX, 182 p.
- Fontaine, J.M., Guastella, G., Jouault, P. & de la Vega, P., 1993. F15-A: a Triassic gas field on the eastern limit of the Dutch Central Graben. In Parker, J.R. (ed.), *Petroleum Geology of Northwest Europe: Proceedings of the 4th conference*. Geological Society, London, *Petroleum Geology Conference Series*, 4, 583–593. <https://doi.org/10.1144/0040583>
- Garcia, A.J.V., Morad, S., de Ros, L.F. & Al-Aasm, I.S., 1998. Palaeogeographical, palaeoclimatic and burial history controls on the diagenetic evolution of reservoir sandstones: evidence from the lower Cretaceous Serraria Sandstones in the Sergipe-Alagoas Basin, NE Brazil. In Morad, S. (ed.), *Carbonate Cementation in Sandstones: Distribution Patterns and Geochemical Evolution*. Blackwell, Oxford, Special Publication of the International Association of Sedimentologists, 26, 107–140. <https://doi.org/10.1002/9781444304893.ch5>
- Garzanti, E. & Vezzoli, G., 2003. A classification of metamorphic grains in sands, based on their composition and grade. *Journal of Sedimentary Research*, 73, 830–837. <https://doi.org/10.1306/012203730830>
- Geluk, M.C., 2005. Stratigraphy and tectonics of Permo-Triassic basins in the Netherlands and surrounding areas. Ph.D. Thesis, Utrecht University, Utrecht, 171 p.
- Giles, M.R., 1997. *Diagenesis: A Quantitative Perspective: Implications for Basin Modelling and Rock-Property Prediction*. Kluwer Academic Publishers, Dordrecht, 526 p.
- Giles, M.R. & Marshall, J.D., 1986. Constraints on the development of secondary porosity in the subsurface: Re-evaluation of processes. *Marine and Petroleum Geology*, 3, 243–255. [https://doi.org/10.1016/0264-8172\(86\)90048-6](https://doi.org/10.1016/0264-8172(86)90048-6)
- Giles, H.A., Indrelid, S.L., Beynon, G.V. & Amthor, J., 2000. The origin of large-scale quartz cementation: evidence from large data sets and coupled heat-fluid mass transport modelling. In Worden, R.H. & Morad, S. (eds), *Quartz Cementation in Sandstones*. Blackwell, Oxford, Special Publication of the International Association of Sedimentologists, 29, 21–38. <https://doi.org/10.1002/9781444304237.ch2>
- Glennie, K.W., Mudd, G.C. & Nagtegaal, P.J.C., 1978. Depositional environment and diagenesis of Permian Rotliegendes sandstones in Lemn Bank and Sole Pit Areas of the UK, Southern North Sea. *Journal of the Geological Society London*, 135, 25–34. <https://doi.org/10.1144/gsjgs.135.1.0025>
- Gluyas, J.H. & Coleman, M.L., 1992. Material flux and porosity changes during sediment diagenesis. *Nature*, 356, 52–53. <https://doi.org/10.1038/356052a0>
- Goldstein, R.H. & Rossi, C., 2002. Recrystallization in quartz overgrowths. *Journal of Sedimentary Research*, 72, 432–440. <https://doi.org/10.1306/110201720432>
- Haszeldine, R.S., Quinn, O., England, G., Wilkinson, M., Shipton, Z.K., Evans, J.P., Heath, J., Crossey, L., Ballentine, C.J. & Graham, C.M., 2005. Natural geochemical analogues for carbon dioxide storage in deep geological porous reservoirs, a United Kingdom perspective. *Oil & Gas Science and Technology*, 60, 33–49. <https://doi.org/10.2516/ogst.2005004>
- Heald, M.T., 1955. Stylolites in sandstones. *Journal of Geology*, 63, 101–114. <https://doi.org/10.1086/626237>
- Heald, M.T., 1959. Significance of stylolites in permeable sandstones. *Journal of Sedimentary Research*, 29, 251–253. <https://doi.org/10.1306/74D708F3-2B21-11D7-8648000102C1865D>
- Heald, M.T. & Larese, R.E., 1974. Influence of coats on quartz cementation. *Journal of Sedimentary Petrology*, 44, 1269–1274. <https://doi.org/10.1306/212F6C94-2B24-11D7-8648000102C1865D>
- Heidsiek, M., Butscher, Ch., Blum, Ph. & Fischer, C., 2020. Small-scale diagenetic facies heterogeneity controls porosity and permeability pattern in reservoir sandstones. *Environmental Earth Sciences*, 79, 425. <https://doi.org/10.1007/s12665-020-09168-z>
- Helsen, S. & Langenaeker, V., 1999. Burial history and coalification modelling of Westphalian strata in the eastern Campine Basin (Northern Belgium). *Geological Survey of Belgium, Professional paper*, 289, 23 p.
- Henares, S., Caracciolo, L., Cultrone, G., Fernández, J. & Viseras, C., 2014. The role of diagenesis and depositional facies on pore system evolution in a Triassic outcrop analogue (SE Spain). *Marine and Petroleum Geology*, 51, 136–151. <https://doi.org/10.1016/j.marpetgeo.2013.12.004>
- Hillier, S., 2003. Quantitative analysis of clay and other minerals in sandstones by X-ray powder diffraction (XRPD). In Worden, R.H. & Morad, S. (eds), *Clay Mineral Cements in Sandstones*. Blackwell, Oxford, International Association of Sedimentologists Special Publication, 34, 213–251. <https://doi.org/10.1002/9781444304336.ch11>
- Houseknecht, D.W., 1984. Influence of grain size and temperature on intergranular pressure solution, quartz cementation, and porosity in

- a quartzose sandstone. *Journal of Sedimentary Petrology*, 54, 348–361. <https://doi.org/10.1306/212F8418-2B24-11D7-8648000102C1865D>
- Irwin, H., Curtis, C. & Coleman, M., 1977. Isotopic evidence for source of diagenetic carbonates formed during burial of organic-rich sediments. *Nature*, 269, 209–213. <https://doi.org/10.1038/269209a0>
- Johnson, H. & Fisher, M., 1998. North Sea plays: geological controls on hydrocarbon distribution. In Glennie, K.W. (ed.), *Petroleum Geology of the North Sea: Basic Concepts and Recent Advances*. 4th ed. Blackwell Science, Oxford, 463–547. <https://doi.org/10.1002/9781444313413.ch12>
- Kastner, M. & Siever, R., 1979. Low temperature feldspars in sedimentary rocks. *American Journal of Science*, 279, 435–479. <https://doi.org/10.2475/ajs.279.4.435>
- Kelly, J.L., Fu, B., Kita, N.T. & Valley, J.W., 2007. Optically continuous silcrete quartz cements of the St. Peter Sandstone: High precision oxygen isotope analysis by ion microprobe. *Geochimica et Cosmochimica Acta*, 71, 3812–3832. <https://doi.org/10.1016/j.gca.2007.05.014>
- Kirkland, D.W., Denison, R.E. & Rooney, M.A., 1995. Diagenetic alteration of Permian strata at oil fields of south central Oklahoma, USA. *Marine and Petroleum Geology*, 12, 629–644. [https://doi.org/10.1016/0264-8172\(95\)98089-N](https://doi.org/10.1016/0264-8172(95)98089-N)
- Knox, R.W.O., Burgess, W.G., Wilson, K.S. & Bath, A.H., 1984. Diagenetic influences on reservoir properties of the Sherwood Sandstone (Triassic) in the Marchwood geothermal borehole, Southampton, UK. *Clay Minerals*, 19, 441–456. <https://doi.org/10.1180/claymin.1984.019.3.12>
- Kunkel, C., Aehnelt, M., Pudlo, D., Kukowski, N., Totsche, K.U. & Gaupp, R., 2018. Surface aquifer heterogeneities of Lower Triassic clastic sediments in central Germany. *Marine and Petroleum Geology*, 97, 209–222. <https://doi.org/10.1016/j.marpetgeo.2018.06.022>
- Laenen, B., 2002. Lithostratigrafie van het pre-Tertiair in Vlaanderen : Deel I: post-Dinantiaan. VITO, Mol, VITO report, ETE/R/063, 46 p.
- Lai, J., Li, D., Wang, G., Xiao, Ch., Cao, J., Wu, C., Han, C., Zhao, X. & Qin, Z., 2019. Can carbonate cementation be inhibited in continental red bed sandstone? *Journal of Petroleum Science and Engineering*, 179, 1123–1135. <https://doi.org/10.1016/j.petrol.2019.05.015>
- Land, L.S., 1983. The application of stable isotopes to studies of the origin of dolomite and to problems of diagenesis of clastic sediments. In Arthur, M.A., Anderson, T.F., Kaplan, I.R., Veizer, J. & Land, L.S. (eds), *Stable Isotopes in Sedimentary Geology*. SEPM Short Course, 10, 4.1–4.22. <https://doi.org/10.2110/scn.83.10>
- Land, L.S., 1997. Mass transfer during burial diagenesis in the Gulf of Mexico sedimentary basin: An overview. In Montañez, I.P., Gregg, J.M. & Shelton K.L. (eds.), *Basin-Wide Diagenetic Patterns: Integrated Petrologic, Geochemical, and Hydrologic Considerations*. SEPM Special Publication, 57, 29–39. <https://doi.org/10.2110/pec.97.57.0029>
- Lane, S.J. & Dalton, J.A., 1994. Electron microprobe analysis of geological carbonates. *American Mineralogist*, 79, 745–749.
- Langenaeker, V., 1998. The Campine Basin: stratigraphy, structural geology, coalification and hydrocarbon potential for the Devonian to Jurassic. Unpublished Ph.D. Thesis, Katholieke Universiteit Leuven, Leuven, 190 p.
- Langenaeker, V., 2000. The Campine Basin. Stratigraphy, structural geology, coalification and hydrocarbon potential for the Devonian to Jurassic. *Aardkundige Mededelingen*, 10, 1–142.
- Lee, M.R. & Parsons, I., 2003. Microtextures of authigenic Or-rich feldspar in the Upper Jurassic Humber Group, UK North Sea. *Sedimentology*, 50, 597–608. <https://doi.org/10.1046/j.1365-3091.2003.00567.x>
- Mahmic, O., Dypvik, H. & Hammer, E., 2018. Diagenetic influence on reservoir quality evolution, examples from Triassic conglomerates/arenites in the Edvard Grieg field, Norwegian North Sea. *Marine and Petroleum Geology*, 93, 247–271. <https://doi.org/10.1016/j.marpetgeo.2018.03.006>
- Maraschin, A.J., Mizusaki, A.M.P. & De Ros, L.F., 2004. Near-surface K-feldspar precipitation in Cretaceous sandstones from the Potiguar Basin, Northeastern Brazil. *Journal of Geology*, 112, 317–334. <https://doi.org/10.1086/382762>
- McBride, E.F., 1989. Quartz cementation in sandstones: a review. *Earth-Science Reviews*, 26, 69–112. [https://doi.org/10.1016/0012-8252\(89\)90019-6](https://doi.org/10.1016/0012-8252(89)90019-6)
- McKinley, J.M., Worden, R.H. & Ruffell, A.H., 2003. Smectite in sandstones a review of the controls on occurrence and behaviour during diagenesis. In Worden, R.H. & Morad, S. (eds), *Clay Mineral Cements in Sandstones*. Blackwell, Oxford, Special Publication of the International Association Sedimentologists, 34, 109–128. <https://doi.org/10.1002/9781444304336.ch5>
- Mijnlieff, H.F., 2020. Introduction to the geothermal play and reservoir geology of the Netherlands. *Netherlands Journal of Geosciences*, 99, e2. <https://doi.org/10.1017/njg.2020.2>
- Milliken, K.L., Mack, L.E. & Land, L.S., 1994. Elemental mobility in sandstones during burial: whole-rock chemical and isotopic data, Frio Formation, south Texas. *Journal of Sedimentary Research*, A64, 788–796. <https://doi.org/10.1306/D4267EC4-2B26-11D7-8648000102C1865D>
- Molenaar, N., 1986. The interrelation between clay infiltration, quartz cementation, and compaction in Lower Givetian terrestrial sandstones, northern Ardennes, Belgium. *Journal of Sedimentary Petrology*, 56, 359–369. <https://doi.org/10.1306/212F8913-2B24-11D7-8648000102C1865D>
- Molenaar, N. & Felder, M., 2018. Clay cutans and the origin of illite rim cement: an example from the siliciclastic Rotliegend sandstone in the Dutch southern Permian Basin. *Journal of Sedimentary Research*, 88, 641–658. <https://doi.org/10.2110/jsr.2018.33>
- Monsees, A.C., Busch, B., Schöner, N. & Hilgers, Ch., 2020. Rock typing of diagenetically induced heterogeneities – A case study from a deeply-buried clastic Rotliegend reservoir of the Northern German Basin. *Marine and Petroleum Geology*, 113, 104163. <https://doi.org/10.1016/j.marpetgeo.2019.104163>
- Moore, D.M. & Reynolds, R.C., 1997. *X-Ray Diffraction and the Identification and Analysis of Clay Minerals*. Oxford University Press, Oxford, 400 p.
- Morad, S., 1998. Carbonate cementation in sandstones: distribution patterns and geochemical evolution. In Morad, S. (ed.), *Carbonate Cementation in Sandstones: Distribution Patterns and Geochemical Evolution*. Blackwell, Oxford, Special Publication of the International Association of Sedimentologists, 26, 1–26. <https://doi.org/10.1002/9781444304893.ch1>
- Morad, S., Ben Ismail, H., Al-Aasm, I. S. & De Ros, L.F., 1994. Diagenesis and formation water chemistry of Triassic reservoir sandstones from southern Tunisia. *Sedimentology*, 41, 1253–1272. <https://doi.org/10.1111/j.1365-3091.1994.tb01452.x>
- Morad, S., Ketzer, J.M. & De Ros, L.F., 2000. Spatial and temporal distribution of diagenetic alterations in siliciclastic rocks: implications for mass transfer in sedimentary basins. *Sedimentology*, 47, 95–120. <https://doi.org/10.1046/j.1365-3091.2000.00007.x>
- Morad, S., Al-Ramadan, K., Ketzer, J.M. & De Ros, L., 2010. The impact of diagenesis on the heterogeneity of sandstone reservoirs: A review of the role of depositional facies and sequence stratigraphy. *American Association of Petroleum Geologist Bulletin*, 94, 1267–1309. <https://doi.org/10.1306/04211009178>
- Moraes, M.A.S. & De Ros, L.F., 1990. Infiltrated clays in fluvial Jurassic sandstones of Recôncavo Basin, Northeastern Brazil. *Journal of Sedimentary Petrology*, 60, 809–819. <https://doi.org/10.1306/212F928C-2B24-11D7-8648000102C1865D>
- Muchez, P. & Viaene, W., 1994. Dolomitization caused by water circulation near the mixing zone: an example from the Lower Viséan of the Campine Basin (northern Belgium). In Purser, B.,

- Tucker, M. & Zenger, D. (eds), Dolomites: a Volume in Honour of Dolomieu. Blackwell, Oxford, Special Publication of the International Association of Sedimentologists, 21, 155–166. <https://doi.org/10.1002/9781444304077.ch10>
- Muchez, P., Boven, J., Bouckaert, J., Leplat, P., Viaene, W. & Wolf, M., 1991. Illite crystallinity in the Carboniferous of the Campine-Brabant Basin (Belgium) and its relationship to organic maturity indicators. *Neues Jahrbuch für Geologie und Paläontologie Abhandlungen*, 182, 117–131. <https://doi.org/10.1127/njgpa/182/1991/117>
- Muchez, P., Viaene, W. & Duser, M., 1992. Diagenetic control on secondary porosity in flood plain deposits: an example of the Lower Triassic of north-eastern Belgium. *Sedimentary Geology*, 78, 285–298. [https://doi.org/10.1016/0037-0738\(92\)90025-M](https://doi.org/10.1016/0037-0738(92)90025-M)
- Murray, R. C., 1990. Diagenetic silica stratification in a paleosilcrete, North Texas. *Journal of Sedimentary Petrology*, 60, 717–720. <https://doi.org/10.1306/212F9255-2B24-11D7-8648000102C1865D>
- Niazi, A.M.K., Jähren, J., Mahmood, I. & Javaid, H., 2019. Reservoir quality in the Jurassic sandstone reservoirs located in the Central Graben, North Sea. *Marine and Petroleum Geology*, 102, 439–454. <https://doi.org/10.1016/j.marpetgeo.2019.01.001>
- Oelkers, E.H., Bjørkum, P.A. & Murphy, W.M., 1996. A petrographic and computational investigation of quartz cementation and porosity reduction in North Sea sandstones. *American Journal of Science*, 296, 420–452. <https://doi.org/10.2475/ajs.296.4.420>
- Oelkers, E.H., Bjørkum, P.A., Walderhaug, O., Nadeau, P.H. & Murphy, W.M., 2000. Making diagenesis obey thermodynamics and kinetics: the case of quartz cementation in sandstones from offshore mid-Norway. *Applied Geochemistry*, 15, 295–309. [https://doi.org/10.1016/S0883-2927\(99\)00047-5](https://doi.org/10.1016/S0883-2927(99)00047-5)
- Ormö, J., Komatsu, G., Chan, M.A., Beitler, B. & Parry, W.T., 2004. Geological features indicative of processes related to the hematite formation in Meridiani Planum and Aram Chaos, Mars: a comparison with diagenetic hematite deposits in southern Utah, USA. *Icarus*, 171, 295–316. <https://doi.org/10.1016/j.icarus.2004.06.001>
- Oye, O.J., Aplin, A.C., Jones, S.J., Gluyas, J.G., Bowen, L., Orland, I.J. & Valley, J.W., 2018. Vertical effective stress as a control on quartz cementation in sandstones. *Marine and Petroleum Geology*, 98, 640–652. <https://doi.org/10.1016/j.marpetgeo.2018.09.017>
- Parry, W.T., Chan, M.A. & Beitler, B., 2004. Chemical bleaching indicates episodes of fluid flow in deformation bands in sandstone. *American Association of Petroleum Geologist Bulletin*, 88, 175–191. <https://doi.org/10.1306/09090303034>
- Patijn, R.J.H. & Kimpe, W.F.M., 1961. De kaart van het Carboon-oppevlak, de profielen en de kaart van het dek-terrein van het zuid-Limburgse mijngebied en Staatsmijn Beatrix en omgeving. *Mededelingen van de Geologische Stichting*, 44, 5–12.
- Patterson, C. & Tatsumoto, M., 1964. The significance of lead isotopes in detrital feldspar with respect to chemical differentiation within the earth's mantle. *Geochimica et Cosmochimica Acta*, 28, 1–22. [https://doi.org/10.1016/0016-7037\(64\)90052-3](https://doi.org/10.1016/0016-7037(64)90052-3)
- Pettijohn, F.J., Potter, P.E. & Siever, R., 1987. *Sand and Sandstone*. Springer-Verlag, Berlin, 532 p. <https://doi.org/10.1007/978-1-4612-1066-5>
- Pimentel, N.L., Wright, V.P. & Azevedo, T.M., 1996. Distinguishing early groundwater alteration effects from pedogenesis in ancient alluvial basins: examples from the Palaeogene of Southern Portugal. *Sedimentary Geology*, 105, 1–10. [https://doi.org/10.1016/0037-0738\(96\)00034-6](https://doi.org/10.1016/0037-0738(96)00034-6)
- Pittman, E.D., Larese, R.E. & Heald, M.T., 1992. Clay coats: occurrence and relevance to preservation of porosity in sandstones. In: Houseknecht, D.W. & Pittman, E.D. (eds), *Origin, Diagenesis and Petrophysics of Clay Minerals in Sandstones*. SEPM Special Publication, 47, 241–264. <https://doi.org/10.2110/pec.92.47.0241>
- Purvis, K. & Okkerman, J.A., 1996. Inversion of reservoir quality by early diagenesis: an example from the Triassic Buntsandstein, offshore the Netherlands. In: Rondeel, H.E., Batjes, D.A.J. & Nieuwenhuijs, W.H. (eds), *Geology of Gas and Oil Under the Netherlands: Selection of Papers Presented at the 1993 International Conference of the American Association of Petroleum Geologists*. Kluwer, Dordrecht, 179–189. [https://doi.org/10.1007/978-94-009-0121-6\\_16](https://doi.org/10.1007/978-94-009-0121-6_16)
- Quandt, D., Busch, B., Schmidt, Ch. & Hilgers, Ch., 2022. Diagenesis and controls on reservoir quality of Lower Triassic red bed sandstones (Buntsandstein) from a marginal basin facies, southwest Germany. *Marine and Petroleum Geology*, 142, 105744. <https://doi.org/10.1016/j.marpetgeo.2022.105744>
- Renard, F., Ortoleva, P. & Gratier, J.P., 1997. Pressure solution in sandstones: influence of clays and dependence on temperature and stress. *Tectonophysics*, 280, 257–266. [https://doi.org/10.1016/S0040-1951\(97\)00039-5](https://doi.org/10.1016/S0040-1951(97)00039-5)
- Renard, F., Park, A., Ortoleva, P. & Gratier, J.P., 1999. An integrated model for transitional pressure solution in sandstones. *Tectonophysics*, 312/2-4, 97–115. [https://doi.org/10.1016/S0040-1951\(99\)00202-4](https://doi.org/10.1016/S0040-1951(99)00202-4)
- Renard, F., Brosse, E. & Gratier, J.P., 2000. The different processes involved in the mechanism of pressure solution in quartz-rich rocks and their interactions. In: Worden, R.H. & Morad, S. (eds), *Quartz Cementation in Sandstones*. Blackwell, Oxford, Special Publication of the International Association of Sedimentologists, 29, 67–78. <https://doi.org/10.1002/9781444304237.ch5>
- Rossi, C., Kálin, O. & Arribas, J., 2002. Diagenesis, provenance and reservoir quality of Triassic TAGI sandstones from Ourhoud field, Berkine (Ghadames) Basin, Algeria. *Marine and Petroleum Geology*, 19, 117–142. [https://doi.org/10.1016/S0264-8172\(02\)00004-1](https://doi.org/10.1016/S0264-8172(02)00004-1)
- Scanlon, B.R., Keese, K., Reedy, R.C., Simunek, J. & Andraski, B.J., 2003. Variations in flow and transport in thick desert vadose zones in response to paleoclimatic forcing (0–90 kyr): field measurements, modeling, and uncertainties. *Water Resource Research*, 39, 3.1–3.18. <https://doi.org/10.1029/2002WR001604>
- Scherer, C.M., Goldberg, K. & Bardola, T., 2015. Facies architecture and sequence stratigraphy of an early post-rift fluvial succession, Aptian Barbalha Formation, Araripe Basin, northeastern Brazil. *Sedimentary Geology*, 322, 43–62. <https://doi.org/10.1016/j.sedgeo.2015.03.010>
- Schmid, S., Worden, R. H. & Fisher, Q. J., 2003. The origin and regional distribution of dolomite cement in sandstones from a Triassic dry river system, Corrib Field, offshore west of Ireland. *Journal of Geochemical Exploration*, 78–79, 475–479. [https://doi.org/10.1016/S0375-6742\(03\)00118-3](https://doi.org/10.1016/S0375-6742(03)00118-3)
- Schmid, S., Worden, R.H. & Fisher, Q.J., 2004. Diagenesis and reservoir quality of the Sherwood Sandstone (Triassic), Corrib field, Slyne Basin, west of Ireland. *Marine and Petroleum Geology*, 21, 299–315. <https://doi.org/10.1016/j.marpetgeo.2003.11.015>
- Schmid, S., Worden, R.H. & Fisher, Q.J., 2006a. Carbon isotope stratigraphy using carbonate cements in the Triassic Sherwood Sandstone Group: Corrib field, west of Ireland. *Chemical Geology*, 225, 137–155. <https://doi.org/10.1016/j.chemgeo.2005.09.006>
- Schmid, S., Worden, R.H. & Fisher, Q.J., 2006b. Sedimentary facies and the context of dolomite in the Lower Triassic Sherwood Sandstone Group: Corrib Field west of Ireland. *Sedimentary Geology*, 187, 205–227. <https://doi.org/10.1016/j.sedgeo.2005.12.028>
- Schmidt, V. & McDonald, D.A., 1979. Texture and recognition of secondary porosity in sandstones. In: Scholle, P.A. & Schluger, P.R. (eds), *Aspects of Diagenesis*. SEPM Special Publication, 26, 209–225. <https://doi.org/10.2110/pec.79.26.0209>
- Schmidt, V. & McDonald, D.A., 1980. Secondary Reservoir Porosity in the Course of Sandstone Diagenesis. *American Association of Petroleum Geologist Continuing Course Note Series*, 12, 125 p. <https://doi.org/10.2110/pec.79.26.0175>
- Schmidt, C., Busch, B. & Hilgers, Ch., 2020a. Compaction and cementation control on bleaching in Triassic fluvial red beds, S-Germany. *Zeitschrift der Deutschen Gesellschaft für*

- Geowissenschaften, 172, 523–539. <https://doi.org/10.1127/zdgg/2020/0233>
- Schmidt, C., Busch, B. & Hilgers, C., 2020b. Lateral variations of detrital, authigenic and petrophysical properties in an outcrop analog of the fluvial Plattensandstein, Lower Triassic, S-Germany. *Zeitschrift der Deutschen Gesellschaft für Geowissenschaften*, 172, 541–564. <https://doi.org/10.1127/zdgg/2020/0234>
- Schöner, O. & Gaupp, R., 2005. Contrasting red bed diagenesis: the southern and northern margin of the Central European Basin. *International Journal of Earth Sciences*, 94, 897–916. <https://doi.org/10.1007/s00531-005-0004-3>
- Scorgie, J.C., Worden, R.H., Utley, J.E.P. & Roche, I.P., 2021. Reservoir quality and diagenesis of Triassic sandstones and siltstones from arid fluvial and playa margin environments: A study of one of the UK's earliest producing oilfields. *Marine and Petroleum Geology*, 131, 105154. <https://doi.org/10.1016/j.marpetgeo.2021.105154>
- Shanmugan, G., 1990. Porosity prediction in sandstones using erosional unconformities. In Meshri, I.D. & Ortoleva, P.J. (eds), *Prediction of Reservoir Quality Through Chemical Modeling*. American Association of Petroleum Geologist Memoir, 49, 1–23. <https://doi.org/10.1306/M49520C1>
- Sheldon, H.A., Wheeler, J., Worden, R.H. & Cheadle, M.J., 2003. An analysis of the roles of stress, temperature, and pH in chemical compaction of sandstones. *Journal of Sedimentary Research*, 73, 64–71. <https://doi.org/10.1306/070802730064>
- Sheldon, H.A., Wheeler, J., Worden, R.H. & Cheadle, M.J., 2004. An analysis of the roles of stress, temperature, and pH in chemical compaction of sandstones: Reply. *Journal of Sedimentary Research*, 74, 449–450. <https://doi.org/10.1306/120203740449>
- Soyk, D., 2015. Diagenesis and reservoir quality of the Lower and Middle Buntsandstein (Lower Triassic), SW Germany. Unpublished Ph.D. Thesis, Ruprecht-Karls-Universität, Heidelberg, 181 p.
- Spain, D.R. & Conrad, C.P., 1997. Quantitative analysis of top-seal capacity: offshore Netherlands, southern North Sea. *Geologie en Mijnbouw*, 76, 217–226. <https://doi.org/10.1023/A:1003056609771>
- Spötl, C. & Wright, V.P., 1992. Groundwater dolocretes from the Upper Triassic of the Paris Basin, France: A case study of an arid, continental diagenetic facies. *Sedimentology*, 39, 1119–1136. <https://doi.org/10.1111/j.1365-3091.1992.tb02000.x>
- Środoń, J., 1980. Precise identification of illite/smectite interstratifications by X-ray powder diffraction. *Clays and clay minerals*, 28/6, 401–411. <https://doi.org/10.1346/CCMN.1980.0280601>
- Suggate, R.P., 1998. Relations between depth of burial, vitrinite reflectance and geothermal gradient. *Journal of Petroleum Geology*, 21, 5–32. <https://doi.org/10.1111/j.1747-5457.1998.tb00644.x>
- Summerfield, M.A., 1983. Petrography and diagenesis of silcrete from the Kalahari Basin, Cape Coastal Zone, southern Africa. *Journal of Sedimentary Petrology*, 53, 895–909. <https://doi.org/10.1306/212F82E2-2B24-11D7-8648000102C1865D>
- Sundal, A., Miri, R., Hellevang, H., Tveranger, J., Midtkandal, I., Zuchuat, V., Aagaard, P. & Braathen, A., 2017. Movement of CO<sub>2</sub> charged fluids in low permeability rocks during deformation: migration patterns in the Carmel Formation, Utah. *Energy Procedia*, 114, 4537–4544. <https://doi.org/10.1016/j.egypro.2017.03.1570>
- Surdam, R.C. & Crossey, L.J., 1985. Organic-inorganic reactions during progressive burial: Key to porosity and permeability enhancement and preservation. *Philosophical Transactions of the Royal Society of London Series A*, 315, 135–156. <https://doi.org/10.1098/rsta.1985.0034>
- Surdam, R.C., Boese, S.W. & Crossey, L.J., 1984. The chemistry of secondary porosity. In McDonald, D.A. & Surdam, R.C. (eds.), *Clastic Diagenesis*. American Association of Petroleum Geologist Memoir, 37, 127–149. <https://doi.org/10.1306/M37435C8>
- Surdam, R.C., Jiao, Z.S. & Macgowan, D.B., 1993. Redox reactions involving hydrocarbons and mineral oxidants: a mechanism for significant porosity enhancement in sandstones. *American Association of Petroleum Geologist Bulletin*, 77, 1509–1518. <https://doi.org/10.1306/BDFF8ED4-1718-11D7-8645000102C1865D>
- Tada, R. & Siever, R., 1989. Pressure solution during diagenesis. *Annual Review of Earth and Planetary Sciences*, 17, 89–118. <https://doi.org/10.1146/annurev.earth.17.050189.000513>
- Thiry, M. & Millot, G., 1987. Mineralogical forms of silica and their sequence of formation in silcretes. *Journal of Sedimentary Petrology*, 57, 343–352. <https://doi.org/10.1306/212F8B25-2B24-11D7-8648000102C1865D>
- Thiry, M. & Milnes, A.R., 1991. Pedogenic and groundwater silcretes at the Stuart Creek Opal Field, South Australia. *Journal of Sedimentary Petrology*, 61, 111–127. <https://doi.org/10.1306/D426769F-2B26-11D7-8648000102C1865D>
- Thorez, J., 1976. *Practical Identification of Clay Minerals: a Handbook for Teachers and Students in Clay Mineralogy*. Edition G. Lelotte, Dison (Belgium), 90 p.
- Trewin, N.H. & Fallick, A.E., 2000. Quartz cement origins and budget in the Tumblagooda Sandstone, Western Australia. In Worden, R.H. & Morad, S. (eds), *Quartz Cementation in Sandstones*. Blackwell, Oxford, Special Publication of the International Association of Sedimentologists, 29, 219–229. <https://doi.org/10.1002/9781444304237.ch15>
- Ullman, W.J. & Welch, S.A., 2002. Organic ligands and feldspar dissolution. In Hellmann, R. & Woods, S.A. (eds), *Water-Rock Interactions, Ore Deposits, and Environmental Geochemistry: A tribute to David A. Crerar*. Geochemical Society Special Publication Series, 7, 3–35.
- Vandewijngaerde, W., Piessens, K., Dusar, M., Bertier, P., Krooss, B.M., Littke, R. & Swennen, R., 2016. Investigations on the shale oil and gas potential of Westphalian mudstone successions in the Campine Basin, NE Belgium (well KB174): Palaeoenvironmental and palaeogeographical controls. *Geologica Belgica*, 19, 225–235. <http://dx.doi.org/10.20341/gb.2016.009>
- Van Hulten, F.F.N., 2006. Reservoir quality distribution as tool for better exploration prospect evaluation and estimation of the resource base in the Netherlands. *Proceedings of the tight gas fields in the Netherlands workshop EBN-TNO*, 13 p.
- Van Keer, I., 1999. Mineralogical variations in sandstone sequences near coal seams, shales and mudstones in the Westphalian of the Campine Basin (NE-Belgium): Its relation to organic matter maturation. Unpublished Ph.D. Thesis, University of Leuven, Leuven, 190 p.
- Van Keer, I., Ondrak, R., Muchez, Ph., Bayer, U., Dusar, M. & Viaene, W., 1998. Burial history and thermal evolution of Westphalian coal-bearing strata in the Campine Basin (NE Belgium). *Geologie en Mijnbouw*, 76, 301–310. <https://doi.org/10.1023/A:1003266317035>
- Van Tongeren, P.C.H., 2001. CO<sub>2</sub>-sequestration possibilities in the deep aquifers of the Campine Basin (northern Belgium). VITO, Mol, VITO report, 2001/ETE/R/030, 20 p.
- Van Tongeren, P.C.H., Laenen, B. & Dreesen, R., 2000. Het koolbed methaan potentieel in Vlaanderen en de mogelijkheden tot geologische opslag van CO<sub>2</sub> in relatie tot de winning van deze gasreserves. VITO, Mol, VITO report, 2000/ETE/R/028, 99 p.
- Wachter, E.A. & Hayes, J.M., 1985. Exchange of oxygen isotopes in carbon dioxide-phosphoric acid systems. *Chemical Geology: Isotope Geoscience Section*, 52, 365–374. [https://doi.org/10.1016/0168-9622\(85\)90046-6](https://doi.org/10.1016/0168-9622(85)90046-6)
- Walderhaug, O., 1994. Precipitation rates for quartz cement in sandstones determined by fluid-inclusion microthermometry and temperature-history modeling. *Journal of Sedimentary Research*, 64, 324–333. <https://doi.org/10.2110/jsr.64.324>
- Walderhaug, O., 1996. Kinetic modeling of quartz cementation and porosity loss in deeply buried sandstone reservoirs. *American Association of Petroleum Geologist Bulletin*, 80, 731–745. <https://doi.org/10.1306/64ED88A4-1724-11D7-8645000102C1865D>

- Walderhaug, O. & Bjørkum, P.A., 2003. The effect of stylolite spacing on quartz cementation in the Lower Jurassic Sto Formation, Southern Barents Sea. *Journal of Sedimentary Research*, 73, 146–156. <https://doi.org/10.1306/090502730146>
- Walderhaug, O., Lander, R.H., Bjørkum, P.A., Oelkers, E.H., Bjørlykke, K. & Nadeau, P.H., 2000. Modelling quartz cementation and porosity in reservoir sandstones: examples from the Norwegian continental shelf. In Worden, R.H. & Morad, S. (eds), *Quartz Cementation in Sandstones*. Blackwell, Oxford, Special Publication of the International Association of Sedimentologists, 29, 39–49. <https://doi.org/10.1002/9781444304237.ch3>
- Walderhaug, O., Oelkers, E.H. & Bjørkum, P.A., 2004. An analysis of the roles of stress, temperature, and pH in chemical compaction of sandstones: Discussion. *Journal of Sedimentary Research*, 74, 447–448.
- Walker, T.R., Waugh, B. & Crone, A.J., 1978. Diagenesis in first-cycle desert alluvium of Cenozoic age, southwestern United States and northwestern Mexico. *Geological Society of America Bulletin*, 89, 19–32. [https://doi.org/10.1130/0016-7606\(1978\)89<19:DIFDAO>2.0.CO;2](https://doi.org/10.1130/0016-7606(1978)89<19:DIFDAO>2.0.CO;2)
- Walvoord, M.A., Plummer, M.A., Phillips, F.M. & Wolfsberg, A.V., 2002. Deep arid system hydrodynamics, I. Equilibrium states and response times in thick desert vadose zones. *Water Resources Research*, 38, 44.1–44.15. <https://doi.org/10.1029/2001WR000824>
- Weber, J. & Ricken, W., 2005. Quartz cementation and related sedimentary architecture of the Triassic Solling Formation, Reinhardswald Basin, Germany. *Sedimentary Geology*, 175, 459–477. <https://doi.org/10.1016/j.sedgeo.2004.12.019>
- Wei, W., Littke, R. & Swennen, R., 2022. Geochemical study of Mississippian to Pennsylvanian Namurian Shale in the Namur Synclinorium and Campine Basin (Belgium and S-Netherlands): Implication for paleo-redox reconstruction and organic matter characteristics. *International Journal of Coal Geology*, in press, 104150. <https://doi.org/10.1016/j.coal.2022.104150>
- Weibel, R., 1998. Diagenesis in oxidising and locally reducing conditions — an example from the Triassic Skagerrak Formation, Denmark. *Sedimentary Geology*, 121, 259–276. [https://doi.org/10.1016/S0037-0738\(98\)00085-2](https://doi.org/10.1016/S0037-0738(98)00085-2)
- Weibel, R. & Friis, H., 2004. Opaque minerals as keys for distinguishing oxidising and reducing diagenetic conditions in the Lower Triassic Bunter Sandstone, North German Basin. *Sedimentary Geology*, 169, 129–149. <https://doi.org/10.1016/j.sedgeo.2004.05.004>
- Wendler, J., Köster, J., Götze, J., Kasch, N., Zisser, N., Kley, J., Pudlo, D., Nover, G. & Gaupp, R., 2012. Carbonate diagenesis and feldspar alteration in fracture-related bleaching zones (Buntsandstein, central Germany): possible link to CO<sub>2</sub>-influenced fluid–mineral reactions. *International Journal of Earth Sciences*, 101, 159–176. <https://doi.org/10.1007/s00531-011-0671-1>
- Wilkinson, M., Darby, D., Haszeldine, R.S. & Couples, G.D., 1997. Secondary porosity generation during deep burial associated with overpressure leakoff: Fulmar Formation, United Kingdom Central Graben. *American Association of Petroleum Geologist Bulletin*, 81, 803–813. <https://doi.org/10.1306/522B484D-1727-11D7-8645000102C1865D>
- Wilson, M.D., 1992. Inherited grain-rimming clays in sandstones from eolian and shelf environments: their origin and control on reservoir properties. In Houseknecht, D.W. & Pittman, E.D. (eds), *Origin, Diagenesis and Petrophysics of Clay Minerals in Sandstones*. SEPM Special Publication, 47, 209–225. <https://doi.org/10.2110/pec.92.47.0209>
- Wooldridge, N.L.J., Worden, R.H., Griffiths, J. & Utley J.E.P., 2017. Clay-coated sand grains in petroleum reservoirs: understanding their distribution via a modern analogue. *Journal of Sedimentary Research*, 87, 338–352. <https://doi.org/10.2110/jsr.2017.20>
- Worden, R.H. & Burley, S.D., 2003. Sandstone diagenesis: the evolution of sand to stone. In Burley, S.D. & Worden, R.H. (eds), *Sandstone Diagenesis: Recent & ancient*. Blackwell, Oxford, Reprint Series of the International Association of Sedimentologists, 4, 3–44. <https://doi.org/10.1002/9781444304459.ch>
- Worden, R.H. & Morad, S., 2000. Quartz cementation in oil field sandstones: a review of the key controversies. In Worden, R.H. & Morad, S. (eds), *Quartz Cementation in Sandstones*. Blackwell, Oxford, Special Publication of the International Association of Sedimentologists, 29, 1–20. <https://doi.org/10.1002/9781444304237.ch1>
- Worden, R.H. & Morad, S., 2003. Clay minerals in sandstones: controls on formation, distribution and evolution. In Worden, R.H. & Morad, S. (eds), *Clay Mineral Cements in Sandstones*. Blackwell, Oxford, Special Publication of the International Association of Sedimentologists, 34, 3–41. <https://doi.org/10.1002/9781444304336.ch1>
- Worden, R.H. & Rushton, J.C., 1992. Diagenetic K-feldspar textures: a TEM study and model for diagenetic feldspar growth. *Journal of Sedimentary Petrology*, 62, 779–789. <https://doi.org/10.1306/D42679D8-2B26-11D7-8648000102C1865D>
- Worden, R.H., Armitage, P.J., Butcher, A., Churchill, J., Csoma, A., Hollis, C., Lander, R.H. & Omma, J., 2018. Petroleum reservoir quality prediction: overview and contrasting approaches from sandstone and carbonate communities. In Armitage, P.J., Butcher, A., Churchill, J., Csoma, A., Hollis, C., Lander, R.H., Omma, J. & Worden, R.H. (eds), *Reservoir Quality of Clastic and Carbonate Rocks: Analysis, Modelling and Prediction*. Geological Society, London, Special Publication, 435, 1–31. <https://doi.org/10.1144/SP435.21>
- Wouters, L. & Vandenberghe, N., 1994. *Geologie van de Kempen: een synthese*. NIRAS-ONDRAF, Brussel, 208 p.
- Xie, D., Yao, S., Cao, J., Hu, W., Wang, X. & Zhu, N., 2021. Diagenetic alteration and geochemical evolution during sandstones bleaching of deep red-bed induced by methane migration in petroliferous basins. *Marine and Petroleum Geology*, 127, 104940. <https://doi.org/10.1016/j.marpetgeo.2021.104940>